2012

Efficient finite element modeling of reinforced concrete columns confined with fiber reinforced polymers

Dan Hu
Louisiana State University and Agricultural and Mechanical College, lsu.hudan@gmail.com

EFFICIENT FINITE ELEMENT MODELING OF REINFORCED CONCRETE COLUMNS CONFINED WITH FIBER REINFORCED POLYMERS

A Thesis

Submitted to the Graduate Faculty of the
Louisiana State University and
Agricultural and Mechanical College
in partial fulfillment of the
requirements for the degree of
Master of Science in Civil Engineering

in

The Department of Civil and Environmental Engineering

by
Dan Hu
B.S., Southwest Jiaotong University, China, 2009
December 2012

This work is sincerely dedicated to my parents.

ACKNOWLEDGMENTS

I would like to express my sincere appreciation and thanks to my advisor, Dr. Michele Barbato for his enormous help and constant guidance through the process of learning and performing this research. Undoubtedly, the completion of this work would have not been possible without such help.

I would also like to thank Dr. Ayman Okeil and Dr. Steve Cai for serving in my defense committee, and providing me support and technical guidance to improve the contents of this thesis.

My genuine gratitude goes to my parents for all their love and support over the years and for always encouraging and supporting me in my studies. I would also like to thank my awesome friends for bearing with me through all the difficulties and their love and support when I needed them the most.

I would also like to thank the funding sources of this research (1) the Louisiana Board of Regents (LA BoR) through the Louisiana Board of Regents Research and Development Program, Research Competitiveness (RCS) subprogram, under Award No. LESQSF (2010-13)-RD-A-01; and (2) the LSU Council on Research through the 2009-2010 Faculty Research Grant Program.

TABLE OF CONTENTS

LIST OF TABLES

LIST OF FIGURES

ABSTRACT

Fiber reinforced polymer (FRP) composites have found extensive applications in the field of Civil Engineering due to their advantageous properties such as high strength-to-weight ratio and high corrosion resistance. This study presents a simple and efficient frame finite element (FE) able to accurately estimate the load-carrying capacity and ductility of reinforced concrete (RC) circular columns confined with externally bonded fiber reinforced polymer (FRP) plates and/or sheets. The proposed FE considers distributed plasticity with fiber-discretization of the cross-sections in the context of a force-based (FB) formulation. The element is able to model collapse due to concrete crushing, reinforcement steel yielding, and FRP rupture.

The frame FE developed in this study is used to predict the load-carrying capacity of FRP-confined RC columns subjected to both concentric and eccentric axial loading. Numerical simulations and experimental results are compared based on experimental tests available in the literature and published by different authors. The numerically simulated responses agree well with the corresponding experiment results. The outstanding features of this FE include computational efficiency, accuracy and ease of use. Therefore, the proposed FE is suitable for efficient and accurate modeling and analysis of RC columns confined with externally retrofitted FRP plates/sheets as for parametric studies requiring numerous FE analyses.

1 INTRODUCTION

1.1 BACKGROUND

A large number of reinforced concrete (RC) columns built in the past are inadequate to meet current seismic design requirements in terms of both strength and ductility [1]. In addition, harsh environmental conditions can have a significant negative effect on the durability and structural integrity of RC columns, and can produce severe corrosion of embedded steel rebars, which is one of the primary reasons of structural damage for RC columns [2]. Inadequate RC columns are very vulnerable to dynamic loads and their failure can lead to significant damage or even complete collapse of the structural system of which they are part (see Figure 1.1). For example, the 1989 Loma Prieta earthquake in the United States, the 1994 Northridge earthquake in the United States, the 1995 Kobe earthquake in Japan, and the 2008 Wenchuan earthquake in China have caused extremely severe loss of lives and properties [3],[4].

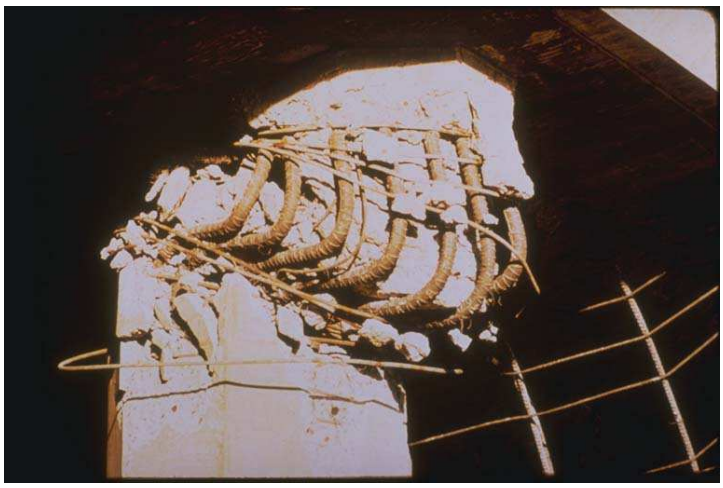

Figure 1.1 - Failure of a spirally-wrapped column during the San Fernando Earthquake, 1971, California (Image credit: NOVV/NGDC, E.V. Leyendecker, U.S. Geological Survey)

The concrete compressive strength and ductility can be significantly increased by providing lateral confinement [5]. Confinement with steel plates has been used to rehabilitate deficient columns for more than four decades [6]. Significant experimental and analytical work has been

performed to understand the behavior of steel-confined RC columns and develop appropriate design provisions for this type of structural retrofit [7],[8]. However, the use of bonded steel plates has several drawbacks, including high cost, possibility of steel corrosion at the steel-concrete interface (which may lead to premature bond failure), and the requirement for specialized heavy equipment at the work site [9].

In the last few decades, structural engineers have been researching substitutes to steel confinement in order to reduce the high costs of repair and maintenance of damaged or inadequate structures. Composite materials, i.e., materials that are formed by the combination of two or more distinct materials at the microscopic scale, have gained widespread use in the retrofit of structural systems. Fiber reinforced polymer (FRP) materials are a relatively new category of composite material manufactured from fibers and resins, which were originally developed in the early 1940's for different type of applications in mechanical and aeronautical engineering [10]. The combination of high-strength high-stiffness structural fibers with low-cost lightweight environmentally-resistant polymers produces composite materials with better mechanical properties and durability than either of the constituents alone. FRP materials can offer designers an excellent combination of properties that can be achieved at a lower cost than with other ordinary structural materials. FRPs can be applied to significantly strengthen (in both flexure and shear) beams, columns, and slabs with only a small increase in structural size and weight. FRP materials do not corrode electrochemically, and have demonstrated excellent durability in harsh environmental conditions [11]. They have high strength-to-weight ratio, and they usually weigh less than one fifth of the weight of steel, with the tensile strength can be as much as eight to ten times as high [12]. The mechanical properties of FRPs make them ideal for extensive applications in construction worldwide.

FRP plates and/or sheets can be bonded to the exterior of concrete structures with high-strength adhesives to provide tensile or confining reinforcement as a supplement provided by internal reinforcing steel. The benefits are twofold: (1) reducing the impact of other degradation processes due to aggressive environmental conditions, and (2) enhancing the strength of concrete due to the confinement of FRP.

Figure 1.2(a) presents a picture of two technicians applying FRP sheets to bridge piers, while Figure 1.2(b) shows a sketch of a RC column confined with external FRP, which is representative of the structural members that are considered in this study.

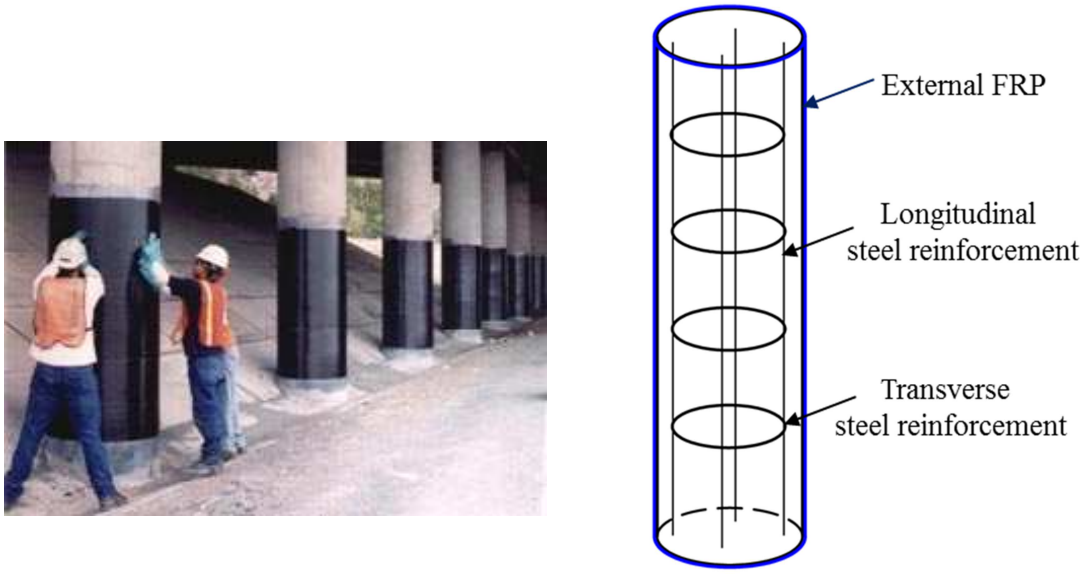

(a) (b)

Figure 1.2 - FRP-confined RC members: (a) bridge piers confined with externally bonded FRP sheets (http://www.luckett-farley.com/frp-strengthening/), and (b) sketch of a RC column confined with external FRP

1.2 RESEARCH MOTIVATIONS

Retrofitting RC members with externally bonded FRP has been widely recognized as an efficient technique to increase the strength, ductility, and durability of these members. Confinement of RC columns with FRP has been widely used, in particular for

retrofit/strengthening of structures located in earthquake-prone regions. The reliable use of FRP plates/sheets for confinement of RC columns requires a proper understanding of and the capability of accurately modeling the stress-strain behavior of FRP-confined concrete. The proper use of this strengthening procedure also requires the analysts to be able to accurately and efficiently predict the improved performance of the FRP-confined columns based on the specific geometry, material properties, and amount of FRP utilized. Thus, numerous numerical tools have been developed to model the structural behavior of FRP-confined columns [14]-[38]. Understanding and modeling the structural behavior of FRP-confined RC columns is still a very active research field, mainly due to the complexity of the problem.

This study focuses on the finite element (FE) modeling of RC columns with circular cross-section confined with externally bonded FRP plates/sheets. The purpose of this study is to properly combine existing modeling tools and develop a new nonlinear frame FE able to model the mechanical behavior of FRP-confined RC columns accurately and efficiently. In addition, this study proposes a mechanics-based material constitutive model able to describe the mechanical behavior of concrete confined simultaneously with transversal reinforcing steel and externally bonded FRP.

1.3 SCOPE

The main part of this research deals with the modeling of response of FRP-confined RC circular columns subjected to concentric monotonic axial load (i.e., increasing axial deformation only) and eccentric axial load (i.e., constant axial load and increasing transversal load). The interaction of confinement effects on the concrete due to transversal reinforcing steel and externally bonded FRP is also studied at the material and structural levels. Modeling of square/rectangular specimens is beyond the scope of this study.

1.4 OBJECTIVES

This research work identifies and achieves the following objectives:

1. Appropriately modifying and implementing existing response-only mechanic-based material constitutive models for concrete confined with FRP in a general-purpose FE program.
2. Developing and validating a new frame FE for nonlinear FE analysis of circular RC columns confined with FRP.
3. Extending the newly developed frame FE in order to directly model the confinement effects due to transversal steel reinforcement and FRP.

The first goal is achieved by implementing the numerical algorithms corresponding to several material constitutive models in FEDEASLab, which is a MATLAB [39] toolbox suitable for linear and nonlinear, static and dynamic structural analysis [40]. FEDEASLab is the primary computational platform for the development of FE models in this study.

The second goal is accomplished by implementing a new force-based frame FE with fiber-section discretization, which uses advanced nonlinear material constitutive models to describe the nonlinear behavior of steel, unconfined concrete, steel-confined concrete, and FRP-confined concrete. A database of experimental results published in the literature, which considers a wide range of different model parameters (e.g., unconfined concrete strength, FRP tensile strength, and FRP modulus) is also developed. This database is used to validate the implemented nonlinear FE models.

The third objective is achieved by developing new numerical algorithms for a concrete material confined at the same time with FRP and steel, and implementing them in FEDEASLab. Another test database is also prepared to validate the newly developed FE model.

1.5 ORGANIZATION OF THE THESIS

This thesis consists of six chapters and five appendices, which present the results of this research and the detailed formulation of the models developed in this study.

The first chapter is an introduction, detailing the background and previous research to model the mechanical behavior of RC columns confined with steel plates and externally bonded FRP. It also gives a brief description of the research motivations, scope, and objectives. Chapter two covers a literature review of previous stress-strain models of FRP-confined concrete and FE modeling of RC columns confined with FRP. Chapter three describes the FE formulation and the material constitutive models used in this study. In chapter four, the newly proposed FE model is validated using two test databases for two different loading conditions (i.e., concentric and eccentric axial loading), which consider a wide range of parameters such as unconfined concrete strength, reinforced steel area, and FRP tensile strength. In chapter five, the newly developed frame FE is extended to model the interaction of the confinement effects due to transversal steel reinforcement and FRP. The same databases are utilized to validate the accuracy of the extended model.

Conclusions and future work are discussed in chapter six, followed by a list of references and the appendices.

2 LITERATURE REVIEW

The proper use of strengthening/retrofit of RC columns with externally bonded FRP requires the accurate prediction of the improved performance of the FRP-confined columns based on the specific geometry, material properties, and amount of FRP utilized. Numerous numerical tools have been developed to model the structural behavior of FRP-confined columns. These tools include (1) stress-strain models of FRP-confined concrete at the material level, (2) stress resultant-section deformation relations at the cross-section level, and (3) FE models of structural components at the structural level. This chapter presents a brief literature review of these three types of numerical tools.

2.1 STRESS-STRAIN MODELS OF FRP-CONFINED CONCRETE

A large number of studies available in the literature have been conducted to develop appropriate stress-strain relations for FRP-confined concrete. These stress-strain models can be classified into two categories: design-oriented models and analysis-oriented models [13]. Design-oriented models (e.g., [14],[16]-[19]) provide closed-form equations directly calibrated on experimental results for predicting the compressive strength, ultimate axial strain and stress-strain behaviors of FRP-confined concrete; whereas analysis-oriented models (e.g., [20]-[23]) derive stress-strain curves that can be used within nonlinear FE models.

Farids and Khalili [14] conducted experimental tests on 46 cylindrical specimens which were encased in four types of glass FRP with the number of FRP layers varying from one to five. It was suggested that both the simple triaxial failure criterion suggested by Richart et al. [15] and a more accurate criterion suggested by Newman and Newman can provide acceptable estimates for ultimate strength of FRP-confined concrete. The failure criteria cited above were employed to quantify the increase in the concrete compressive strength and to obtain an equation to predict

the confined concrete strength by using the maximum confining pressure that the FRP plates/sheets can exert.

Karbhari and Gao [16] obtained a large set of experimental data based on variety of reinforcing fiber types, orientations and jacket thickness. Then, they developed simple design equations able to estimate the response of FRP-confined concrete and verified these equations based on their experimental data. However, the authors stressed the importance of developing a true mechanics-based model of concrete confined with FRP rather than rely on empirical models.

Samaan et al. [17] presented a simple model to predict the complete bilinear stress-strain response of FRP-confined concrete in both axial and lateral directions based on their experimental tests. The experimental test results indicated that the initial softening or yielding occurs at the level of the unconfined strength of concrete and the secondary slope is proportional to the stiffness of the confining jacket in this bilinear response. The model is based on correlation between the dilation rate of concrete and the hoop stiffness of the restraining member. It was shown that this new model can provide an accurate prediction of the failure of FRP-confined concrete.

Toutanji [18] performed experimental and analytical work on the performance of concrete columns externally confined with carbon and glass FRP composite sheets. Different types of unidirectional FRP composites were applied to the cylinder specimens. The confined and unconfined specimens were loaded in uniaxial compression. An analytical model was developed to predict the stress-strain relationship of concrete specimens wrapped with FRP composites sheets. Comparison between the experimental and analytical results indicated that the model provides satisfactory predictions of the stress-strain response.

Xiao and Wu [19] described the axial compression test results of concrete cylinders confined by carbon FRP jackets. The test results indicated that concrete strength and confinement modulus, defined as the ratio of transverse confinement stress and transverse strain, were the most influential factors affecting the stress-strain behavior of confined concrete. Based on the theory of elasticity and the monotonically increasing behavior observed from the experimental tests, and the theory of elasticity, a simple bilinear model was proposed. This new model was shown to compare well with test results from previous studies by other researchers.

Mirmiran and Shahawy [20] developed a novel type of composite column that consisted of a RC core cast in a composite FRP shell. Previous models assumed a constant lateral strain and confining pressure throughout the loading history, which was unsuitable for the proposed composite jackets. Behavior of the proposed column was studied by two analytical tools: a new passive confinement model for externally confined RC columns, and a composite action model that explicitly evaluated the lateral stiffening effect of the jacket. It was shown that the new passive confinement model provided significantly more accurate results than the direct use of Mander's steel-confined concrete model [7].

Spoelstra and Monti [21] proposed a uniaxial concrete model that explicitly accounts for the continuous interaction with the confining device, which can be used for concrete confined with either steel or FRP. The model is suitable to be used in conjunction with fiber-type beam column models for the analysis of FRP-strengthened RC structures. This model relies on an iterative procedure through which the actual stress-strain curve of the FRP-confined concrete is obtained point by point from a family of stress-strain curves at constant confinement pressure (i.e., Mander's curves). At each point the confinement pressure is equal to that induced by the FRP jacket subjected to the corresponding lateral expansion. Through the use of this model, predictive

equations were also derived to determine the ultimate compressive strength and strain of FRP-confined concrete.

Fam and Rizkalla [22] aimed to predict the behavior of axially loaded circular columns confined by FRP tubes. They proposed a new FRP-confined concrete model, which is an extension of the confinement model developed by Mander et al. [7] for concrete confined by steel reinforcement. This model can be used to predict the behavior of prefabricated FRP tubes totally filled or partially filled with concrete, as well as concrete wrapped with FRP sheets. A parametric study was conducted to study the effects of the stiffness of the FRP tubes, axial loading the FRP tube, and presence of an inner hole inside the concrete core. The model was based on equilibrium, compatibility, and the biaxial strength failure criteria of FRP tubes. It was verified through a comparison of numerical predictions and experimental results reported by the authors and other researchers.

Shao et al. [23] tested 24 FRP-confined concrete stub specimens in uniaxial compression under different levels of loading and unloading, with different FRP types, FRP wrap thickness, and loading patterns. A constitutive model that includes cyclic rules of loading and unloading, plastic strains, and stiffness and strength degradations was then developed based on a regression analysis of the tests results. The proposed model was validated by comparing analytical predictions with experimental results obtained from an independent test series.

2.2 STRESS RESULTANT-SECTION DEFORMATION RELATIONS

A few models for sectional analysis of FRP-confined RC columns have been developed in the last decade. For the sectional analysis of FRP-confined RC sections, the classical Bernoulli-Euler theory was adopted under plane assumption. It was assumed that the confining stress was the largest at the extreme compression fiber, decreased with the decreasing distance to the neutral

axis and vanished at the neutral axis location. A similar assumption was employed by many researchers for the sectional analysis of FRP-confined RC sections.

Monti et al. [24] used a fiber-section model which discretized the cross-section of RC members confined with FRP into fibers of unconfined concrete, confined concrete, steel rebar, and FRP jacket. This fiber-section model was employed to determine (through numerical integration) the nonlinear moment-curvature response of the plastic hinge at the base of a pier. The relation between applied force and displacement at the top of the pier was derived by assuming a plastic hinge length measured directly or estimated using equation provided by Priestley et al. [25] and a linear elastic behavior for the remaining portion of the pier.

Yuan et al. [26] presented a two-dimensional sectional analysis of RC columns confined with FRP, in which the bending moment strength was determined through analytical integration of the stresses corresponding to material constitutive models used for design.

2.3 FE MODELS OF STRUCTURAL COMPONENTS

The FE method has been widely used as a powerful tool to effectively model the behavior of FRP-confined RC columns.

Mirmiran et al. [27] developed a nonlinear FE model for the analysis of FRP-confined concrete using a non-associative Drucker-Prager plasticity model. A parametric analysis routine was developed inside the ANSYS software [28] to automatically generate the mesh for various geometric shapes and material properties. The jacket was modeled by linear-elastic membrane shell elements, and the concrete core was modeled by solid elements. The results presented in Mirmiran et al. [27] showed that the Drucker-Prager plasticity can effectively predict the axial stress-strain response of the FRP confined columns.

Parvin and Wang [29] modeled large-scale control (i.e., unretrofitted) and FRP-wrapped RC columns under combined axial and cyclic lateral loadings using the nonlinear FE analysis software MARC^{TM} [30]. The concrete was modeled using three-dimensional eight-node solid brick elements, the steel rebars were modeled as three-dimensional truss elements, and the nonlinear behavior of the confined concrete material was simulated by employing the Mohr-Coulomb yield criterion combined with an isotropic hardening rule. The proposed FE analysis model was validated through the comparisons of numerically simulated and experimental results obtained from scaled specimens. The FE model proposed in the above study was developed to obtain high-resolution simulated response of structural systems as a substitute of significantly more expensive experimental tests of large-scale structural members and systems.

Malvar et al. [31] developed a numerical model for cylinders and prisms confined by different types of FRP in order to study the effects of blast loading on RC structures. The numerical analyses were performed using the research software DYNA3D [32] and closely reproduced the strength enhancements observed in experimental tests for various levels of confinement.

Varma et al. [33] performed uniaxial cyclic and monotonic compression tests on concrete cylinders that were partially and fully wrapped with carbon FRP sheets. A constitutive model for carbon FRP-confined circular RC columns was proposed and implemented in the FE research program FEMIX [34]. The results obtained from the experimental tests were used to calibrate some of the parameters of this model, and to assess the model performance. This model allowed the simulation of RC members by using Timoshenko one-dimensional elements. Good agreement was obtained between numerical simulations and experimental results for both monotonic and cyclic loading tests.

Karabinis et al. [35] proposed a new Drucker-Prager plasticity model for confined concrete and implemented it into ABAQUS [36], which already contained other suitable material models for concrete, steel, and FRP. Steel and concrete were modeled using eight-node solid elements, whereas the FRP jacket was modeled as quadrilateral lamina element with membrane properties. The FE response predictions were in close agreement with test results available in literature.

Yu et al. [37] proposed a modified plastic-damage model within the theoretical framework of the Concrete Damage Plasticity Model (CDPM) for the modeling of confined concrete. The FE models used eight-node solid elements for concrete and four-node shell elements for the FRP jacket in ABAQUS. FE models incorporating the CDPM were developed for concrete in a number of confinement scenarios. Also in this case, the FE response predictions were in close agreement with test results available in literature.

Binici and Mosalam [38] implemented appropriate material constitutive models in the framework of fiber-discretized frame elements using a displacement-based formulation. This computational model employed a variable confinement relation based on a non-uniform confinement distribution in the compression zone.

As shown by this brief literature review, a significant number of previous FE studies employed refined FE meshes of three-dimensional solid elements using commercially available and research software. When a proper numerical model is used, FE models can effectively predict the behavior of the FRP-confined concrete columns. However, the computational cost of similar structural response analyses is usually extremely high, because of the large number of elements and degrees of freedom involved, and the need to use three-dimensional constitutive models for all materials considered in the FE analyses.

3 FINITE ELEMENT MODELING

3.1 FINITE ELEMENT FORMULATION

A two-node one-dimensional frame FE able to model FRP-confined RC columns was developed using a force-based formulation [41],[42] with Euler-Bernoulli kinematic assumptions with small deformations and small displacements (i.e., linear geometry). A fiber-discretization was employed to evaluate the cross-section nonlinear behavior [42]. Figure 3.1 shows the local reference system for a frame FE with the monitored sections discretized into fibers.

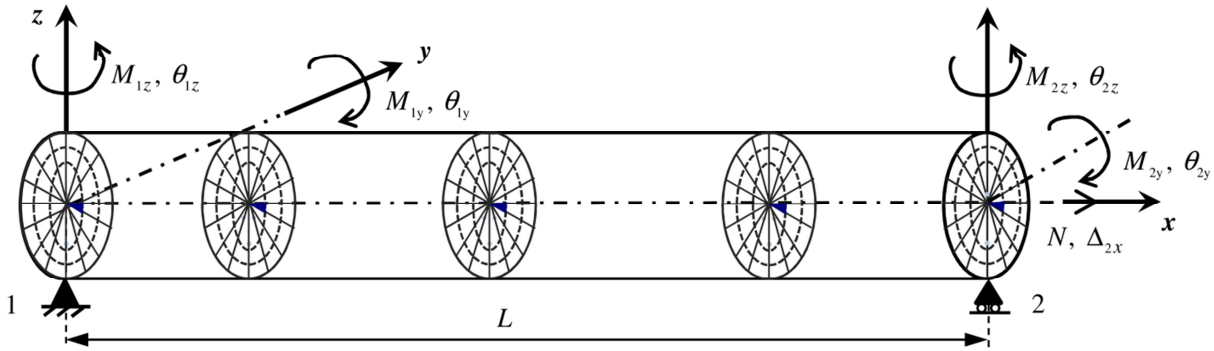

Figure 3.1 - Force-based frame element: local reference system and fiber-discretization of the monitored cross-sections

Realistic one-dimensional nonlinear constitutive models were employed to describe the stress-strain behavior of unconfined, steel-confined, and FRP-confined concrete, as well as reinforcing steel. In this study, the element state determination was based on the non-iterative algorithm proposed by Neuenhofer and Filippou [43], whereas the integrals in the element formulation are evaluated numerically following a Gauss-Lobatto integration scheme with a user-defined number of integration points (i.e., monitored cross-sections). It is noteworthy that other element state determination algorithms (e.g., an iterative algorithm proposed by Spacone et al. [42],[44]) and numerical integration schemes (e.g., Gauss-Legendre integration) can be also used in conjunction with the frame FE element developed in this study.

The force-based formulation for a frame-FE element is based on the following relations [42]

$$\mathbf{D}(x) = \mathbf{b}(x) \cdot \mathbf{Q} \quad : \text{equilibrium (strong form)} \tag{2.1}$$

$$\mathbf{d}(x) = \mathbf{f}(x) \cdot \mathbf{D}(x) \quad : \text{section constitutive law} \tag{2.2}$$

$$\mathbf{q} = \mathbf{F} \cdot \mathbf{Q} \quad : \text{compatibility (weak form)} \tag{2.3}$$

where

$\mathbf{D}(x) = \left\{ N(x) \;\; M_y(x) \;\; M_z(x) \right\}^{\mathrm{T}}$ = cross-section stress resultants;

$\mathbf{Q} = \left\{ N \;\; M_{1y} \;\; M_{1z} \;\; M_{2y} \;\; M_{2z} \right\}^{\mathrm{T}}$ = element end node forces;

$\mathbf{d}(x) = \left\{ \bar{\varepsilon}(x) \;\; \chi_y(x) \;\; \chi_z(x) \right\}^{\mathrm{T}}$ = section deformations;

$\mathbf{q} = \left\{ \Delta_{2x} \;\; \theta_{1y} \;\; \theta_{1z} \;\; \theta_{2y} \;\; \theta_{2z} \right\}^{\mathrm{T}}$ = element end node displacements;

$\mathbf{F} = \int_0^L \mathbf{b}^{\mathrm{T}}(x) \cdot \mathbf{f}(x) \cdot \mathbf{b}(x) \cdot \mathbf{d}(x)$ = element flexibility matrix;

$\mathbf{b}(x)$ = force interpolation function matrix;

$\mathbf{f}(x)$ = cross-section flexibility matrix;

$N(x), M_y(x), M_z(x)$ = axial force along x axis, section bending moment about local y and z axis, respectively.

$\bar{\varepsilon}(x)$, $\chi_y(x)$, $\chi_z(x)$ = section strain along local x axis, section curvature about local y and z axis, respectively.

The generalized section forces and deformations are shown in Figure 3.2.

The outstanding features of the proposed frame FE include computational efficiency, accuracy, and ease of use. The computational efficiency of the proposed frame element derives from the use of (1) the force-based formulation, which for frame elements imposes exactly

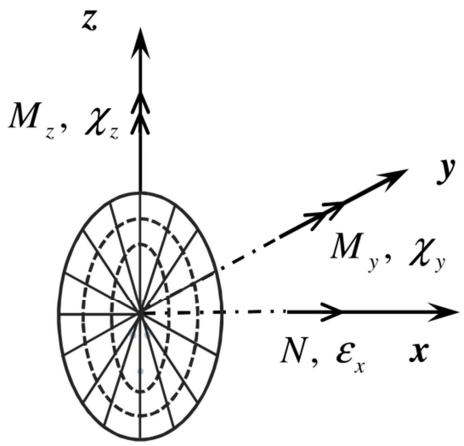

Figure 3.2 - Generalized section forces and deformations

equilibrium and reduces the number of elements needed for an appropriate mesh of the FE model compared to a displacement-based formulation [41]-[43], and (2) the cross-section fiber-discretization that allows the structural analyst to use one-dimensional material constitutive models only, which are computationally less demanding than their three-dimensional counterparts [45],[46]. The accuracy of the proposed frame FE element derives from the capability of the fiber-section models to closely represent the nonlinear interaction between axial forces and bending moments at the cross-section level, and the high fidelity of the uni-dimensional material constitutive models in describing the actual stress-strain relations for the different materials used in FRP-confined RC columns. The ease of use of the proposed frame FE is due to the fact that FE models built by using force-based frame elements are virtually mesh-independent, in the sense that the same mesh discretization can be used for linear and nonlinear FE analysis without loss of accuracy.

3.2 COMPUTATION OF CROSS-SECTION STRESS RESULTANTS

In the proposed FE, the cross-section stress resultants (axial force and bending moment) are computed using a fiber-discretization of the cross-section [24], as shown in Figure 3.3. The concrete fibers are defined through a radial discretization (defined by parameters R_i = internal radius, R_e = external radius, R_c = confined radius, n_{r1} = number of steel-confined radial layers, and n_{r2} = number of unconfined radial layers) and an angular discretization (defined by θ_i = initial angle, θ_e = end angle, and n_a = number of angular subdivision) of the cross-section. In addition, each reinforcing steel rebar corresponds to an additional fiber, which is described by the parameters A_{b_i} = area of the *i*-th steel rebar, θ_{b_i} = angle for the *i*-th steel rebar and R_{b_i} = radius at which the *i*-th steel rebar is located (with i = 1, 2, ..., n_b, n_b = number of reinforcing steel bars). The nonlinear stress-strain response of each discretization fiber is described by appropriate one-dimensional nonlinear material constitutive models.

The cross-section stress resultants, $\mathbf{D}(x)$, are computed as follows

$$\mathbf{D}(x) = \begin{Bmatrix} N \\ M_y \\ M_z \end{Bmatrix} = \begin{Bmatrix} \sum_{j=1}^{j_{total}} \sigma_j A_j \\ \sum_{j=1}^{j_{total}} \sigma_j A_j z_j \\ \sum_{j=1}^{j_{total}} \sigma_j A_j y_j \end{Bmatrix} \tag{2.4}$$

where σ_j = axial stress at the *j*-th fiber; A_j = area of the *j*-th fiber; z_j = distance between the center of the *j*-th fiber and the *y* axis; y_j = distance between the center of the *j*-th fiber and the *z* axis; and j_{total} = total number of fibers, given by $(n_{r1} + n_{r2}) \cdot n_a$.

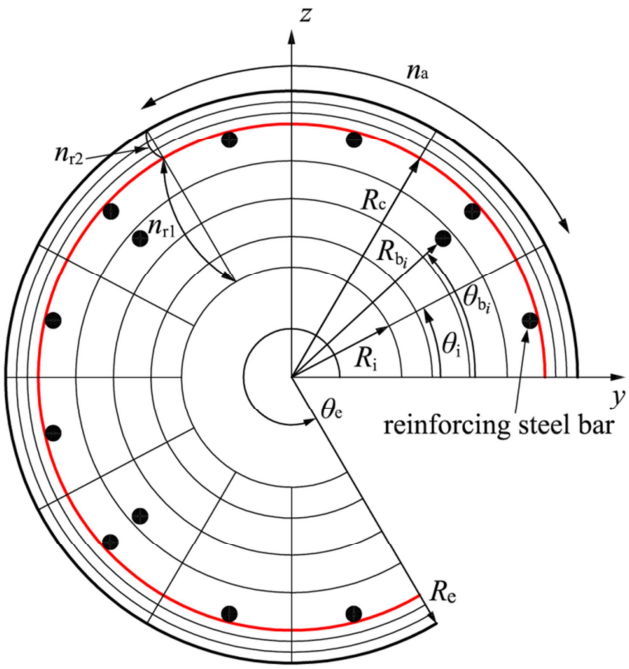

Figure 3.3 - Fiber-discretization of the cross-section

3.3 MATERIAL CONSTITUTIVE MODELS

3.3.1 Menegotto-Pinto steel model

Numerous researchers have proposed models to characterize the response of reinforcing steel used in RC structures [47],[48]. In this study, the constitutive behavior of the steel reinforcement is modeled using the Menegotto-Pinto constitutive model [49], as extended by Filippou et al. [50] to account for isotropic strain hardening. The Menegotto-Pinto one-dimensional plasticity model is a computationally efficient smooth inelastic model typically used for structural steel, which showed very good agreement with experimental results. The model states explicitly the current stress as a function of the current strain, thus it is computationally more efficient compared with other models such as the Ramberg-Osgood model [51]. In addition, the Menegotto-Pinto model can accommodate modifications to account for local buckling of steel bars in RC members [52], and can be used for macroscopic modeling of hysteretic behavior of structures or substructures with an appropriate choice of the modeling parameters. It is also noteworthy that the Menegotto-

Pinto model is a physically motivated model of structural material hysteresis, whose performance in representing structural physical behavior is not undermined by mathematical features that can lead to non-physical analysis results.

The response of reinforcing steel is defined by the following non-linear equation:

$$\sigma^* = b \cdot \varepsilon^* + \frac{(1-b) \cdot \varepsilon^*}{(1+\varepsilon^{*R})^{1/R}} \tag{2.5}$$

$$\varepsilon^* = \frac{\varepsilon - \varepsilon_r}{\varepsilon_y - \varepsilon_r} \tag{2.6}$$

$$\sigma^* = \frac{\sigma - \sigma_r}{\sigma_y - \sigma_r} \tag{2.7}$$

Equation (3.5) represents a smooth curved transition from an asymptotic straight line with initial stiffness E_0 to another asymptotic straight line with to final tangent stiffness E_1, where $b = E_1 / E_0$ denotes the hardening ratio; the effective strain and stress (ε^*, σ^*) are functions of the unload/reload interval; R is a parameter that defines the curvature of the transition curve between the two asymptotes; ε_y and σ_y are the coordinates in the strain-stress plane of the intersection point of the two asymptotes; ε_r and σ_r (initially set to zero) are the coordinates in the strain-stress plane of the point where the last strain reversal event took place; and ε and σ are the current strain and stress, respectively. The model is completed by the updating rules for the history parameters at each strain reversal event. For example, the updating rule for the history parameter *R* is given by

$$R = R_0 - \frac{a_1 \cdot \xi}{a_2 + \xi} \tag{2.8}$$

where R_0 is the value of the parameter R during the first loading; a_1 and a_2 are experimentally determined material dependent parameters; ξ is the ratio of the maximum plastic strain $\varepsilon^p_{\max} = \max_{\varepsilon} \left| \varepsilon_{\max} - \varepsilon_y \right|$ over the initial yield strain ε_{y0}.

To account for the isotropic cyclic strain hardening, Filippou et al. [50] proposed a stress shift σ_{sh} in the linear yield asymptote depending on the maximum plastic strain as

$$\frac{\sigma_{sh}}{\sigma_{y0}} = a_3 \cdot \left(\frac{\varepsilon_{max}}{\varepsilon_{y0}} - a_4 \right) \tag{2.9}$$

in which a_3 and a_4 are experimentally determined parameters; $\varepsilon_{\max}$ is the absolute maximum total strain at the instant of strain reversal and σ_{yo} is the initial yield stress. The equations that are needed to update all history dependent parameters from load/time step *n* to the next load/time step *n*+1 can be found in [53].

A typical cyclic stress-strain response behavior is shown in Figure 3.4.

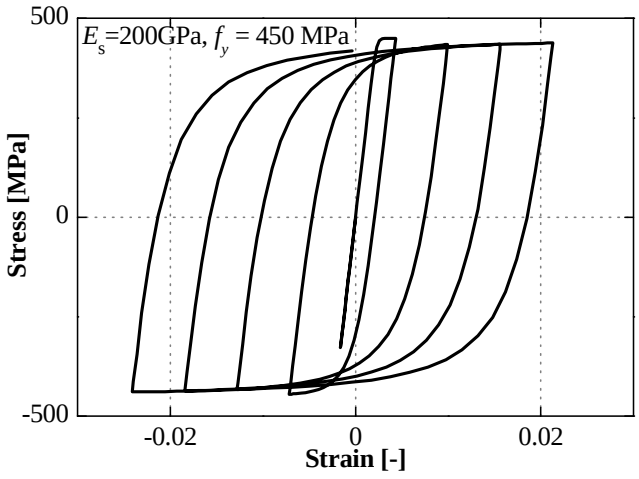

Figure 3.4 - Menegotto-Pinto material constitutive model for structural steel: typical cyclic stress-strain response

3.3.2 Popovics-Saenz unconfined concrete model

The selected constitutive law for the concrete material is a uniaxial cyclic law with a monotonic envelope given by the Popovics-Saenz law [54]-[56], which is defined by the following single equation for the compressive stress-strain response:

$$\sigma = f_c \cdot \frac{K \cdot \eta}{1 + A \cdot \eta + B \cdot \eta^2 + C \cdot \eta^3 + D \cdot \eta^r} \tag{2.10}$$

where $\eta = \varepsilon / \varepsilon_c$, $K = E_c \cdot \varepsilon_c / f_c$, $K_\varepsilon = \varepsilon_h / \varepsilon_c$, $K_\sigma = f_c / f_h$, $r = K \cdot (K - 1)$, E_c = initial modulus of elasticity, ε_c and f_c = strain and stress at the compressive peak, respectively; ε_h and f_h = strain and stress at the inflection point on the descending branch of the monotonic envelope

If $\eta < 1$ (Popovics curve): $A = B = C = 0$, $D = K - 1$.

If $\eta \geq 1$ (Saenz curve): $A = C + K - 2$, $B = 1 - 2C$, $C = K \cdot \frac{(K_\sigma - 1)}{(K_\varepsilon - 1)^2} - \frac{1}{K_\varepsilon}$, $D = 0$.

The tension stress-strain response is described by the same equations used for the compression behavior, with the same initial stiffness and appropriate (scaled down) values for the other parameters.

The cyclic behavior is modeled assuming linear unloading and reloading between the monotonic envelope and the zero stress line. The linear branches are described by:

$$\sigma = E_{ur} \cdot (\varepsilon - \varepsilon_p) \tag{2.11}$$

where E_{ur} is the unloading stiffness and ε_p is the residual strain (intersection of the unloading branch with the strain axis). When unloading occurs before the strength peak, then the linear path is defined by a stiffness equal to that at zero strain, i.e., $E_{ur} = E_c$, and the residual strain is

$\varepsilon_p = \varepsilon_r - \sigma_r / E_c$, where ε_r and σ_r are the coordinates of the point of unloading from the monotonic envelope. When unloading occurs after the strength peak, then the linear branch connects the point of unloading from the monotonic envelope to the point which is the intersection between the strain axis and the unloading branch with stiffness E_c from the strength peak point with coordinates ε_c and f_c. In this case, $E_{ur} = \sigma_r / (\varepsilon_r - \varepsilon_p)$, with $\varepsilon_p = \varepsilon_c - f_c / E_c$ and the unloading/reloading stiffness degrades progressively. When the unloading linear branches reach the strain axis, the strain unloading continues on the strain axis (zero stress) until positive strains are reached (i.e., tension, with response depending on the specific tension behavior adopted). Stress paths along the monotonic envelope can be used only once; reloading always occurs along the linear paths; thus the monotonic envelope is reached only when the absolute value of the largest deformation previously attained is surpassed. A typical cyclic stress-strain response in compression of the concrete material model employed in this study is shown in Figure 3.5.

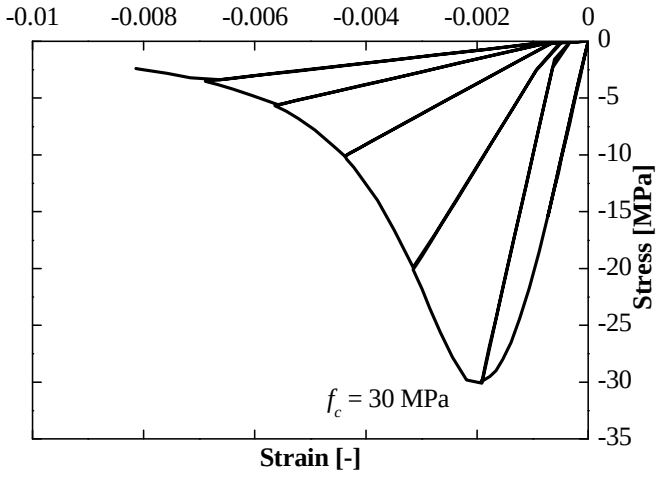

Figure 3.5 - Hysteretic Popovics-Saenz concrete material model: typical cyclic stress-strain response in compression

3.3.3 Mander steel-confined concrete model

Mander et al. [7] proposed a stress-strain model for steel-confined concrete subjected to uniaxial compressive loading, which is based on the axial compressive tests of concrete with a quasi-static strain rate and monotonic loading. A typical monotonic response of the constitutive material model compared with the Popovics-Saenz unconfined concrete model is shown in Figure 3.6.

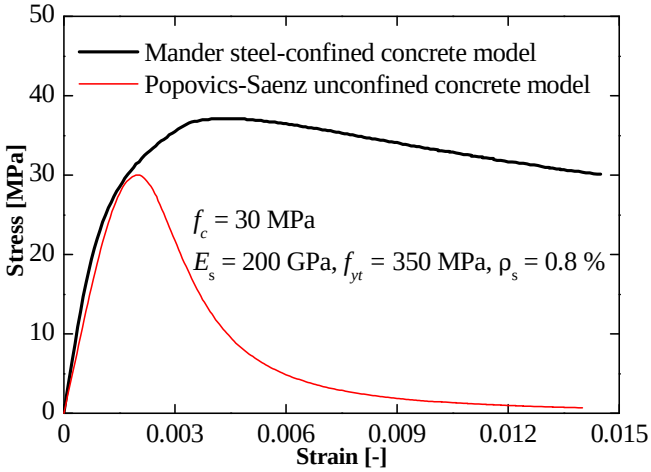

Figure 3.6 - Comparison of stress-strain relation under monotonic loading of unconfined and steel-confined concrete

The stress-strain model proposed by Mander et al. [7] is based on the equations suggested by Popovics [57], i.e.,

$$\sigma = \frac{f_{cc} \cdot x \cdot r}{r - 1 + x^r} \tag{2.12}$$

where

f_{cc} = peak strength of confined concrete

$$x = \frac{\varepsilon}{\varepsilon_{cc}} \tag{2.13}$$

$$r = \frac{E_c}{E_c - E_{\text{sec}}} \tag{2.14}$$

ε = longitudinal compressive concrete strain

ε_{cc} = compressive strain at confined peak strength f_{cc}

$$\varepsilon_{cc} = \varepsilon_c \cdot \left[1 + 5 \cdot \left(\frac{f_{cc}}{f_c} - 1\right)\right] \tag{2.15}$$

E_c = tangent modulus of elasticity of the concrete, given by $5000\sqrt{f_c}$ MPa

E_{sec} = secant modulus of confined concrete at peak stress, equal to $\frac{f_{cc}}{\varepsilon_{cc}}$

f_c and ε_c = the unconfined concrete strength and corresponding strain, respectively.

The confined peak strength f_{cc} is expressed in terms of a constant effective confining pressure f_l as follows:

$$f_{cc} = f_c \cdot \left(2.254 \cdot \sqrt{1 + 7.94 \cdot \frac{f_l}{f_c}} - 2 \cdot \frac{f_l}{f_c} - 1.254\right) \tag{2.16}$$

The effective confining pressure is a function of the transverse steel volumetric ratio ρ_s and its yield stress f_{yt}, and is given by:

$$f_l = 0.5 \cdot k_e \cdot \rho_s \cdot f_{yt} \tag{2.17}$$

where

$\rho_s = \frac{4 \cdot A_{\text{st}}}{s \cdot d_c}$

A_{st} = cross-section area of a transverse reinforcing bar

s = clear distance between adjacent hoops or spiral turns

d_c = diameter of the hoop or spiral

k_e = confinement effectiveness coefficient, given by

$$k_e = \frac{\left(1 - \frac{s}{2 \cdot d_c}\right)^2}{1 - \rho_{cc}} \quad \text{(for circular hoops)} \tag{2.18}$$

$$k_e = \frac{1 - \frac{s}{2 \cdot d_c}}{1 - \rho_{cc}} \quad \text{(for circular spirals)} \tag{2.19}$$

ρ_{cc} = ratio of volume of longitudinal reinforcement to volume of concrete core

The ultimate strain is defined as the strain at first hoop/spiral fracture and is calculated from an energy balance approach.

3.3.4 Spoelstra and Monti FRP-confined concrete model

Spoelstra and Monti [21] proposed an incremental iterative numerical model (referred to as SM model hereinafter) for concrete confined with FRP as well as with steel jackets or conventional transverse reinforcement. The model proposed by Pantazopoulou and Mills [58] for unconfined concrete under uniaxial load was adopted and extended to model the dilation behavior of confined concrete:

$$\varepsilon_f(\varepsilon, f_l) = \frac{E_c \cdot \varepsilon - \sigma(\varepsilon, f_l)}{2 \cdot \beta \cdot \sigma(\varepsilon, f_l)} \tag{2.20}$$

where

β = constant depending on the concrete properties and approximated to be a function of unconfined concrete strength as follow

$$\beta = \frac{E_c}{|f_c|} - \frac{1}{|\varepsilon_c|} \tag{2.21}$$

$\sigma(\varepsilon, f_l)$ = confined concrete stress at axial strain equal to ε and with lateral confining stress equal to f_l.

For the case of axially loaded concrete columns, the strain in the confining jacket ε_f can be identified equal to ε_l. Thus the corresponding confining pressure f_l can be evaluated as:

$$f_l = 0.5 \cdot \rho_f \cdot \sigma_f \tag{2.22}$$

where

$\rho_f = \frac{4 \cdot t_f}{D}$

E_f = elastic modulus of the composite material of the jacket

t_f = thickness of the jacket

D = diameter of the jacket

$$\sigma_f = \begin{cases} E_f \cdot \varepsilon_l & \text{for} \quad \max(\varepsilon_l) < f_{fu}/E_f \\ 0 & \text{for} \quad \max(\varepsilon_l) \geq f_{fu}/E_f \end{cases} \tag{2.23}$$

The peak strain ε_{cc} and confined concrete strength f_{cc} were determined using Equation (3.15) and (3.16), respectively. The Popovics model was applied to find the stress-strain response of concrete for each f_l using Equation (3.12) through (3.14). The iterative incremental procedure is shown in Figure 3.7.

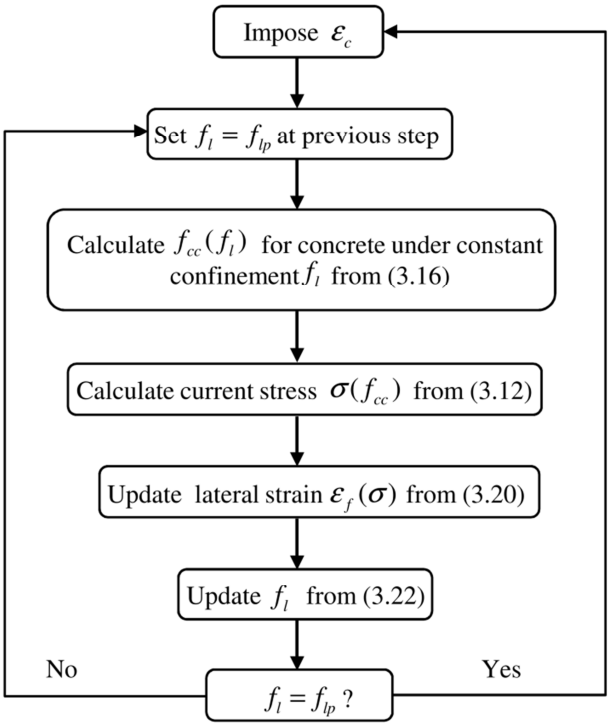

Figure 3.7 - Iterative procedure for the SM model

3.3.5 Shao, Zhu, and Mirmiran FRP-confined model

Shao et al. [23] developed a constitutive model for FRP-confined concrete (referred to as SZM model hereinafter) including cyclic rules for loading and unloading, plastic strains, and stiffness/strength degradations. Numerical techniques were employed to eliminate discontinuities or non-smoothness without reducing the prediction capabilities of the model.

The constitutive model of Samaan et al. [17] for monotonic loading was used as the envelope curve for cyclic loading. The entire stress-strain ($\sigma - \varepsilon$) response is defined as:

$$\sigma = \frac{(E_1 - E_2)\cdot\varepsilon}{\left[1+\left(\frac{(E_1 - E_2)\cdot\varepsilon}{f_0}\right)^n\right]^{1/n}} + E_2\cdot\varepsilon \qquad (2.24)$$

where E_1 and E_2 = first and second slope of the response, respectively, given by

$$E_1 = 3950 \cdot \sqrt{f_c} \quad \text{MPa} \tag{2.25}$$

$$E_2 = 245.61 \cdot f_c^{0.2} + 1.3456 \cdot \frac{E_f \cdot t_f}{D} \quad \text{MPa} \tag{2.26}$$

f_0 = the Y-intercept of the second slope, given by

$$f_0 = 0.872 \cdot f_c + 0.371 \cdot f_l + 6.258 \quad \text{MPa} \tag{2.27}$$

where

f_l = the confining pressure from FRP, calculated as $f_l = \frac{2 \cdot E_f \cdot \varepsilon_f \cdot t_f}{D}$

n = the curve shape parameter for the transition zone, selected as 1.5.

The ultimate strength of FRP-confined concrete is given by

$$f_{cu}^{'} = f_c + 6.0 \cdot f_l^{0.7} \quad \text{MPa} \tag{2.28}$$

Finally, the ultimate strain of FRP-confined concrete can be calculated as

$$\varepsilon_{cu} = \frac{f_{cu}^{'} - f_0}{E_2} \tag{2.29}$$

The SZM model is completed by appropriate unloading/reloading rules for cyclic behavior, which are described in detail in Shao [86].

Figure 3.8 compares the monotonic stress-strain relations of the SM model and the SZM model for the same concrete material with the same FRP confinement.

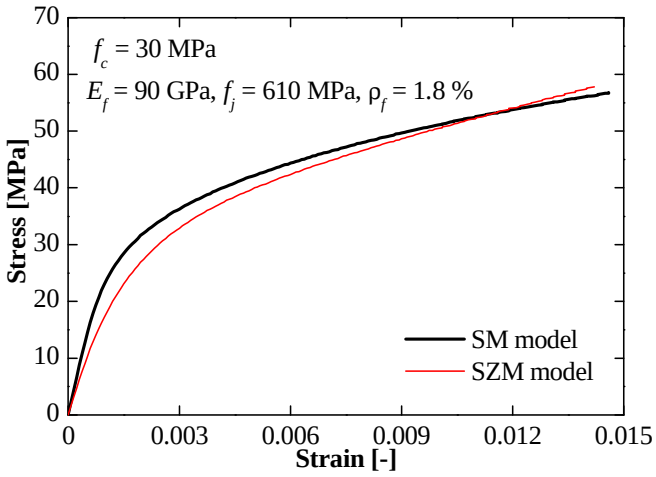

Figure 3.8 - Stress-strain relation for monotonic loading of the SM model and the SZM model

3.4 COMPUTER IMPLEMENTATION

The proposed frame FE for nonlinear FE response analysis of RC columns confined with externally bonded FRP was implemented in FEDEASLab. FEDEASLab contains several different options for load and time stepping schemes, as well as for iterative schemes for the solution of systems of nonlinear equations. By taking advantage of the modularity of FEDEASLab, the existing element, section and material libraries were extended (i.e., 6-degrees-of-freedom force-based RC column element confined with FRP, circular fiber-discretized cross-section with FRP confinement, SM and SZM constitutive models for FRP-confined concrete) to enable accurate modeling and response simulation of RC columns confined with externally bonded FRP. These FE libraries can be easily updated and/or extended to reflect the state-of-the-art in modeling such structures.

4 CORRELATION BETWEEN NUMERICAL SIMULATIONS AND EXPERIMENTAL RESULTS

The proposed FE is validated through a detailed comparison of experimentally recorded and numerically simulated response results corresponding to a significant number of FRP-retrofitted circular RC columns with a static scheme corresponding to a cantilever structure. The FRP-retrofitted columns considered in this study are subjected to two different quasi-static loading conditions that are referred to as (1) concentric axial loading, which corresponds to the application of a monotonically increasing axial deformation; and (2) eccentric axial loading, which corresponds to the application of a monotonically increasing transversal deformation at the free end of the cantilever under a constant axial load (see Figure 4.1).

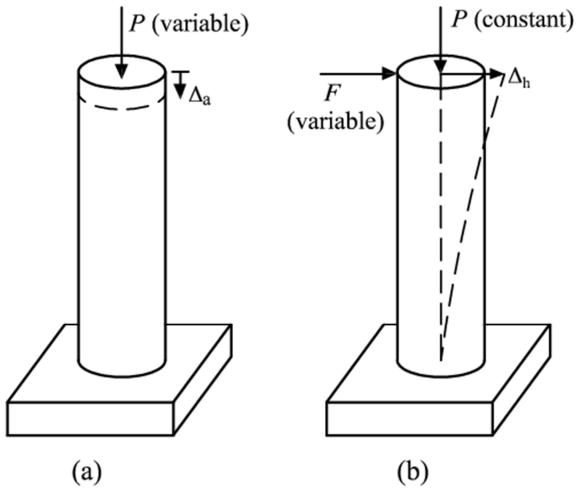

Figure 4.1 - Experimental loading conditions:
(a) concentric axial loading, and (b) eccentric axial loading

A careful literature review is completed in order to collect the experimental data used in this study. The selected response experimental data were complemented in the original reference papers, by a description of the column specimens' geometry and material properties, which was sufficiently detailed to build the corresponding FE model. The description of the selected experimental column specimens, as well as the references from which the data were taken, is

provided in Table 1 for the columns subjected to concentric axial loading and in Table 4 for the columns subjected to eccentric axial loading. For the concentric axial loading case, this study considered a set of 41 RC columns, of which nine were control specimens (without FRP retrofit) and 32 were RC columns confined using externally-bonded FRP. For the eccentric axial loading case, this study considered a set of 23 RC columns, of which six were control specimens (without FRP retrofit) and 17 were RC columns confined using externally bonded FRP. All FE analyses performed in this study are quasi-static nonlinear analyses based on an incremental displacement-controlled technique and the Newton-Raphson iterative procedure [59].

4.1 FINITE ELEMENT MODEL CONVERGENCE STUDY

A convergence analysis study was performed to determine an appropriate FE mesh and cross-section discretization to be used in the comparison between experimental and numerical results. This convergence analysis study considered the following ranges of modeling parameters: (1) n_{FE} = 1, 2, 3 (where n_{FE} denotes the number of FEs); (2) n_{GL} = 3, 5, 10 (where n_{GL} denotes the number of G-L integration points); (3) n_r = 20, 40; and (4) n_a = 20, 40. The computational cost of each FE analysis increases proportionally to the increasing resolution of the FE mesh and cross-section discretization. Thus, it is useful to find the FE mesh and cross-section discretization with smallest resolution for which the FE response results are converged.

The results of the convergence analysis are reported here for the column specimen denoted ST3NT in Sheikh and Yau [60]. The ST3NT specimen consisted of a column with diameter d = 356 mm and a shear span length L = 1,470 mm, cast integrally with a 510×760×810 mm stub. The layout of the specimen is shown in Figure 4.2 and the other geometric and material properties for the specimen are given in Table 4.1. The column was tested under eccentric axial loading.

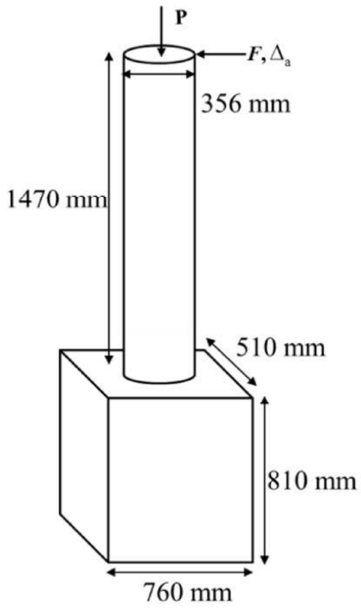

Figure 4.2 - Layout of the test specimen ST3NT

Figure 4.3 provides the moment-curvature response results computed at the fixed end section using FE models with different meshes and cross-section discretizations. The inset of Figure 4.3 shows a zoom view of the moment-curvature curve, which highlights that response convergence is practically obtained for the FE model with one FE, 5 G-L integration points, 20 radial layers, and 20 angular subdivisions.

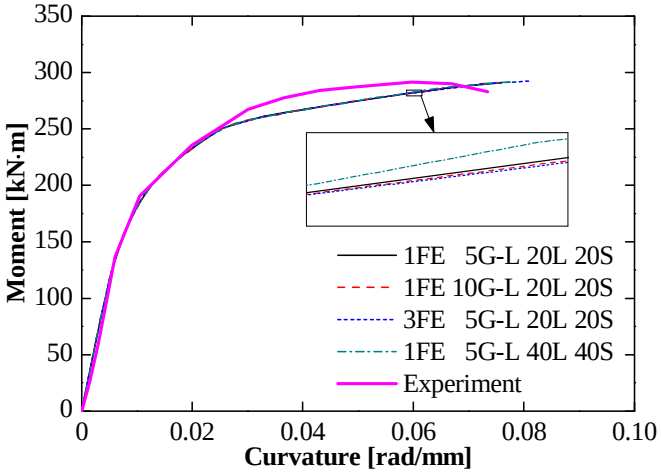

Figure 4.3 - Convergence analysis results for the test specimen ST3NT: moment-curvature response at the fixed end

This convergence analysis was repeated for several specimens with and without FRP retrofit, subjected to both concentric and eccentric axial loading. In all cases considered, the FE response was already practically converged using n_{FE} = 1, n_{GL} = 5, n_r = 20, and n_a = 20. Thus, in the remainder of this study, for all specimens with constant cross-section properties along their length, a FE model with a single FE mesh and five G-L integration points was adopted. For specimens with variable cross-section properties, each portion with constant cross-section properties was modeled using one FE and five G-L points. All cross-sections were discretized using 20 radial layers and 20 angular subdivisions.

4.2 Prediction of Ultimate Load-carrying Capacity and Strain at Peak Strength for Columns Subjected to Concentric Axial Loading

In this part, the performance of the newly developed frame FE is evaluated through a comparison between the experimentally measured and the numerically predicted axial load-carrying capacity and strain at peak strength of the columns included in the experimental database and subjected to concentric axial loading (see Table 4.1). The geometric properties of the specimens and mechanical properties of the used materials are taken from the experimental information provided in the literature [61]-[69].

The considered database contains specimens with a wide range of heights *L* (from 320 mm to 2000 mm), cross-section diameters *d* (from 150 mm to 508 mm), unconfined compressive strength of concrete f_c (from 25.5 MPa to 61.81 MPa), longitudinal steel reinforcement area $A_s = n_b \cdot A_b$ (from 168 mm^2 to 3,040 mm^2) and yield strength f_y (from 391 MPa to 620 MPa). The experimental database used in this comparison considers also a wide variety of FRP reinforcement configurations, with three materials (carbon FRP, glass FRP and hybrid FRP),

elastic modulus in the hoop direction E_f, varying in the range from 19.1 GPa to 241 GPa, and tensile strength in the hoop direction f_{fu}, varying in the range from 330 MPa to 3,937 MPa.

Table 4.2 presents the comparison between experimental results and numerical simulations of the load-carrying capacity and strain at peak strength for the reference RC columns (i.e., for the RC columns without FRP retrofit) subjected to concentric axial loading. The accuracy of the numerical model is investigated by using the ratio of the numerically simulated and experimentally measured load-carrying capacity, $R = P_{\text{FE}} / P_{\text{exp}}$ (where P_{FE} and P_{exp} = maximum axial load numerically predicted and experimentally measured, respectively), and strain at peak strength, $S = \varepsilon_{\text{FE}} / \varepsilon_{\text{exp}}$ (where ε_{FE} and ε_{exp} = axial strain at peak strength numerically predicted and experimentally measured, respectively). The agreement in terms of load-carrying capacity between experimental results and numerical simulations is excellent, with $\mu_R = 1.05$ (where μ_R = mean value of R) and $COV_R = 0.06$ (where COV_R = coefficient of variation of R). The agreement in terms of axial strain at peak strength between experimental results and numerical simulations is also very good, with $\mu_S = 0.94$ (where μ_S = mean value of S) and $COV_S = 0.08$ (where COV_S = coefficient of variation of S). These results are consistent with similar results reported in the existing literature [70]-[72].

Table 4.3 compares the experimentally measured and numerically simulated values of the load-carrying capacities and strain at peak strength of the selected FRP-confined RC columns under concentric axial loading. The numerical simulations were performed for both SM and SZM models. In this case, the statistics of both R and S (i.e., mean, standard deviation, coefficient of variation, and minimum and maximum values) are provided for both models.

Table 4.1 - Experimental test database for RC columns subjected to concentric axial loading: specimens' identification, geometry, and material properties

Ref.	ID	d (mm)	L (mm)	f_c (MPa)	n_b (-)	A_b (mm^2)	f_y (MPa)	FRP Type	t_f (mm)	E_f (GPa)	f_{fu} (MPa)
[61]	C01-L0-20	356	1524	29.8	6	300	402	CFRP	1	41.2	885
	C02-L0-26	356	1524	29.8	6	300	402	CFRP	2	41.2	885
[62]	00-LS320-3	356	1524	29.8	6	300	402	-	-	-	-
	G01-L0-9	356	1524	29.8	6	300	402	GFRP	1	22.6	535
	G02-L0-13	356	1524	29.8	6	300	402	GFRP	2	22.6	535
[63]	C1	508	1830	26.2	8	380	450	-	-	-	-
	C2	508	1830	26.2	8	380	450	GFRP	3	19.1	330
	C3	508	1830	26.2	8	380	450	GFRP	3	21.6	383
	C4	508	1830	26.2	8	380	450	CFRP	3	38.1	580
[64]	C10	150	750	37.7	6	28	400	CFRP	0.167	210	3371
	C15	150	750	37.7	6	28	400	CFRP	0.167	210	3371
	C19	150	750	37.7	6	28	400	CFRP	0.167	210	3371
[65]	DB450-C	200	914	25.5	8	78	393	CFRP	0.270	125.6	1689
[66]	K1	400	2000	31.8	10	113	620	-	-	-	-
	K2	400	2000	34.3	10	113	620	CFRP	0.585	198	2600
	K3	400	2000	34.3	10	113	620	CFRP	0.94	480	1100
	K4	400	2000	39.3	10	113	620	GFRP	1.8	60	780
	K5	400	2000	39.3	10	113	620	GFRP	0.6	60	780
	K8	400	2000	34.3	10	113	620	HFRP	0.492	120	1100
[67]	A5NP2C	303	1200	29.4	6	201	423	CFRP	0.762	78	1050
	C4NP0C	303	1200	31.7	6	201	423	-	-	-	-
	C4NP2C	303	1200	31.7	6	201	423	CFRP	0.762	78	1050
	C4NP4C	303	1200	31.7	6	201	423	CFRP	1.524	78	1050
	B4NP2C	303	1200	31.7	6	201	550	CFRP	0.762	78	1050
	C4MP0C	303	1200	50.8	6	201	423	-	-	-	-
	C4MP2C	303	1200	50.8	6	201	423	CFRP	0.762	78	1050
[68]	I.RCC.0L	160	320	25.93	4	113	500	-	-	-	-
	I.RCC.1L	160	320	25.93	4	113	500	CFRP	1	34	450
	I.RCC.3L	160	320	25.93	4	113	500	CFRP	3	34	450
	II.RCC.0L	160	320	49.46	4	113	500	-	-	-	-
	II.RCC.1L	160	320	49.46	4	113	500	CFRP	1	34	450
	II.RCC.3L	160	320	49.46	4	113	500	CFRP	3	34	450
	III.RCC.0L	160	320	61.81	4	113	500	-	-	-	-
	III.RCC.1L	160	320	61.81	4	113	500	CFRP	1	34	450
	III.RCC.3L	160	320	61.81	4	113	500	CFRP	3	34	450
[69]	C10	150	750	38	6	28	391	CFRP	0.334	226	3339
	C30	250	750	35.2	6	113	458	-	-	-	-
	C41	250	750	35.2	6	113	458	CFRP	0.176	241	3937
	C34	250	750	35.2	6	113	458	CFRP	0.352	241	3937
	C43	250	750	35.2	6	113	458	CFRP	0.528	241	3937
	C44	250	750	35.2	6	113	458	CFRP	0.704	241	3937

These statistics show that both models provide very good results in terms of load-carrying capacity, with the SZM model ($\mu_{R_{SZM}} = 0.98$ and $\sigma_{R_{SZM}} = 0.08$) providing results that are slightly better than the SM model ($\mu_{R_{SM}} = 1.06$ and $\sigma_{R_{SM}} = 0.10$). The FE analyses performed using both material constitutive models overestimate the experimentally measured strains at peak strength, with the SM model ($\mu_{S_{SM}} = 1.22$ and $\sigma_{S_{SM}} = 0.29$) performing better than the SZM model ($\mu_{S_{SZM}} = 1.64$ and $\sigma_{S_{SZM}} = 0.53$).

Table 4.2 - Comparison between experimental results and numerical simulations for reference RC columns subjected to concentric axial loading: axial load-carrying capacity and strain at peak strength

Ref.	ID	Maximum axial load (kN)			Axial strain at peak strength (mm/m)		
		Exp.	FE	R	Exp.	FE	S
[62]	00-LS320-3	3130	3709	1.18	2.38	2.36	0.99
[63]	C1	6648	6618	0.99	2.6	2.21	0.85
[66]	K1	4685	4705	1.00	2.8	2.8	1.00
[67]	C4NP0C	2930	2845	0.97	2.2	2.29	1.04
	C4MP0C	3917	4205	1.07	3.1	2.63	0.85
[68]	I.RCC.0L	594	624	1.05	3.77	3.87	1.03
	II.RCC.0L	1171	1210	1.03	3.02	2.53	0.84
	III.RCC.0L	1267	1341	1.06	2.69	2.53	0.94
[69]	C30	1917	2058	1.07	2.7	2.53	0.94
			Mean	St. Dev.	COV	Min.	Max.
Max. axial load			1.05	0.06	0.06	0.97	1.18
Axial strain at peak strength			0.94	0.08	0.08	0.84	1.04

Figure 4.4 and Figure 4.5 graphically reproduce the results relative to the load-carrying capacity and strain at peak strength, respectively, provided in Table 4.2 and Table 4.3. These two figures have the experimental results on the vertical axis and the FE results on the horizontal axis. The dashed line on the main diagonal corresponds to perfect agreement between experimental values and numerical simulations, i.e., R = 1.00 and S = 1.00 for Figure 4.4 and 4.5, respectively.

Table 4.3 - Comparison between experimental results and numerical simulations for FRP-confined RC columns subjected to concentric axial loading: axial load-carrying capacity and strain at peak strength

Ref.	ID	Maximum axial load (kN)					Axial strain at peak strength (mm/m)				
		Exp.	SM	R_{SM}	SZM	R_{SZM}	Exp.	SM	S_{SM}	SZM	S_{SZM}
[61]	C01-L0-20	4370	5202	1.19	4911	1.12	8.90	19.16	2.15	22.05	2.48
	C02-L0-26	5903	6905	1.17	6070	1.03	17.30	25.72	1.49	29.86	1.73
[62]	G01-L0-9	3895	4439	1.14	4570	1.17	7.39	10.83	1.46	17.50	2.37
	G02-L0-13	5500	6091	1.11	5784	1.05	12.51	21.32	1.70	24.93	1.99
[63]	C2	7479	7114	0.95	7797	1.04	8.80	7.65	0.87	7.27	0.83
	C3	7884	7139	0.91	8025	1.02	9.50	8.20	0.86	8.50	0.89
	C4	10134	8118	0.80	8991	0.89	11.60	23.14	1.99	12.02	1.04
[64]	C10	1438	1346	0.94	1256	0.87	1.3	1.64	1.26	2.24	1.72
	C15	1450	1346	0.93	1256	0.87	1.47	1.64	1.12	2.24	1.52
	C19	1465	1346	0.92	1256	0.86	1.36	1.64	1.21	2.24	1.65
[65]	DB450-C	1715	1639	0.96	1563	0.91	1.49	1.64	1.10	1.72	1.16
[66]	K2	7460	7745	1.04	7115	0.95	11.1	11.3	1.02	15.70	1.41
	K3	7490	7590	1.01	7311	0.98	4.30	4.25	0.99	8.25	1.92
	K4	7580	7777	1.03	7510	0.99	6.90	8.2	1.19	15.00	2.17
	K5	5325	5458	1.02	5558	1.04	3.80	5.8	1.53	4.80	1.26
	K8	6230	6665	1.07	6333	1.02	5.90	6	1.02	8.8	1.49
[67]	A5NP2C	3326	3360	1.01	3231	0.97	6.30	6.75	1.07	8.75	1.39
	C4NP2C	3704	3809	1.03	3504	0.95	7.70	8.25	1.07	10.50	1.36
	C4NP4C	5468	5675	1.04	4866	0.89	20.80	22	1.06	22.75	1.09
	B4NP2C	4182	4255	1.02	4065	0.97	13.6	14.25	1.05	16.25	1.19
	C4MP2C	5434	5422	1.00	4994	0.92	8.80	10.75	1.22	14.75	1.67
[68]	I.RCC.1L	1003	1128	1.12	1129	1.12	15.34	15.94	1.04	18.75	1.22
	I.RCC.3L	1435	1595	1.11	1544	1.08	22.98	24.25	1.05	23.44	1.02
	II.RCC.1L	1558	1809	1.16	1594	1.02	8.36	8.75	1.05	20.62	2.47
	II.RCC.3L	2019	2561	1.27	2049	1.01	13.58	15.25	1.12	25.63	1.89
	III.RCC.1L	1532	1709	1.12	1586	1.03	3.75	4.53	1.21	11.25	3
	III.RCC.3L	1906	2164	1.14	1892	0.99	6.18	7.81	1.26	15.47	2.50
[69]	C10	1485	1670	1.12	1381	0.93	13.10	16.93	1.29	25.73	1.96
	C41	2767	3065	1.11	2804	1.01	9.10	11.73	1.29	17.60	1.93
	C34	3742	4033	1.08	3463	0.93	15.50	17.6	1.14	24.93	1.61
	C43	3967	4515	1.14	3700	0.93	16.60	18.4	1.11	23.47	1.41
	C44	4828	5363	1.11	4481	0.93	22.50	26.4	1.17	28.67	1.27

	Mean	St. Dev.	COV	Min.	Max.
Max. axial load (SM model)	1.06	0.10	0.09	0.8	1.27
Axial strain at peak strength (SM model)	1.22	0.29	0.24	0.86	2.15
Max. axial load (SZM model)	0.98	0.08	0.08	0.86	1.17
Axial strain at peak strength (SZM model)	1.64	0.53	0.32	0.83	3

These results suggest that, for the specimen sizes considered here, the accuracy of the proposed frame FE in predicting the load-carrying capacity is not affected by scale effects. In addition, it is observed that the FE models employed in this study can predict with good accuracy the strain at peak strength for RC columns that are not confined with FRP, whereas they overestimate, sometimes even significantly, the strain at peak strength for RC columns confined with FRP, particularly for larger values of the strains. This observation may be related to possible size effects.

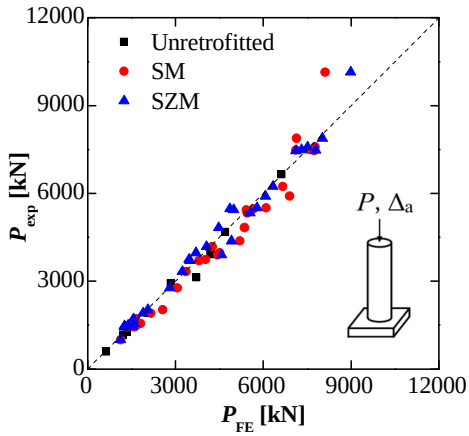

Figure 4.4 - Comparison between experimental and numerical results for columns subjected to concentric axial loading: ultimate load-carrying capacity

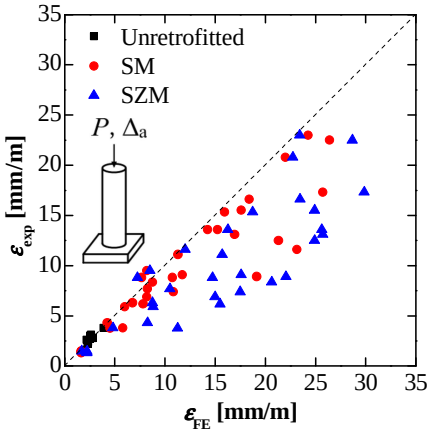

Figure 4.5 - Comparison between experimental and numerical results for the columns subjected to concentric axial loading: strain at peak strength

4.3 PREDICTION OF ULTIMATE LOAD-CARRYING CAPACITY FOR COLUMNS SUBJECTED TO ECCENTRIC AXIAL LOADING

The performance of the newly developed frame FE was also evaluated through a comparison between the experimentally measured and the numerically predicted load-carrying capacity of the columns included in the experimental database and subjected to eccentric axial loading (see Table 4.4). The geometric properties of the specimens and mechanical properties of the materials are taken from experimental information provided in the literature [3],[60],[73]-[76]. The considered database contains specimens with a wide range of heights L (from 1,200 mm to 3,658 mm), cross-section diameters d (from 270 mm to 610 mm), unconfined compressive strength of concrete f_c (from 34.45 MPa to 90.1 MPa), longitudinal steel reinforcement areas A_s (from 1,608 mm^2 to 7,384 mm^2) and yield strength f_y (from 303 MPa to 500 MPa), as well as a wide variety of FRP reinforcement configurations, FRP material jacket thickness t_f varying in the range from 0.33 mm to 6.3 mm, elastic modulus in the hoop direction E_f varying in the range from 18.6 GPa to 227 GPa, and FRP tensile strength in the hoop direction f_{fu} varying in the range from 400 MPa to 3,800 MPa. Since the proposed frame FE does not model shear failure, this study considers only specimens with a ratio L/d between the shear span length, L, and the diameter, d, larger than 3.0, in order to avoid specimens failing in shear. In addition, the selected experimental database considers only columns strengthened via FRP-confinement (i.e., with FRP fibers oriented orthogonally to the column axis); thus, it excludes specimens retrofitted in flexure or in flexure-confinement (i.e., with FRP fiber oriented not orthogonally to the column axis). It is noteworthy that the frame FE proposed in this study can be easily combined with a frame FE previously developed by Barbato [77] to model flexural retrofit of beam/column components with externally bonded FRP.

Table 4.5 presents the comparison between experimental results and numerical simulations of the load-carrying capacity for the reference RC columns (i.e., for the RC columns without FRP retrofit) subjected to eccentric axial loading. The accuracy of the numerical model is investigated by using the ratio of the numerically simulated and experimentally measured load-carrying capacity, $R = F_{FE} / F_{\exp}$. The agreement in terms of load-carrying capacity between experimental results and numerical simulations is excellent, with $\mu_R = 1.02$ and $COV_R = 0.04$.

Table 4.6 compares the experimentally measured and numerically simulated values of the load-carrying capacities (in terms of maximum lateral load) for the FRP-confined RC columns subjected to eccentric axial loading. The numerical simulations were performed using both the SM and SZM models. The statistics of R (i.e., mean, standard deviation, coefficient of variation, and minimum and maximum values) are provided for both models. These statistics show that both models provide excellent results in terms of load-carrying capacity, with $\mu_{R_{\mathrm{SM}}} = 1.04$ and $\sigma_{R_{\mathrm{SM}}} = 0.07$ for the SM model, and $\mu_{R_{\mathrm{SZM}}} = 1.02$ and $\sigma_{R_{\mathrm{SZM}}} = 0.06$ for the SZM model, respectively.

Figure 4.6 graphically reproduces the results relative to the load-carrying capacities for the column specimens subjected to eccentric axial load, which are provided in Table 4.5 and Table 4.6. The result indicates that, for all sizes of the specimens considered here, the FE models employed in this study can predict the load-carrying capacity for both reference columns and FRP-confined columns with very good accuracy.

Table 4.4 - Experimental test database for RC columns subjected to eccentric axial loading: specimens' identification, geometry, and material properties

Ref.	ID	d (mm)	L (mm)	f_c (MPa)	n_b (-)	A_s (mm^2)	f_y (MPa)	FRP Type	t_f (mm)	E_f (GPa)	f_{fu} (MPa)
[3]	As-Built	610	3658	34.45	26	284	303	-	-	-	-
	#1	610	3658	34.45	26	284	303	CFRP	5.1	124	1300
	#2	610	3658	34.45	26	284	303	CFRP	6.3	124	1300
[60]	S-2NT	356	1470	40.1	6	500	450	-	-	-	-
	S-3NT	356	1470	39.2	6	500	450	-	-	-	-
	S-4NT	356	1470	39.2	6	500	450	-	-	-	-
	ST-2NT	356	1470	40.4	6	500	450	GFRP	1.25	20	400
	ST-3NT	356	1470	40.4	6	500	450	CFRP	1.00	20	900
	ST-4NT	356	1470	44.8	6	500	450	CFRP	0.5	75	900
	ST-5NT	356	1470	40.8	6	500	450	GFRP	1.25	20	400
[73]	As-Built	305	1892	34.5	9	201	358	-	-	-	-
	Upgraded	305	1892	34.5	9	201	358	GFRP	4.8	18.6	532
[74]	A2	400	1350	30	12	201	296	CFRP	0.11	243	4277
	A3	400	1350	27.5	12	201	296	CFRP	0.22	243	4277
	B2	400	1350	30	12	201	296	CFRP	0.11	243	4277
	B3	400	1350	27.5	12	201	296	CFRP	0.22	243	4277
[75]	BR-C8	508	2000	38	12	302	400	-	-	-	-
	BR-C8-1	508	2000	38	12	302	400	CFRP	3.6	60	700
	BR-C8-2	508	2000	38	12	302	400	CFRP	1.8	60	700
[76]	RC-1	270	2000	90.1	8	201	500	CFRP	0.66	227	3800
	RC-2	270	2000	75.2	8	201	500	CFRP	0.33	227	3800
	RC-3	270	2000	49.7	8	201	500	CFRP	0.33	227	3800
	RC-4	270	1200	75.3	8	201	500	CFRP	0.33	227	3800

Table 4.5 - Comparison between experimental results and numerical simulations for reference RC columns under eccentric axial loading: lateral load-carrying capacity

Ref.	ID	Maximum lateral load (kN)		
		Exp	Model	R
[3]	As-Built	208	226	1.09
[60]	S-2NT	133	136.7	1.03
	S-3NT	126	130.6	1.04
	S-4NT	135	133.3	0.99
[73]	As-Built	64	64.1	1.00
[75]	BR-C8	210	208.5	0.99

	Mean	St. Dev.	COV	Min.	Max.
Max. lateral load	1.02	0.04	0.04	0.99	1.09

Table 4.6 - Comparison between experimental results and numerical simulations for FRP-confined RC columns subjected to eccentric axial loading: load-carrying capacity

Ref.	ID	Maximum lateral load (kN)				
		Exp.	SM	R_{SM}	SZM	R_{SZM}
[3]	#1	272	297	1.09	290	1.07
	#2	310	302	0.97	293	0.95
[60]	ST-2NT	203	204.1	1.01	200.7	0.99
	ST-3NT	199	210.2	1.06	215	1.08
	ST-4NT	185	175.5	0.95	182.3	0.99
	ST-5NT	179	176.2	0.98	176.9	0.99
[73]	Upgraded	84	87.5	1.04	84.7	1.01
[74]	A2	112	115	1.03	113	1.01
	A3	102	120	1.18	119	1.17
	B2	112	114	1.02	114	1.02
	B3	106	117	1.10	119	1.12
[75]	BR-C8-1	256	259	1.01	252	0.98
	BR-C8-2	263	244.5	0.93	242	0.92
[76]	RC-1	101	114	1.13	105	1.04
	RC-2	86	95	1.10	90.5	1.05
	RC-3	84	85.8	1.02	80.6	0.96
	RC-4	153	158	1.03	163	1.07
		Mean	St. Dev.	COV	Min.	Max.
Max. lateral load (SM model)		1.04	0.07	0.06	0.93	1.18
Max. lateral load (SZM model)		1.02	0.06	0.06	0.92	1.17

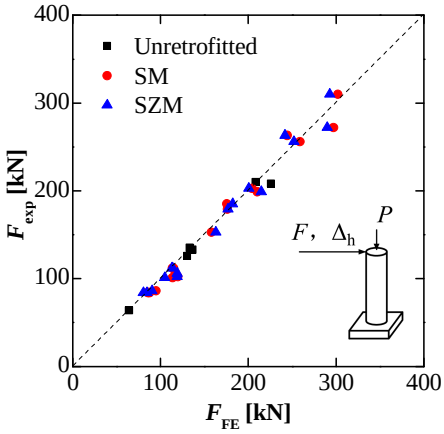

Figure 4.6 - Comparison between experimental and numerical results for the columns subjected to eccentric axial loading: maximum lateral force

4.4 COMPARISON OF FORCE-DISPLACEMENT RESPONSE

The accuracy of the newly developed frame FE was also investigated through a comparison between the experimentally measured and the numerically predicted force-displacement response of the FRP confined circular columns included in the experimental database considered in this study. This section describes in detail the force-displacement results corresponding to (1) the specimens identified as C4NP0C (unconfined specimen) and B4NP2C (FRP-confined specimen) in Eid et al. [67], as representative of columns subjected to concentric axial loading; and (2) the specimens identified as “as-built” (unconfined specimen) and “upgraded” (FRP-confined specimen) in Saadatmanesh et al. [73], as representative of columns subjected to eccentric axial loading. The results corresponding to the other specimens considered in this study are shown in Appendix A.

Figure 4.7 plots the axial force-displacement response for the unretrofitted column (C4NP0C) and the FRP-confined column (B4NP2C) subjected to concentric axial load. The thick lines correspond to the results for the C4NP0C specimen, whereas the thin lines correspond to the results for the B4NP2C specimen. For the unretrofitted column, the agreement between numerical simulations and experimental records is excellent up to the peak strength and very good in the softening branch of the response, where the FE results slightly overestimate the post-peak residual strength of the column. These results are consistent with the results reported in Mander et al. [70]. For the FRP-confined column, the SM model provided results that are in excellent agreement with the experimental data in terms of initial stiffness, force at the yield point, post-yielding stiffness, peak strength, and displacement at the peak strength of the specimen. The SZM model appeared to (1) slightly underestimate the initial stiffness and the force at the yield point, (2) accurately capture the post-yielding stiffness and the peak strength,

and (3) overestimate the displacement at the peak strength of the FRP-confined specimen. Both models did not capture the experimentally recorded behavior of the specimens after the peak strength is achieved. This disagreement between experimental and numerical results may be due to the fact that, in the FE models, the FRP confinement fails along the entire length of the column during a single load step; whereas, in the experimental test, the FRP confinement may have failed locally at different locations for different values of the imposed axial displacement. Similar results were obtained also for the other FRP-confined columns subjected to concentric axial load and considered in this study. These results suggest that, in general, the SM model can capture very well the initial stiffness of the specimens, but tends to slightly overestimate their peak strength and strain at peak strength; whereas the SZM can capture very well the specimens' peak strength, but tends to overestimate the strain at peak strength and underestimate the initial stiffness of the column specimens.

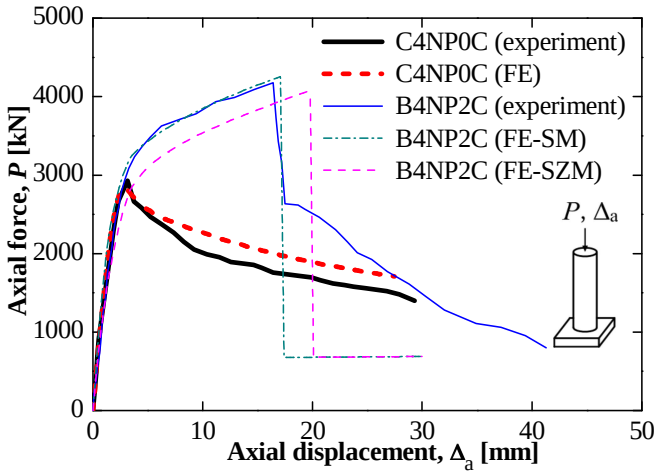

Figure 4.7 - Comparison between experimental and numerical results for columns subjected to concentric axial loading: axial force-displacement response

Figure 4.8 plots the lateral force-displacement response for the reference column ("as-built") and the FRP-confined column ("upgraded") subjected to concentric axial load. In this figure, the

thick lines correspond to the results for the “as-built” specimen, whereas the thin lines correspond to the results for the “upgraded” specimen. In this case, the agreement between numerical simulations and experimental records is excellent for the reference column, and very good for the FRP-confined column considering both the SM and SZM models. The SM model slightly overestimated the lateral force after yielding and the peak strength, whereas the SZM model slightly underestimated the stiffness of the specimen after the initial cracking of the concrete.

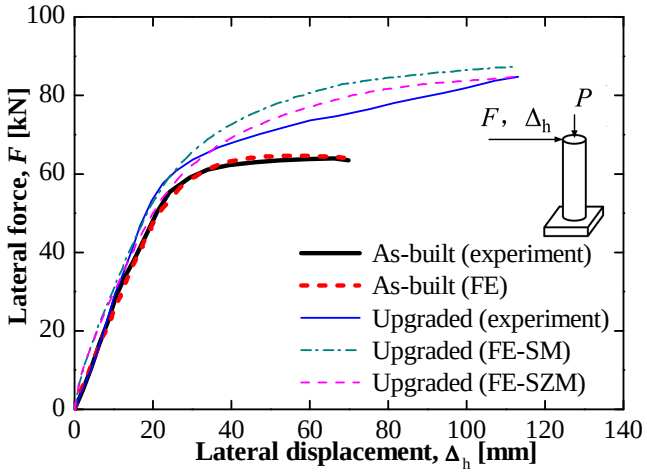

Figure 4.8 - Comparison between experimental and numerical results for columns subjected to eccentric axial loading: lateral force-displacement response

The results presented in this section of the study show that the proposed frame FE is able to accurately predict the nonlinear force-displacement response of FRP-confined columns under different loading conditions. This accuracy is achieved at a low computational cost, by using a very small number of FEs (only one in this case) to discretize the structural components under study.

5 NONLINEAR FE MODEL FOR RC COLUMNS CONFINED BY BOTH LATERAL STEEL AND EXTERNAL FRP

5.1 INTRODUCTION

According to the structural design standards for RC structures established by the building and design codes [78],[79], the amount of longitudinal and transverse reinforcement in RC columns must satisfy minimum requirements in terms of flexural and shear strength. As a result, RC columns that need to be retrofitted with FRP plates/sheets also contain transverse steel. Thus, most of the confined concrete in these retrofitted RC columns need is subjected to two simultaneous actions of confinement: the action due to transversal steel reinforcement and the action due to FRP.

The majority of (both design-oriented and analysis-oriented) stress-strain models for concrete confined with FRP available in existing literature [14],[16]-[23] considered only separately the confinement actions due to transversal steel and FRP, i.e., they did not take account for the influence of the existing transversal steel reinforcement on the mechanical behavior of the concrete confined through externally-bonded FRP plates/sheets.

Kawashima et al. [74] proposed two different stress-strain models; a first model for concrete confined with carbon FRP only, and a second model for concrete confined simultaneously by carbon FRP and transversal steel ties. They used a regression analysis based on the experimental results obtained through two-phase loading tests on RC specimens with circular and rectangular sections to calibrate the parameters defining the two proposed stress-strain confined concrete models.

Li et al. [80] developed a combined theoretical and experimental constitutive model for carbon FRP-confined concrete columns. The peak strength of the confined concrete was derived from the Mohr-Columb failure criterion, and the strain at the peak strength was obtained from

the regression analysis of experimental results. The model was modified for concrete confined by both steel reinforcement and carbon FRP. In the modified model, the strength of the confined concrete was obtained as the sum of the unconfined concrete strength and the increments of strength due to the confinement of carbon FRP and steel reinforcement considered independently. The strength increment due to the lateral confinement produced by the carbon FRP was computed from the model proposed in [80]. The strength increment due to the lateral steel reinforcement was calculated using the Mander's model [7]. This confined concrete modified model was verified by comparisons with experimental tests, and proved to be more accurate than the Kawashima's model [74].

Ilki et al. [81] also proposed empirical equations for the compressive strength and corresponding axial deformation of FRP jacketed columns considering the effects of internal transverse and longitudinal steel reinforcement. The equation for compressive strength of the confined concrete was obtained based on experimental work that was carried out on nearly full size specimens [82]. The corresponding axial strain was estimated using the equation proposed by Mander et al. [7]. An extensive database consisting of 448 specimens was compiled to evaluate the performance of the proposed model. The proposed model predicted the compressive strength and corresponding axial strains with a reasonable accuracy.

Pellegrino and Modena [83] considered internal steel reinforcement configuration had an important influence on concrete packing pattern at failure, and thus, on the efficiency of FRP confinement. They proposed an analytical model to predict the strength and ductility of RC columns. This model provides a complete stress-strain curve for FRP-confined concrete, which takes into account the interaction mechanisms between internal steel reinforcement and external FRP wrapping. Their new model was found to be more accurate than existing models.

5.2 NEWLY PROPOSED MATERIAL CONSTITUTIVE MODEL FOR CONCRETE CONFINED SIMULTANEOUSLY BY STEEL AND FRP

The constitutive material model proposed by Spoelstra and Monti [21] (SM model) was extended in this study to consider the simultaneous confinement actions on the concrete due to transverse steel reinforcement (which is applied internally and used to provide additional shear strength to the RC member) and FRP sheets/plates (which are externally bonded and used to provide confinement to the RC member). The original SM model is based on an iterative numerical procedure (see Figure 3.7) and is suitable to model concrete confined separately with externally-bonded FRP, as well as with steel jackets or conventional transverse reinforcement.

The newly proposed material constitutive model (referred to as modified SM model hereinafter) evaluates the lateral confinement pressure as the sum of the confinement pressure due to the externally-bonded FRP and internal transversal steel reinforcement, with an approach similar to some of the previous studies [74],[80],[81].

The total confinement pressure for the Modified SM model is calculated as follows

$$f_l^{'} = \frac{1}{2} \cdot k_e \cdot \rho_s \cdot \sigma_{st} + \frac{1}{2} \cdot \rho_f \cdot E_f \cdot \varepsilon_f \tag{5.1}$$

The first term in the right hand side of Equation (5.1) represents the confinement action due to the transversal reinforcement steel, where k_e = confinement effectiveness coefficient (the equations for which can be found in Mander et al. [7]), ρ_s = transversal steel reinforcement ratio defined as

$$\rho_s = \frac{4 \cdot A_{st}}{s \cdot d_c} \tag{5.2}$$

where A_{st} = cross-section area of a transversal reinforcing stirrup/spiral, s = clear distance between adjacent hoops or spiral turns, and d_c = diameter of the confined concrete core, and σ_{st} = the strength of the transversal reinforcing stirrup/spiral, which is given by

$$\sigma_{st} = \begin{cases} E_{st} \cdot \varepsilon_l & \text{for} \quad \max(\varepsilon_l) < \varepsilon_y \\ f_{yt} & \text{for} \quad \varepsilon_y \le \max(\varepsilon_l) < \varepsilon_{su} \\ 0 & \text{for} \quad \max(\varepsilon_l) \ge \varepsilon_{su} \end{cases} \tag{5.3}$$

where E_{st} = elastic modulus of the transversal reinforcing steel stirrup/spiral, f_{yt} = yield strength of the transversal reinforcing stirrup/spiral, ε_l = updated lateral strain, ε_y = yield strain of the transversal reinforcing steel stirrup/spiral, and ε_{su} = rupture strain of the transversal reinforcing steel stirrup/spiral.

The second term in the right hand side of Equation (5.1) represents the confinement action due to the externally-bonded FRP, where ρ_f = FRP volume ratio defined as

$$\rho_f = \frac{4 \cdot t_f}{D} \tag{5.4}$$

where t_f = thickness of the jacket, D = diameter of the FRP jacket/sheet, and E_f = elastic modulus of the FRP; and

$$\sigma_f = \begin{cases} E_f \cdot \varepsilon_l & \text{for} \quad \max(\varepsilon_l) < f_{fu}/E_f \\ 0 & \text{for} \quad \max(\varepsilon_l) \ge f_{fu}/E_f \end{cases} \tag{5.5}$$

where f_{fu} = ultimate strength of the FRP material.

The confining pressure for concrete confined simultaneously by steel and FRP is shown in Figure 5.1 as a function of the radial strain.

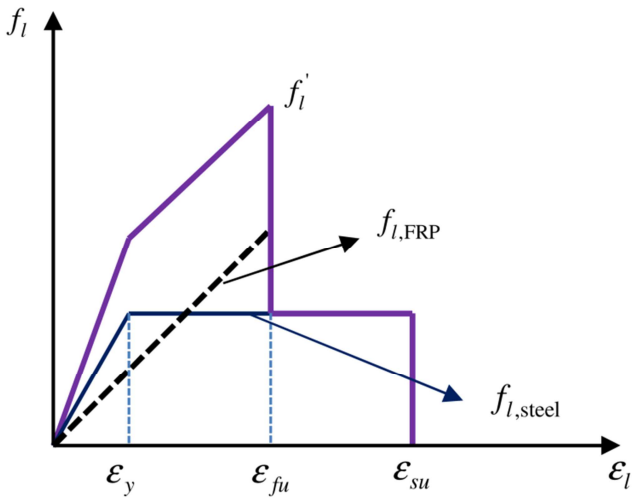

Figure 5.1 - Confine scheme for columns confined simultaneously by steel and FRP

The calculation of the stress-strain relation is performed using the same iterative process described in Figure 3.7, with the only modification being the evaluation of the confinement pressure using Equation (5.1) instead of Equation (3.22). Typical monotonic stress-strain response curves for the SM model and the modified SM model are compared in Figure 5.2.

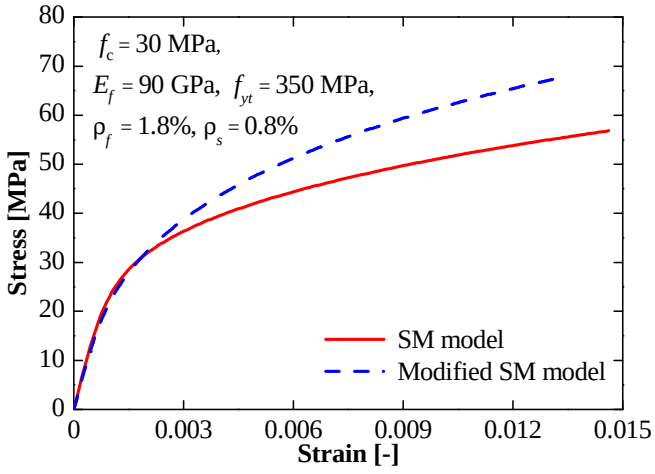

Figure 5.2 - Comparison of stress-strain relations for the SM and Modified SM model under monotonic loading

5.3 PREDICTION OF ULTIMATE LOAD-CARRYING CAPACITY AND STRAIN AT PEAK STRENGTH FOR COLUMNS SUBJECTED TO CONCENTRIC AXIAL LOADING USING THE MODIFIED SM MODEL FOR CORE CONCRETE

The performance of the newly developed frame FE used in conjunction with the Modified SM model was evaluated through a comparison between the experimentally measured and the numerically predicted load-carrying capacity and strain at peak strength of the columns subjected to concentric axial loading and included in the experimental database selected for this study, [63]-[69]. In addition to the parameters given in Table 4.1, Table 5.1 provides the geometric properties of the specimens and mechanical properties of the materials that are needed to completely define the FE model using the modified SM model for the core concrete of the specimens. The elastic modulus of the transversal steel E_{st} and rupture strain of the transversal steel ε_{su} are assumed to be the same in all the tests, with values 200 GPa and 0.1, respectively.

Table 5.2 shows the experimental values and numerical simulations of the load-carrying capacity and strain at peak strength of the RC columns under concentric axial loading. The modified SM model was employed to model the fibers of core concrete, which are confined by both lateral steel and FRP. Both the SM and SZM models were used to simulate the fibers of concrete cover, which are confined by FRP only. The statistics of both *R* and S (i.e., mean, standard deviation, coefficient of variation, and minimum and maximum values) are provided for both models options, i.e., (1) core concrete modeled using the modified SM model and cover concrete modeled using the SM model, and (2) core concrete modeled using the modified SM model and cover concrete modeled using the SZM model. In addition to the results for these two new sets of models, Table 5.2 also provides in parentheses the mean and standard deviations for the FE models used in the previous section and neglecting the simultaneous confining action of FRP and transverse steel.

Table 5.1 - Experimental test database for FPR-confined RC column subjected to concentric axial loading: specimens' identification, geometry, and material properties

Ref.	ID	d (mm)	L (mm)	c (mm)	A_{st} (mm^2)	s (mm)	f_{yt} (MPa)	k_e (-)	ρ_s (%)	ρ_f (%)	FRP Type
[63]	C2	508	1830	30	71	700	450	0.049	0.091	2.36	GFRP
	C3	508	1830	30	71	700	450	0.049	0.091	2.36	GFRP
	C4	508	1830	30	71	700	450	0.049	0.091	2.36	CFRP
[64]	C10	150	750	15	7	10	400	0.927	2.333	0.445	CFRP
	C15	150	750	15	7	15	400	0.887	1.556	0.445	CFRP
	C19	150	750	15	7	5	400	0.967	4.667	0.445	CFRP
[65]	DB450-C	200	914	20	28	50	517	0.726	1.4	0.54	CFRP
[66]	K2	400	2000	15	50	140	560	0.663	0.386	0.585	CFRP
	K3	400	2000	15	50	140	560	0.663	0.386	0.94	CFRP
	K4	400	2000	15	50	140	560	0.663	0.386	1.8	GFRP
	K5	400	2000	15	50	140	560	0.663	0.386	0.6	GFRP
	K8	400	2000	15	50	140	560	0.663	0.386	0.492	HFRP
[67]	A5NP2C	303	1200	25	71	150	602	0.503	0.748	1.006	CFRP
	C4NP2C	303	1200	25	100	100	456	0.654	1.581	1.006	CFRP
	C4NP4C	303	1200	25	100	100	456	0.654	1.581	2.012	CFRP
	B4NP2C	303	1200	25	100	100	456	0.654	1.581	1.006	CFRP
	C4MP2C	303	1200	25	100	100	456	0.654	1.581	1.006	CFRP
[68]	I.RCC.1L	160	320	18	50	140	235	0.194	1.152	2.5	CFRP
	I.RCC.3L	160	320	18	50	140	235	0.194	1.152	7.5	CFRP
	II.RCC.1L	160	320	18	50	140	235	0.194	1.152	2.5	CFRP
	II.RCC.3L	160	320	18	50	140	235	0.194	1.152	7.5	CFRP
	III.RCC.1L	160	320	18	50	140	235	0.194	1.152	2.5	CFRP
	III.RCC.3L	160	320	18	50	140	235	0.194	1.152	7.5	CFRP
[69]	C10	150	750	20	7	100	323	0.3	0.255	0.891	CFRP
	C41	250	750	20	28	150	391	0.419	0.356	0.282	CFRP
	C34	250	750	20	28	150	391	0.419	0.356	0.563	CFRP
	C43	250	750	20	28	150	391	0.419	0.356	0.845	CFRP
	C44	250	750	20	28	150	391	0.419	0.356	1.126	CFRP

It is observed that the results in terms of the maximum axial load capacity obtained using the modified SM model for the core concrete in conjunction with the SZM model for the cover concrete ($\mu_{R_{SZM}} = 1.06$ and $\text{COV}_{R_{SZM}} = 0.07$) are slightly more accurate than the results obtained using the SM model for the cover concrete, with $\mu_{R_{SM}} = 1.11$ and $\text{COV}_{R_{SM}} = 0.06$. Both models provide very good estimates of the strain at peak strength, with the SM model that performs

slightly better giving $\mu_{S_{SM}} = 1.04$ and $\text{COV}_{S_{SM}} = 0.19$, while the SZM models gives $\mu_{S_{SZM}} = 1.08$ and $\text{COV}_{S_{SZM}} = 0.23$. Compared with the simulation results obtained without taking into consideration the simultaneous confinement of transversal steel reinforcement and FRP, the results of the FE analyses performed using the modified SM model and accounting for the simultaneous confinement action of FRP and steel for the core concrete are similar to the FE results obtained by negelecting the simultaneous confinement action in terms of load-carrying capacity, whereas they present a significant improvement in terms of strain at peak strength when compared with the original models that are neglecting the simultaneous confinement actions of FRP and steel.

Figure 5.3 and Figure 5.4 graphically reproduce the results relative to the load-carrying capacity and strain at peak strength, respectively, provided in Table 5.2. The two figures have the experimental results on the vertical axis and the FE results on the horizontal axis. The dashed line on the main diagonal corresponds to 100% percent agreement between experimental values and numerical simulations for the two figures. These results suggest that the FE models with the Modified SM model employed in this study can predict with very good accuracy the load-carrying capacity and axial strain at peak strength for FRP-confined RC columns.

5.4 Prediction of Ultimate Load-carrying Capacity for Columns Subjected to Eccentric Axial Loading with the Modified SM Model for Core Concrete

The performance of the newly developed frame FE with the Modified SM model was also assessed through a comparison between the experimentally measured and the numerically predicted load-carrying capacity of the columns subjected to eccentric axial loading and included in the experimental database selected for this study [3],[60],[73]-[76].

Table 5.2 - Comparison between experimental results and numerical simulation with the Modified SM model of load-carrying capacity of RC column specimens subjected to concentric axial loading

Ref.	ID	Maximum axial load (kN)					Axial strain at peak strength (mm/m)				
		Exp.	SM	R_{SM}	SZM	R_{SZM}	Exp.	SM	S_{SM}	SZM	S_{SZM}
[63]	C2	7479	7894	1.06	7668	1.03	8.8	8.14	0.93	7.86	0.89
	C3	7884	8359	1.06	7979	1.01	9.5	7.39	0.78	6.94	0.73
	C4	10134	9945	0.98	9837	0.97	11.6	10.1	0.87	10.1	0.87
[64]	C10	1438	1458	1.01	1399	0.97	1.3	1.55	1.19	1.87	1.44
	C15	1450	1411	0.97	1337	0.92	1.47	1.55	1.05	1.76	1.20
	C19	1465	1586	1.08	1563	1.07	1.36	1.55	1.14	2.15	1.58
[65]	DB450-C	1715	1799	1.05	1793	1.05	1.49	1.63	1.09	1.83	1.23
[66]	K2	7460	8148	1.09	7861	1.05	11.1	9.9	0.89	9.3	0.84
	K3	7490	7687	1.03	7331	0.98	4.3	4.50	1.05	4.35	1.01
	K4	7580	8716	1.15	8511	1.12	6.9	7.35	1.07	7.65	1.11
	K5	5325	6325	1.23	6336	1.24	3.8	4.5	1.18	5.4	1.09
	K8	6230	7091	1.14	7017	1.13	5.9	4.5	0.76	4.8	0.81
[67]	A5NP2C	3326	3651	1.09	3542	1.06	6.3	6.25	0.99	6.25	0.99
	C4NP2C	3704	4092	1.10	3952	1.07	7.7	8	1.04	8	1.04
	C4NP4C	5468	5870	1.07	5601	1.02	20.8	19.75	0.95	19.75	0.95
	B4NP2C	4182	4823	1.15	4670	1.12	13.6	14	1.03	14	1.03
	C4MP2C	5434	5811	1.07	5587	1.03	8.8	5.5	0.63	5.5	0.63
[68]	I.RCC.1L	1003	1245	1.24	1197	1.19	15.34	19.37	1.26	18.75	1.22
	I.RCC.3L	1435	1662	1.16	1649	1.15	22.98	25.62	1.12	25	1.09
	II.RCC.1L	1558	1845	1.18	1630	1.05	8.36	7.5	0.90	7.50	0.90
	II.RCC.3L	2019	2528	1.25	2153	1.07	13.58	10.63	0.78	10.63	0.78
	III.RCC.1L	1532	1682	1.10	1581	1.03	3.75	4.37	1.17	4.31	1.15
	III.RCC.3L	1906	2188	1.15	2069	1.09	6.18	6.41	1.04	8.28	1.34
[69]	C10	1485	1699	1.14	1503	1.01	13.10	17.86	1.36	18.93	1.45
	C41	2767	3219	1.16	3078	1.11	9.10	13.87	1.52	14.13	1.55
	C34	3742	4210	1.13	3932	1.05	15.50	20.26	1.31	20.26	1.31
	C43	3967	4411	1.11	4231	1.07	16.60	18	1.08	19.33	1.16
	C44	4828	4926	1.02	4720	0.98	22.50	20.4	0.91	22	0.98

	Mean	St. Dev.	COV	Min.	Max.
Max. axial load (SM model)	1.11 (1.06)	0.07 (0.10)	0.06	0.97	1.25
Axial strain at peak strength (SM model)	1.04 (1.22)	0.20 (0.29)	0.19	0.63	1.52
Max. axial load (SZM model)	1.06 (0.98)	0.07 (0.08)	0.07	0.92	1.24
Axial strain at peak strength (SZM model)	1.08 (1.64)	0.25 (0.53)	0.23	0.63	1.58

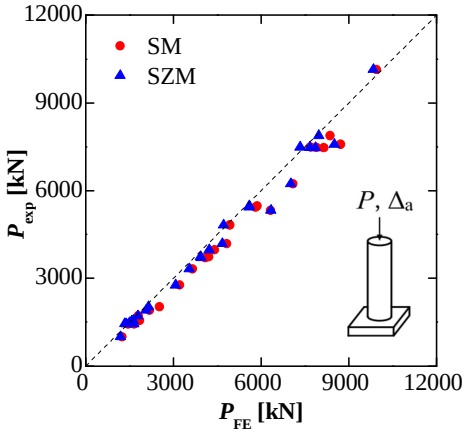

Figure 5.3 - Comparison between experimental results and FE simulations for columns subjected to concentric axial loading and modeled using the modified SM model for the core concrete: ultimate load-carrying capacity

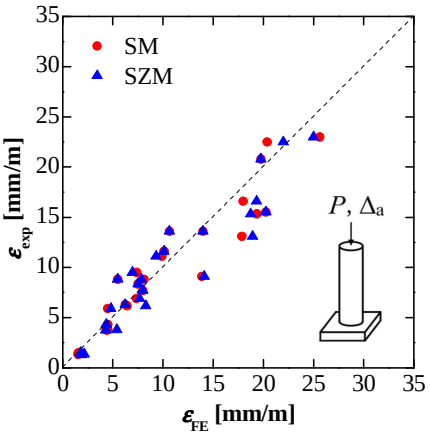

Figure 5.4 - Comparison between experimental results and FE simulations for columns subjected to concentric axial loading and modeled using the modified SM model for the core concrete: stain at peak strength

In addition to the parameters given in Table 4.4, Table 5.3 provides the geometric properties of the specimens and mechanical properties of the materials that are needed to completely define the FE model using the Modified SM model for the core concrete of the specimens.

Table 5.3 - Experimental test database for FRP-confined RC column subjected to eccentric axial loading: specimens' identification, geometry, and material properties

Ref.	ID	d (mm)	L (mm)	c (mm)	A_{st} (mm^2)	s (mm)	f_{yt} (MPa)	k_e (-)	ρ_s (%)	ρ_f (%)	FRP Type
[3]	#1	610	3658	19	32	127	303	0.793	0.176	3.344	CFRP
	#2	610	3658	19	32	127	303	0.793	0.176	4.131	CFRP
[60]	ST-2NT	356	1470	20	71	300	450	0.277	0.3	1.404	GFRP
	ST-3NT	356	1470	20	71	300	450	0.277	0.3	1.124	CFRP
	ST-4NT	356	1470	20	71	300	450	0.277	0.3	0.562	CFRP
	ST-5NT	356	1470	20	71	300	450	0.277	0.3	1.404	GFRP
[73]	Upgraded	305	1892	20	51	450	301	0.023	0.171	6.295	GFRP
[74]	A2	400	1350	35	28	150	296	0.599	0.226	0.11	CFRP
	A3	400	1350	35	28	150	296	0.599	0.226	0.22	CFRP
	B2	400	1350	35	28	300	296	0.298	0.113	0.11	CFRP
	B3	400	1350	35	28	300	296	0.298	0.113	0.22	CFRP
[75]	BR-C8-1	508	2000	49	100	300	400	0.405	0.325	2.835	CFRP
	BR-C8-2	508	2000	49	100	300	400	0.405	0.325	1.417	CFRP

Table 5.4 compares the experimentally measured and numerically simulated results of the load-carrying capacities (in terms of maximum lateral load) of the RC columns subjected to eccentric axial loading. The numerical simulations were performed using the modified SM model for the fibers of core concrete, which are confined by both transversal steel reinforcement and FRP, and both the SM and SZM models for the fibers of cover concrete, which are confined by FRP only. The agreement in terms of load-carrying capacity between experimental results and numerical simulations is excellent, with $\mu_{R_{SM}} = 1.02$ and $\sigma_{R_{SM}} = 0.07$ for the FE models using the SM model for the cover concrete, and $\mu_{R_{SZM}} = 1.03$ and $\sigma_{R_{SZM}} = 0.06$ for the FE model using the SZM model for the cover concrete, respectively. These results are very similar to the ones obtained using the SM and SZM models also for the core concrete, i.e., by neglecting the simultaneous confinement actions of FRP and transversal steel on the core concrete.

Table 5.4 - Comparison between experimental results and numerical simulations for FRP-confined RC columns subjected to eccentric axial loading and modeled using the modified SM model: load-carrying capacity

Ref.	ID	Maximum lateral load (kN)				
		Exp.	SM	R_{SM}	SZM	R_{SZM}
[3]	#1	272	305	1.12	302	1.11
	#2	310	307	0.99	304	0.98
[60]	ST-2NT	203	207	1.02	207	1.02
	ST-3NT	199	201	1.01	204	1.03
	ST-4NT	185	184	0.99	181	0.98
	ST-5NT	179	185	1.03	189	1.06
[73]	Upgraded	84	87.6	1.04	86.1	1.02
[74]	A2	112	108	0.96	113	1.01
	A3	102	118	1.16	116	1.14
	B2	112	108	0.96	113	1.01
	B3	106	116	1.09	119	1.12
[75]	BR-C8-1	256	255	1.00	256	1.00
	BR-C8-2	263	246	0.94	245	0.93
		Mean	St. Dev.	COV	Min.	Max.
Max. lateral load (SM model)		1.02 (1.04)	0.07 (0.07)	0.06	0.94	1.16
Max. lateral load (SZM model)		1.03 (1.02)	0.06 (0.06)	0.06	0.93	1.14

Figure 5.5 graphically reproduces the results relative to the load-carrying capacities for the column specimens subjected to eccentric axial load, which are provided in Table 5.4. The result indicates that the FE simulations with the Modified SM model can predict the load-carrying capacity for FRP-confined columns subjected to eccentric axial loading with very good accuracy. The material constitutive model used to describe the mechanical behavior of the cover concrete has only a minor effect on the numerical estimates of the load-carrying capacity. The comparison with the previous simulation results (which were obtained without taking into consideration the simultaneous confinement of transversal steel reinforcement and FRP) show that the interaction between the confinement actions of transversal steel reinforcement and externally-bonded FRP has only a minor effect on the estimates of the load-carrying capacity of RC columns subjected to eccentric axial loading, at least for the level of constant axial loading considered in this study.

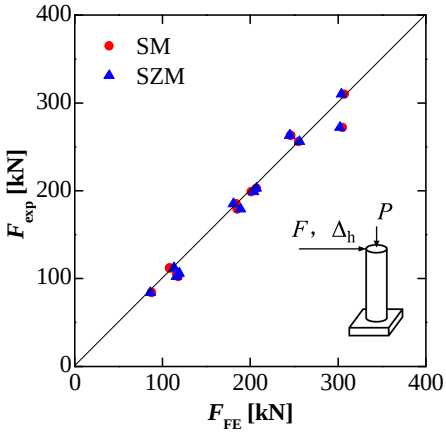

Figure 5.5 - Comparison between experimental results and FE simulations for columns subjected to eccentric axial loading and modeled using the modified SM model for the core concrete: maximum lateral force

5.5 Force-displacement Response of FE Models with the Modified SM Model for Core Concrete

This section describes in detail the force-displacement results corresponding to (1) the specimen identified as C2 in Pessiki et al. [63], as a representative of columns subjected to concentric axial loading; and (2) the specimen identified as ST2NT in Sheikh and Yau [60], as a representative of columns subjected to eccentric axial loading.

Figure 5.6 plots the axial force-displacement response for column C2 subjected to concentric axial load. The dotted line corresponds to the experimental result, the thin lines correspond to the FE results obtained ignoring the confining effect of lateral steel reinforcement, and the thick lines correspond to the FE results with the modified SM model for the core concrete. It was observed that the FE models built with the modified SM model for the core concrete and both the SM and SZM models for the cover concrete can estimate very accurately the axial force-displacement response of RC columns subjected to concentric axial loading.

Figure 5.7 plots the lateral moment-curvature response for the column ST2NT subjected to eccentric axial load. The dotted line corresponds to the experimental result, the thin lines

correspond to the FE results obtained ignoring the confining effect of lateral steel reinforcement, and the thick lines correspond to the FE results using the modified SM model for the core concrete. It was observed that the agreement between numerical simulations and experimental records is excellent for both the SM and SZM models used for the cover concrete and the modified SM model for the core concrete.

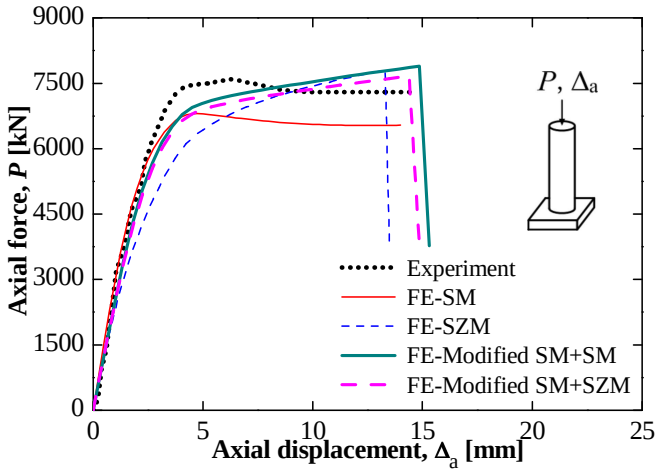

Figure 5.6 - Comparison between experimental and numerical results for columns subjected to concentric axial loading and modeled using the modified SM model for the core concrete: axial force-displacement response

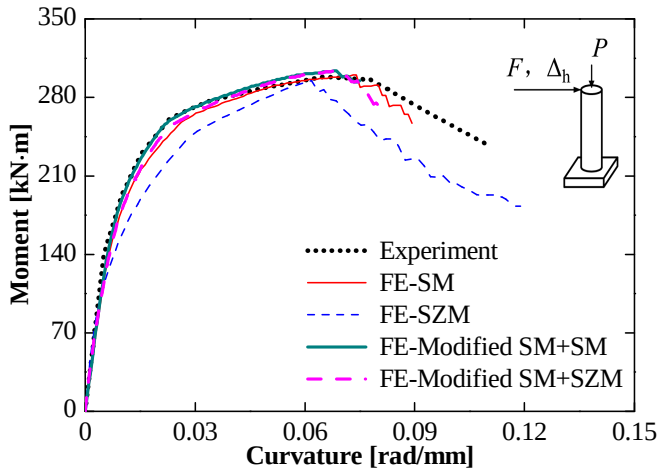

Figure 5.7 - Comparison between experimental and numerical moment-curvature response at the fixed end of column ST2NT subjected to eccentric axial loading

6 CONCLUSION AND RECOMMENDATIONS FOR FUTURE WORK

The research presented in this thesis focus on the modeling of RC columns confined with externally-bonded FRP plates/sheets. A new efficient frame FE which is able to accurately simulate the nonlinear response of circular RC columns confined using external FRP plates/sheets, is proposed.

This new frame FE employs a force-based formulation. A circular cross-section using fiber discretization is developed to represent the concrete cover, concrete core, and steel rebars. Advanced response-only mechanic-based material constitutive models are adopted and implemented in FEDEASLab to describe the nonlinear stress-strain behavior of steel, unconfined concrete, steel-confined concrete, and FRP-confined concrete.

The frame FE is used to predict the ultimate load-carrying capacity of columns subjected to concentric axial load (i.e., variable axial deformation) and eccentric axial load (i.e., constant axial load and variable transversal deformation). The study presented in this thesis provides an extensive comparison of numerical simulations and experimental results based on data that are available in the literature. The agreement between numerical simulations and experimental measurements is excellent in terms of peak strength for FRP-confined RC columns subjected to concentric and eccentric axial loading, and very good in terms of strain at peak strength for FRP-confined RC columns subjected to concentric axial loading.

The SM model is extended into the modified SM model in order to directly model the simultaneous confinement effects due to lateral steel reinforcement and FRP in conjunction with the newly developed frame FE. The same databases are employed to verify the accuracy of FE models built using the modified SM model to describe the behavior of the core concrete. When compared with the FE results obtained neglecting the simultaneous confinement actions of

transversal steel and FRP, the FE simulation results obtained using the modified SM model for the concrete core are found (1) more accurate in terms of strain at peak strength for FRP-confined RC columns subjected to concentric axial loading; and (2) as accurate in terms of load-carrying capacity for FRP-confined RC columns subjected to both concentric and eccentric axial loading.

The outstanding features of this frame FE are its simplicity, computational efficiency, and accuracy in predicting the structural behavior of circular columns confined with FRP even when a very coarse FE discretization is used to model a structural component. For the FE mesh used in this study, a nonlinear FE analysis can be performed in less than two minutes on a common personal computer.

Based on the research work performed and presented in this thesis, the following recommendations for future research are made.

(1) The material constitutive models considered in this study were used in conjunction with the newly developed frame FE to study the nonlinear response behavior of FRP-confined square/rectangular RC columns using the relations provided in [21],[23] to account for shape effects. However, the comparison between experimentally measured and FE simulated results is not satisfactory (see Appendix B). Additional research is needed to extend the newly proposed frame FE and the considered material constitutive models in order to obtain accurate nonlinear response predictions for FRP-confined RC columns with square/rectangular cross-sections.

(2) The newly developed frame FE provides a very useful tool for structural reliability analysis of FRP-retrofitted RC structures, and can be used to improve the calibration of the partial resistance factors that are needed for design.

REFERENCES

[1] Clyde, C., Pantelides, C.P., and Reaveley, L.D. Performance-based evaluation of exterior reinforced concrete building joints for seismic excitation. A report on research conducted under Grant No.SA1810JB from the National Science Foundation, 2000.

[2] Broomfield, J. Corrosion of steel in concrete, E & FN Spon, London, 1997.

[3] Seible, F., Priestley, M.J.N., Hegemier, G.A., and Innamorato, D. Seismic retrofit of RC columns with continuous carbon fiber jacket. Journal of Composites for Construction. 1997; 1(2):52-62.

[4] Kawashima, K., Takahashi, Y., Ge, H.B., Wu, Z.S., and Zhang, J.D. Damage of bridges in 2008 Wenchuan, China, earthquake. Journal of Earthquake Engineering. 2009; 13:956-998.

[5] Saatcioglu, M. and Razvi, S.R. Strength and ductility of confined concrete. Journal of Structural Engineering. ASCE 1992; 118 (6):1590-1607.

[6] Norris, T., Saadatmanesh, H., and Ehsani, M.R. Shear and flexural strengthing of R/C beams with carbon fiber sheets. Journal of Structural Engineering. ASCE 1997; 123(7):903-911.

[7] Mander, J.B., Priestly, M.J.N., and Park, R. Theoretical stress-strain model for confined concrete. Journal of Structural Engineering. ASCE 1988a; 114(8):1804-1826.

[8] Cheong, H.K., and Zeng, H. Stress-strain relationship for concrete confined by lateral steel reinforcement. Materials Journal. 2002; 99(3):250-255.

[9] Mosallam, A.S. Structural upgrade of reinforced concrete column-tie beam assembly using FRP composites. Seismic strengthen of concrete buildings using FRP composites, ACI 2008, SP-258-4.

[10] Seible, F., and Karbhari, V. Advanced composites for Civil Engineering applications in the United States. First International Conference on Composites in Infrastructure, 1996; 21-37.

[11] Bisby, L.A, and Williams, B.K. An introduction to FRP strengthening of concrete structures. ISIS Educational Module 4, 2004; ISIS Canada.

[12] Bisby, L.A, Ranger, M., and Williams, B.K. An introduction to FRP-reinforced concrete. ISIS Education Module 3, 2006; ISIS Canada.

[13] Lam, L., and Teng, J.G. Design-oriented stress-strain model for FRP-confined concrete. Construction and Building Materials. 2003; 17(6-7):471-489.

[14] Fardis, M.N., and Khalili, H.H. FRP-encased concrete as a structural material.Magazine of Concrete Research. 1982; 34(121):191-202.

[15] Richart, F.E., Brandtzaeg, A. and Brown, R.L. A Study of failure of concrete under combined compressive stress. Bulletin No.185, Univ. of Illinois, Engineering Experimental Station, Urvana, IL, USA. 1928.

[16] Karbhari, V.M., and Gao, Y. Composite jacketed concrete under uniaxial compression-verification of simple design equations. Journal of Materials in Civil Engineering. ASCE 1997; 9(4):185-193.

[17] Samaan, M., Mirmiran, A., and Shahawy, M. Model of concrete confined by fiber composites. Journal of Structural Engineering. ASCE 1998; 124(9):1025-1031.

[18] Toutanji, H.A. Stress-strain characteristics of concrete columns externally confined with advanced fiber composite sheets. ACI Material Journal. 1999; 96(3):397-404.

[19] Xiao, Y., and Wu, H. Compressive behavior of concrete confined by carbon fiber composite jackets. Journal of Materials in Civil Engineering. 2000; 12(2):139-146.

[20] Mirmiran A., and Shahawy M. A new concrete-filled hollow FRP composite column. Composites, Part B. 1996; 27B (3-4):263-268.

[21] Spoelstra, M.R., and Monti, G. FRP-confined concrete model. Journal of Composites for Construction. 1999; 3(3):143-150.

[22] Fam A.Z., and Rizkalla S.H. Confinement model for axially loaded concrete confined by circular fiber-reinforced polymer tubes. ACI Structural Journal. 2001; 98(4):451-461.

[23] Shao, Y., Zhu, Z., and Mirmiran, A. Cyclic modeling of FRP-confined concrete with improved ductility. Cement & Concrete Composites. 2006; 28(10):959-968.

[24] Monti, G., Nistico, N., and Santini, S. Design of FRP jackets for upgrade of circular bridge piers. Journal of Composites for Construction. ASCE 2001; 5(2):94-101.

[25] Priestley, M.J.N., Seible, F., and Calvi, M. Seismic design and retrofit of bridges. Wiley, New York. 1996.

[26] Yuan, X.F., Xia, S.H., Lam, L., and Smith, S.T. Analysis and behavior of FRP-confined short concrete columns subjected to eccentric loading. Journal of Zhejiang University Science A. 2007; 9(1):38-49.

[27] Mirmiran, A., Zagers, K., and Yuan, W.Q. Nonlinear finite element modeling of concrete confined by fiber composites. Finite Element in Analysis and Design. 2000; 35(1):79-96.

[28] ANSYS user's manual 10.0, Release 10.0, ANSYS, Inc.,2005.

[29] Parvin, A., and Wang, W. Concrete columns confined by fiber composite wraps under combined axial and cyclic lateral loads. Composite Structures. 2002; 58(4):539-549.

[30] MARC user's guide. MSC software corportation. Palo Alto, CA, 2000.

[31] Malvar, L.J., Morrill, K.B., and Crawford, J.E. Numerical modeling of concrete confined by fiber-reinforced composites. Journal of Composites for Construction. ASCE 2004; 8(4):315-322.

[32] Lin, J.I., DYNA3D: A nonlinear, explicit, three-dimensional finite element code for solid and structural mechanics, User Manual. UCRL-MA-107254, June, 2005.

[33] Varma, R.K., Barros, J.A.O., and Sena-Cruz, J.M. Numerical model for CFRP confined concrete elements subject to monotonic and cyclic loadings. Composites: Part B. 2009; 40(8):766-775

[34] FEMIX V4.0 Finite Element package. http://www.alvaroazevedo.com/femix/.

[35] Karabinis, A.I., Rousakis, T.C., and Manolitsi, G.E. 3D finite-element analysis of substandard RC columns strengthened by fiber-reinforced polymer sheets. Journal of Composites for Construction. ASCE 2008; 12(5):531:540.

[36] ABAQUS user's manual 6.5, ABAQUS, Inc.,2004.

[37] Yu, T., Teng, J.G., Wong, Y.L., and Dong, S.L. Finite element modeling of confined concrete-II: Plastic-damage model. Engineering Structures. 2010; 32(3):680-691.

[38] Binici, B., and Mosalam, K.M. Analysis of reinforced concrete columns retrofitted with fiber reinforced polymer lamina. Composites: Part B. 2007; 38(2):265-276.

[39] MathWorks Inc. Matlab - High performance numeric computation and visualization software. User's guide, 1997; Natick, MA, USA.

[40] Filippou, F.C., and Constantinides, M. FEDEASLab getting started guide and simulation examples. Technical Report NEESgrid-2004-22. www.neesgrid.org.

[41] Spacone, E., Filippou, F.C., and Taucer F.F. Fiber beam-column element for seismic response analysis of reinforced concrete structures. UCB/EERC Rep. 91/17, Earthquake Engineering Research Center, University of California, Berkeley, California, USA. 1991.

[42] Spacone, E., Filippou, F.C., and Taucer F.F. Fiber beam-column element for nonlinear analysis of R/C frames. Part I: formulation. Earthquake Engineering Structural Dynamics. 1996a; 25(7):11-25.

[43] Neuenhofer, A., and Filippou, F.C. Evaluation of nonlinear frame finite-element models. Journal of Structural Engineering. ASCE 1997; 123(7):958-966.

[44] Spacone, E., Filippou, F.C., and Taucer F.F. Fiber beam-column element for nonlinear analysis of R/C frames. Part II: application. Earthquake Engineering Structural Dynamics. 1996b; 25(7):27-42.

[45] Ranzo, G. and Petrangeli, M. A fibre finite beam element with section shear modeling for seimic analysis of RC structure. Journal of Earthquake Engineering. 1998; 2(3):443-473.

[46] Petrangeli, M., Pinto, P.E., and Ciampi, V. Fibre element for cyclic bending and shear of RC structures. I: Theory. Journal of Engineering Mechanics. 1999; 125(9):994-1001.

[47] King D.J., Priestley, M.J.N., and Park, R. Computer program for concrete column design. Research Report 86/12, Department of Civil Engineering, University of Canterbury, New Zealand, May, 1986.

[48] Kunnath, S.K., Heo, Y., and Mohle, J.F. Nonlinear uniaxial material model for reinforcing steel bars. Journal of Structural Engineering. ASCE 2009; 135(4):335-343.

[49] Menegotto M., and Pinto P.E. Method of analysis for cyclically loaded reinforced concrete plane frames including changes in geometry and nonelastic behavior of elements under combined normal force and bending. Proceedings, IABSE symposium on resistance and ultimate deformability of structures acted on by well-defined repeated loads, Lisbon, Portugal.

[50] Filippou, F.C., Popov, E.P., and Bertero, V.V. Effects of bond deterioration on hysteretic behavior of reinforced concrete joints. Report EERC 83–19, Earthquake Engineering Research Center, University of California, Berkeley, California, USA. 1983.

[51] Ramberg, W., and Osgood, W. R. Description of stress-strain curves by three parameters. Tech. Note 902, National Advisory Committee on Aeronautics. 1943.

[52] Monti, G., and Nuti, C. Nonlinear cyclic behavior of reinforcing bars including buckling. Journal of Structural Engineering. ASCE 1992; 118(12):3268–3284.

[53] Barbato, M., and Conte, J.P. Finite element structural response sensitivity and reliability analyses using smooth versus non-smooth material constitutive models.

[54] Balan, T.A., Filippou, F.C., and Popov, E.P. Constitutive model for 3D cyclic analysis of concrete structures. Journal of Engineering Mechanics. ASCE 1997; 123(2):143-153.

[55] Balan, T.A., Spacone, E., and Kwon, M.A. 3D hypoplastic model for cyclic analysis of concrete structures. Engineering Structures. 2001; 23(4):333-342.

[56] Kwon, M., and Spacone, E. Three dimensional finite element analyses of reinforced concrete columns. Computers and Structures. 2002; 80(2):199-212.

[57] Popovics, S. A numerical approach to the complete stress strain curve for concrete. Cement and concrete research, 1973; 3(5), 583-599.

[58] Pantazopoulou, S.J., and Mills, R.H. Microstrucutural aspects of the mechanical response of plain concrete. ACI Materials Journal. 1995; 92(6):605-616.

[59] Bathe, K.J. Finite element procedures. Prentice-Hall, Englewood Cliffs, NJ, USA.1995.

[60] Sheikh, S.A., and Yau, G. Seismic behavior of concrete columns confined with steel and fiber-reinforced polymers. ACI Structural Journal. 2002; 99(1):72-80.

[61] Cairns, S.W. Circular concrete columns externally reinforced with pre-fabricated carbon polymer shells. Master Thesis, Department of Civil Engineering, University of Toronto, Toronto, Canada. 2001.

[62] Jaffry, S.A.D. Concrete-filled glass fiber reinforced polymer (GFRP) shells under concentric compression. Master Thesis, Department of Civil Engineering, University of Toronto, Toronto, Canada. 2001.

[63] Pessiki, S., Harries, K.A, Kestner, J.T., Sause, R., and Ricles, J.M. Axial behavior of reinforced concrete columns confined with FRP jackets. Journal of Composites for Construction. 2001; 5(4):237-245.

[64] Rodrigues, C.C., and Silva, M.G. Experiment investigation of CFRP reinforced concrete columns under uniaxial cyclic compression. FRPRCS-5, Thomas Telford, London, 2001.

[65] Parretti, R., and Nanni, A. Axial testing of concrete columns confined with carbon FRP:effect of fiber orientation. 2002.

[66] Matthys, S., Toutanji, H., and Taerwe, L. Stress-strain behavior of large-scale circular columns confined with FRP composites. Journal of Structural Engineering. ASCE 2006; 132(1):123-133.

[67] Eid, R., Roy, N., and Paultre, P. Normal- and high-strength concrete circular elements wrapped with FRP composites. Journal of Composites for Construction. 2009; 13(2):113-124.

[68] Benzaid, R., Mesbah, H., and Chikh, N.E. FRP-confined concrete cylinders: axial compression experiments and strength model. Journal of Reinforced Plastics and Composites. 2010; 29(16):2469-2488.

[69] Chastre, C., and Silva, M.A.G. Monotonic axial behavior and modeling of RC circular columns confined with CFRP.”Engineering Structure. 2010; 32(8):2268-2277.

[70] Mander, J.B., Priestley, M.J.N., and Park, R. Observed stress-strain behavior of confined concrete. Journal of Structural Engineering, ASCE 1988b; 114(8):1827-1849.

[71] Taucer, F.F, Spacone, E., and Filippou, F.C. A fiber beam-column element for seismic response analysis of reinforced concrete structures. Report No. UCB/EERC-91/17, Earthquake Engineering Research Center, College of Engineering, University of California, Berkeley, 1991.

[72] Lee, T.H., and Mosalam, K.M. Probabilistic fiber element modeling of reinforced concrete structures. Computers and Structures. 2004; 82(27):2285-2299.

[73] Saadatmanesh, H., Ehsani, M.R., and Jin, L. Seismic strengthening of circular bridge piers with fiber composites. ACI Structural Journal. 1997; 93(6):639-647.

[74] Kawashima, K., Hosotani, M., and Yoneda, K. Carbon fiber sheet retrofit of reinforced concrete brige piers. International Workshop on Anuual Commemoration of Chi-Chi Earthquake, Vol.II. National Center for Research on Earthquake Engineering, Taipei, Taiwan, 2000.

[75] Elnabelsy, G., and Saatcioglu, M. Design of FRP jackets for seismic retrofit of circular concrete columns. Emirates Journal for Engineering Research. 2004; 9(2):65-69.

[76] Ozbakkaloglu, T., and Saatcioglu, M. Seismic behavior of high-strength concrete columns confined by fiber-reinforced polymer tubes. Journal of Composites for Construction. 2006; 10(6):538-549.

[77] Barbato, M. Efficient finite element modelling of reinforced concrete beams retrofitted with fibre reinforced polymers. Computers and Structures. 2009; 87(3-4):167-176.

[78] American Concrete Institute. Building code requirements for structural concrete and commentary. ACI 318-11.

[79] International Code Council. International Building Code. 2009.

[80] Li, Y.F., Lin, C.T., and Sung, Y.Y. A constitutive model for concrete confined with carbon fiber reinforced plastics. Mechanics of Materials 2003; 35(3-6):603-619.

[81] Ilki, A., Peker, O., Karamuk, E., Demir, C., and Kumbasar, N. FRP retrofit of low and medium strength circular and rectangular reinforced concrete columns. Journal of Material in Civil Engineering. ASCE, 2008; 20(2):169-188.

[82] Ilki, A., Kumbasar, N., Ozdemir, P., and Fukuta, T. A trilinear stress-strain model for confined concrete. Structural Engineering and Mechchanics. 2004; 18(5):541–563.

[83] Pellegrino, C., and Modena, C. Analytical model for FRP confinement of concrete columns with and without internal steel reinforcement. Journal of Composites for Construction. ASCE,2010; 14(6):693-705.

[84] Rousakis, T.C. and Karabinis A.I. Adequately FRP confined reinforced concrete columns under axial compressive monotonic or cyclic loading. Materials and Structures. 2012; 45(7):957-975.

[85] Turgay, T., Polat, Z., Koksal, H.O., Doran, B., and Karakoc, C. Compressive behavior of large-scale square reinforced concrete columns confined with carbon fiber reinforced polymer jackets. Materials and Design. 2010; 31(1):357-364.

[86] Shao, Y.T. Behavior of FRP-concrete beam-columns under cyclic loading. Ph.D. dissertation, North Carolina State University, Raleigh, USA. 2003.

APPENDIX A : COMPARISON OF EXPERIMENTAL AND NUMERICAL RESPONSES FOR THE CONSIDERED DATABASE

This appendix provides the comparison between experimentally recorded and numerically simulated force-displacement responses of the reference (unconfined) and FRP-confined RC columns. Figure A.1 to A.15 plot the comparisons of the experimental and FE simulated force-displacement responses of the RC columns subjected to concentric axial loading.

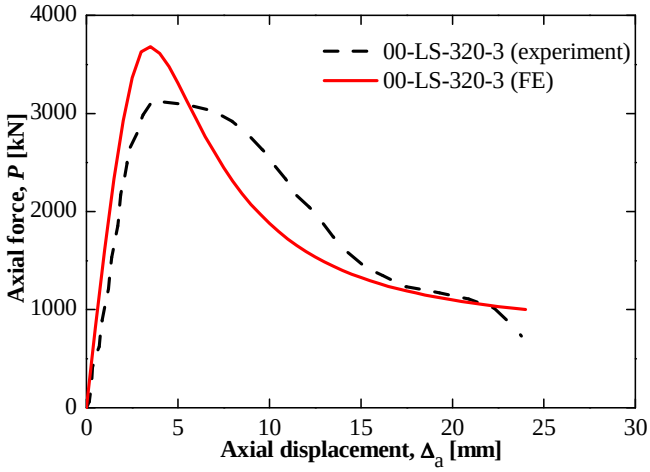

Figure A.1 - Comparison between experimental and numerical result for unconfined RC column subjected to concentric axial loading in [62]: force-displacement response

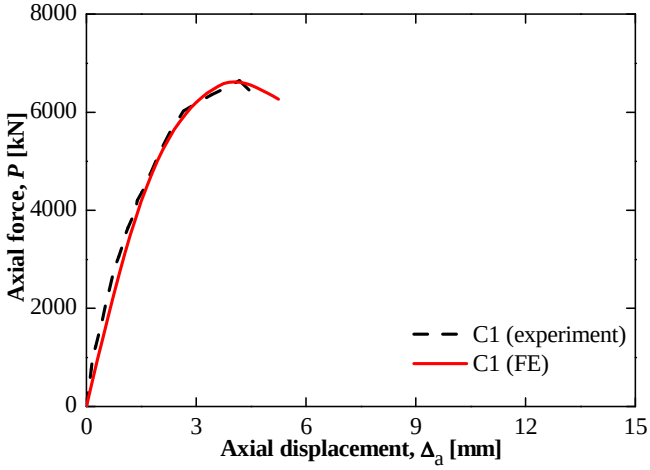

Figure A.2 - Comparison between experimental and numerical result for unconfined RC column subjected to concentric axial loading in [63]: force-displacement response

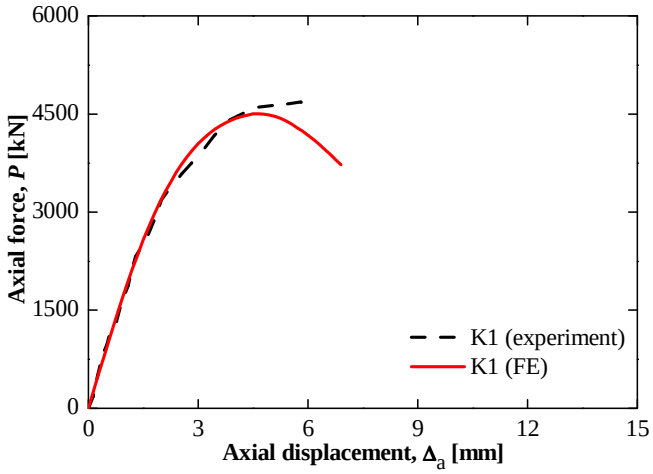

Figure A.3 - Comparison between experimental and numerical result for unconfined RC column subjected to concentric axial loading in [66]: force-displacement response

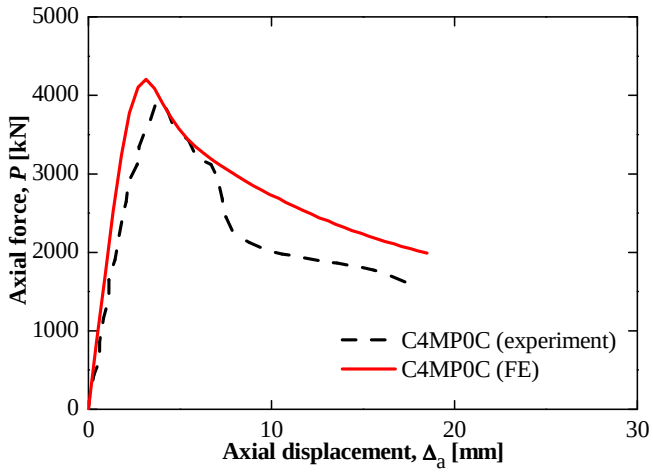

Figure A.4 - Comparison between experimental and numerical result for unconfined RC column subjected to concentric axial loading in [67]: force-displacement response

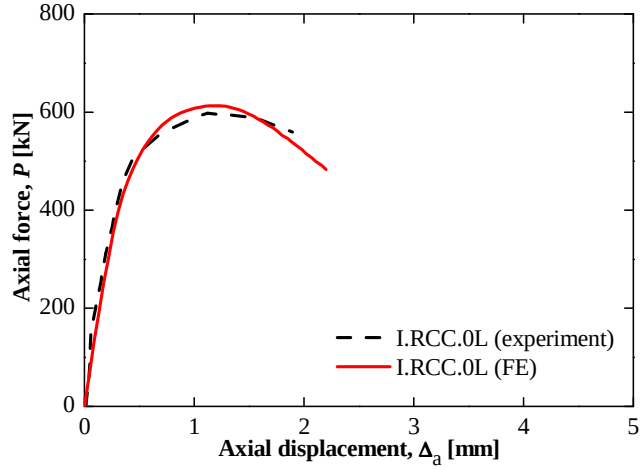

(a)

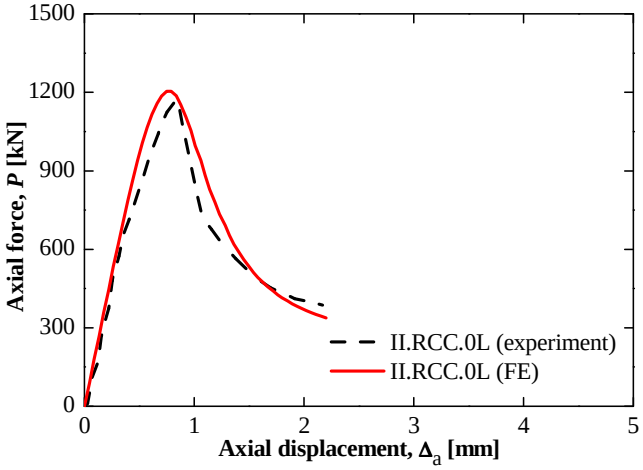

(b)

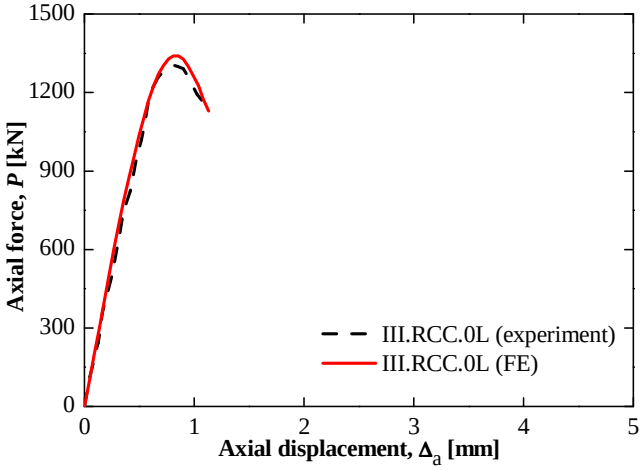

(c)

Figure A.5 - Comparison between experimental and numerical result for unconfined RC column subjected to concentric axial loading in [68]: force-displacement response (a) I.RCC.0L specimen, (b) II.RCC.0L specimen, (c) III.RCC.0L specimen

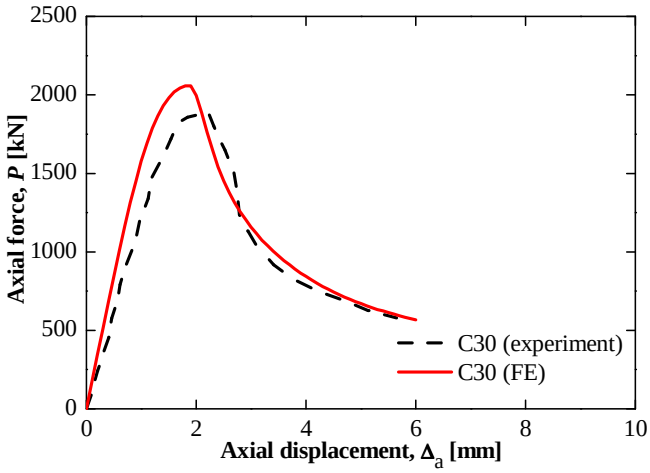

Figure A.6 - Comparison between experimental and numerical result for unconfined RC column subjected to concentric axial loading in [69]: force-displacement response

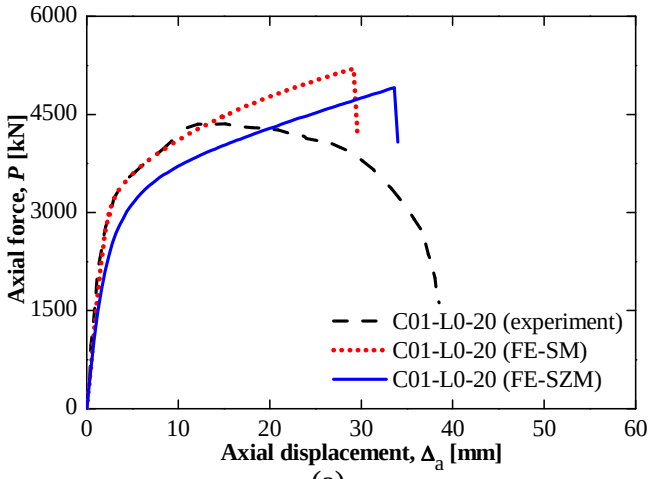

(a)

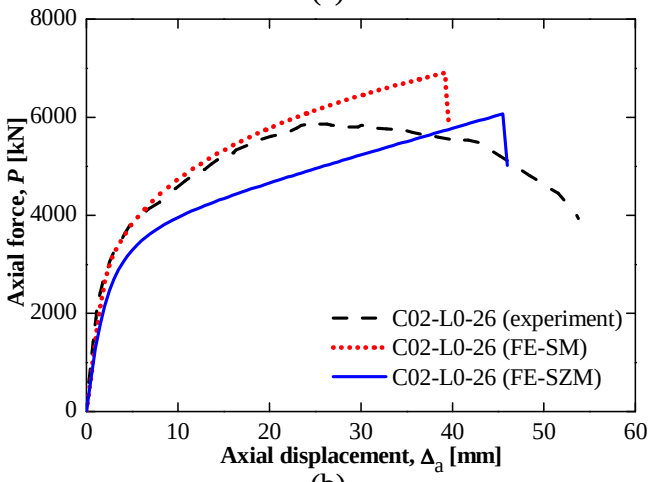

(b)

Figure A.7 - Comparison between experimental and numerical result for FRP-confined RC column subjected to concentric axial loading in [61]: force-displacement response (a) C01-L0-20 specimen, (b) C02-L0-26 specimen

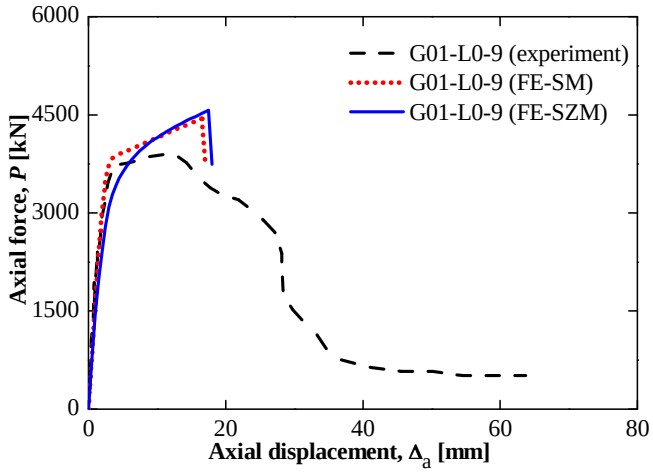

(a)

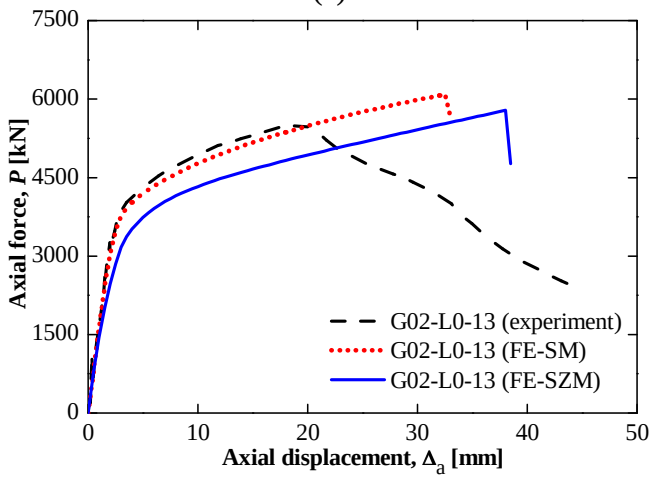

(b)

Figure A.8 - Comparison between experimental and numerical result for FRP-confined RC column subjected to concentric axial loading in [62]: force-displacement response (a) G-01-L0-9 specimen, (b) G-02-L0-13 specimen

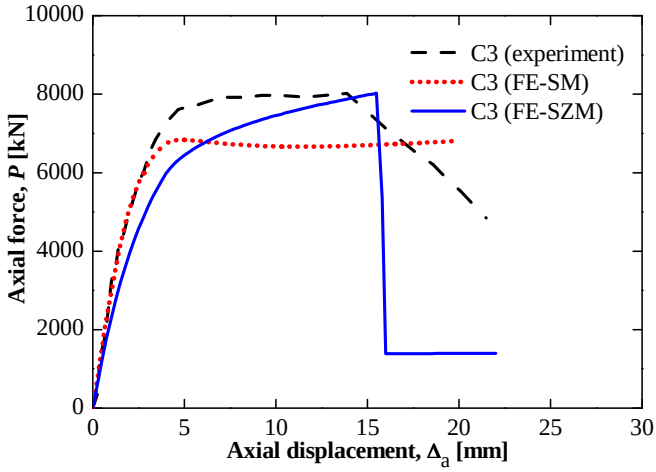

(a)

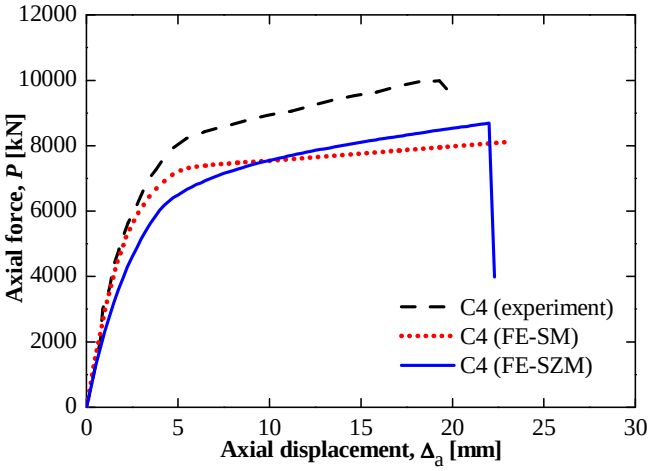

(b)

Figure A.9 - Comparison between experimental and numerical result for FRP-confined RC column subjected to concentric axial loading in [63]: force-displacement response (a) C3 specimen, (b) C4 specimen

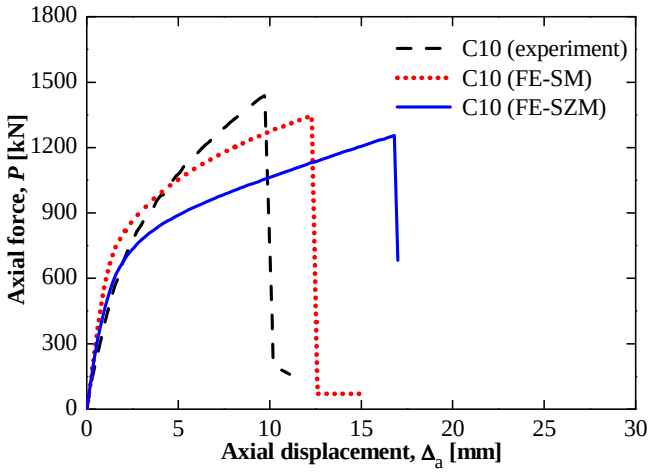

(a)

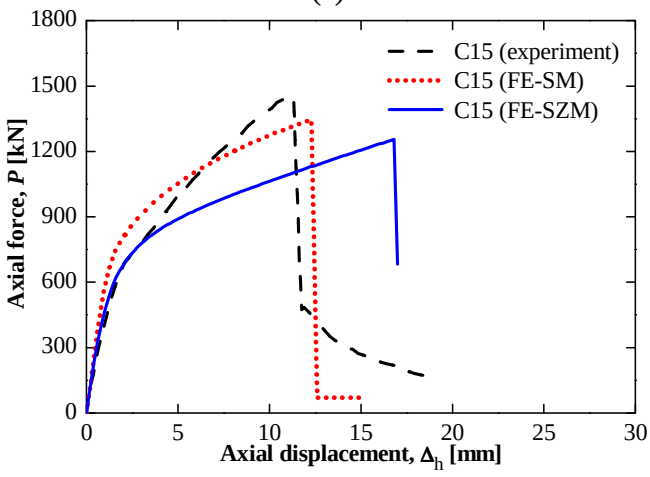

(b)

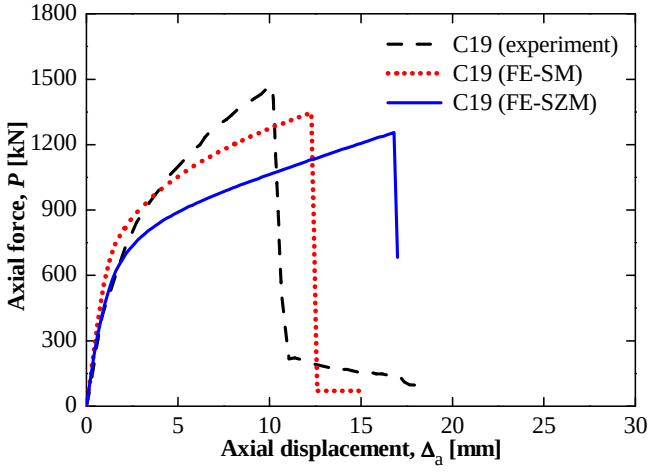

(c)

Figure A.10 - Comparison between experimental and numerical result for FRP-confined RC column subjected to concentric axial loading in [64]: force-displacement response (a) C10 specimen, (b) C15 specimen, (c) C19 specimen

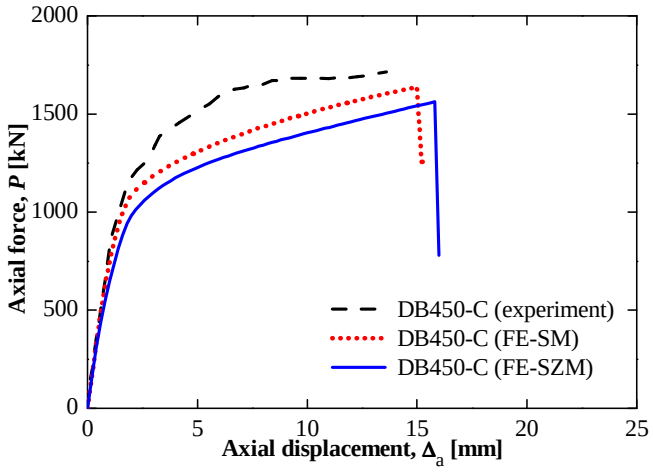

Figure A.11 - Comparison between experimental and numerical result for FRP-confined RC column subjected to concentric axial loading in [65]: force-displacement response

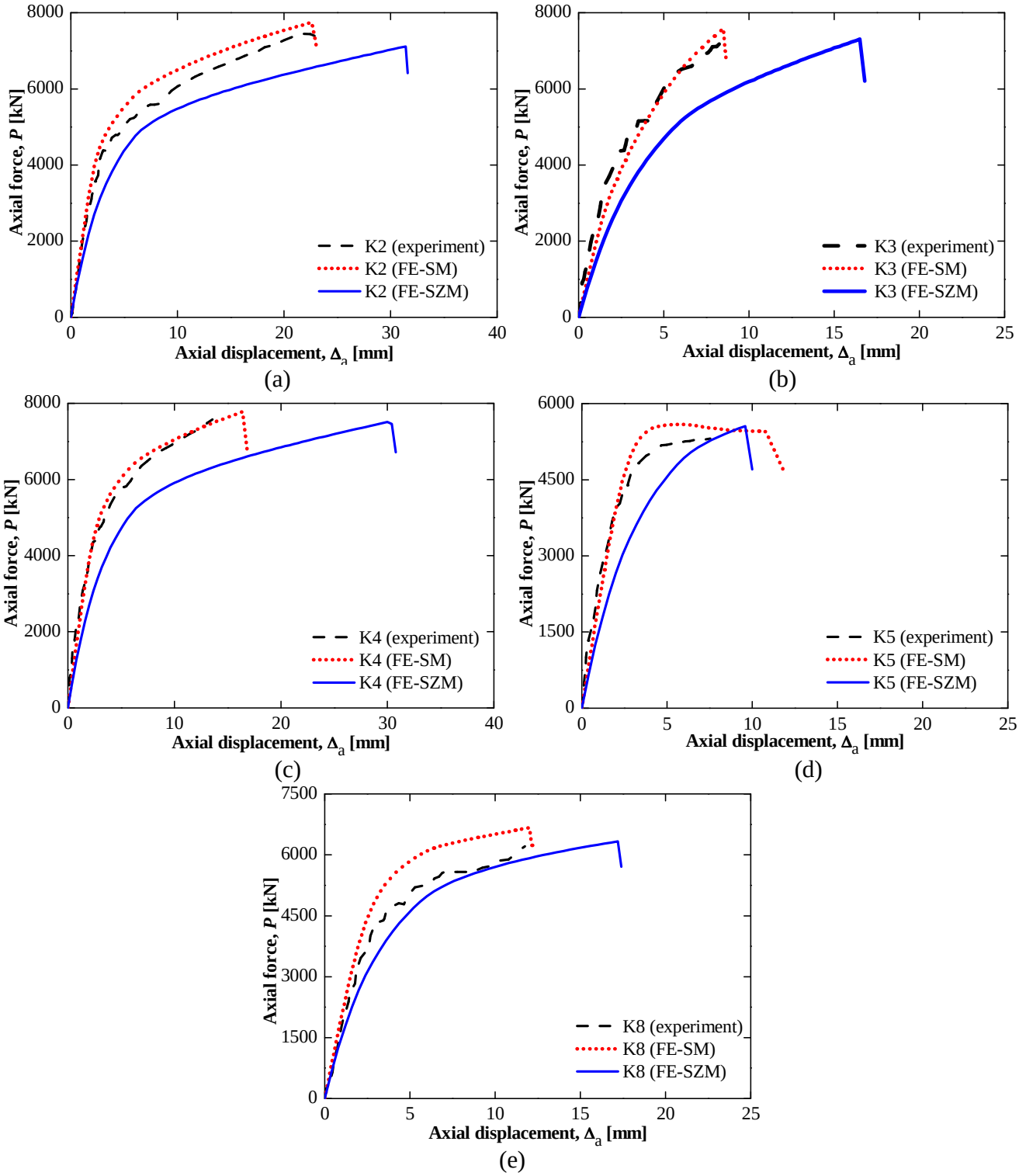

Figure A.12 - Comparison between experimental and numerical result for FRP-confined RC column subjected to concentric axial loading in [66]: force-displacement response (a) K2 specimen, (b) K3 specimen, (c) K4 specimen, (d) K5 specimen, (e) K8 specimen

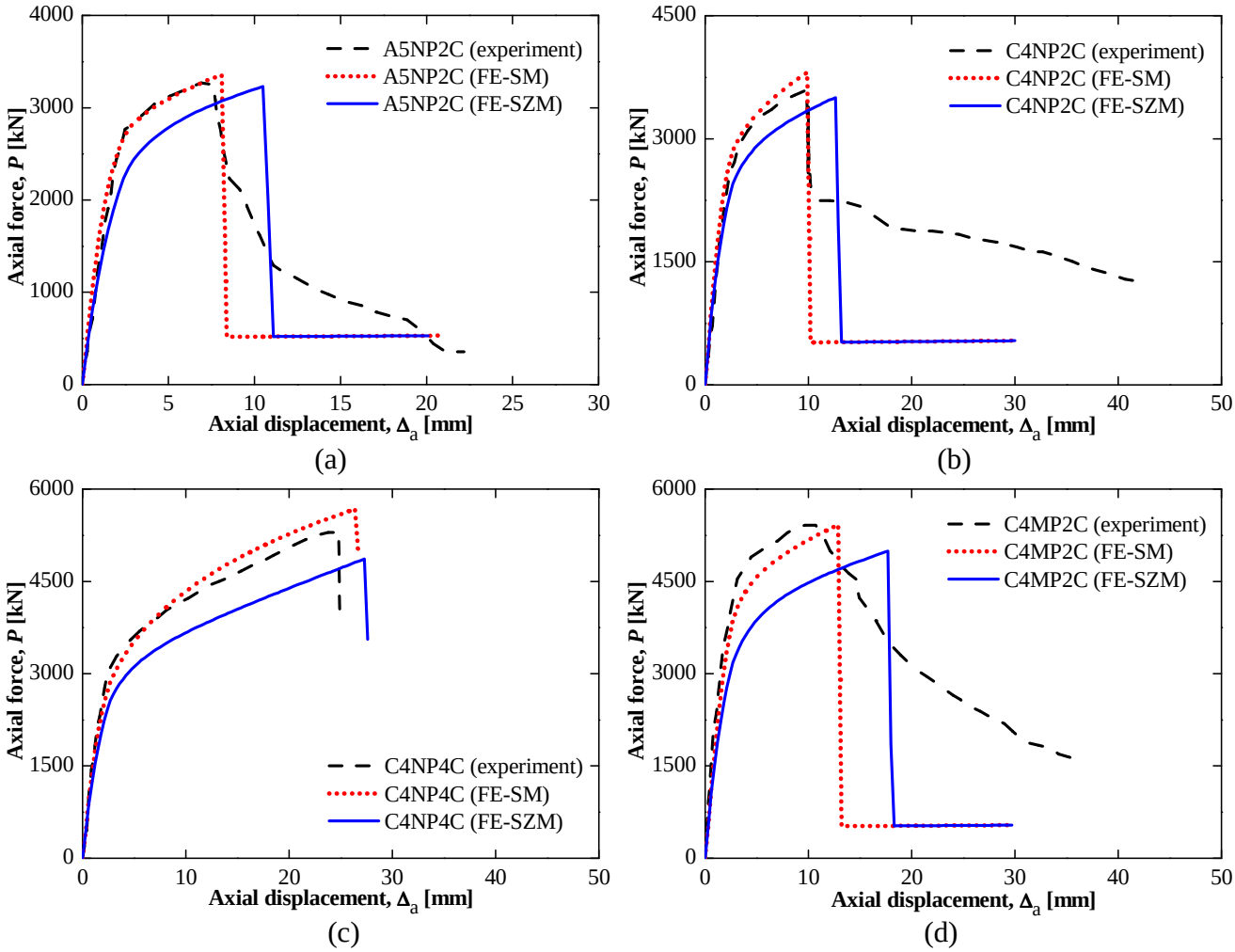

Figure A.13 - Comparison between experimental and numerical results for FRP-confined RC columns subjected to concentric axial loading in [67]: force-displacement response (a) A5NP2C specimen, (b) C4NP2Cspecimen, (c) C4NP4C specimen, (d) C4MP2C specimen

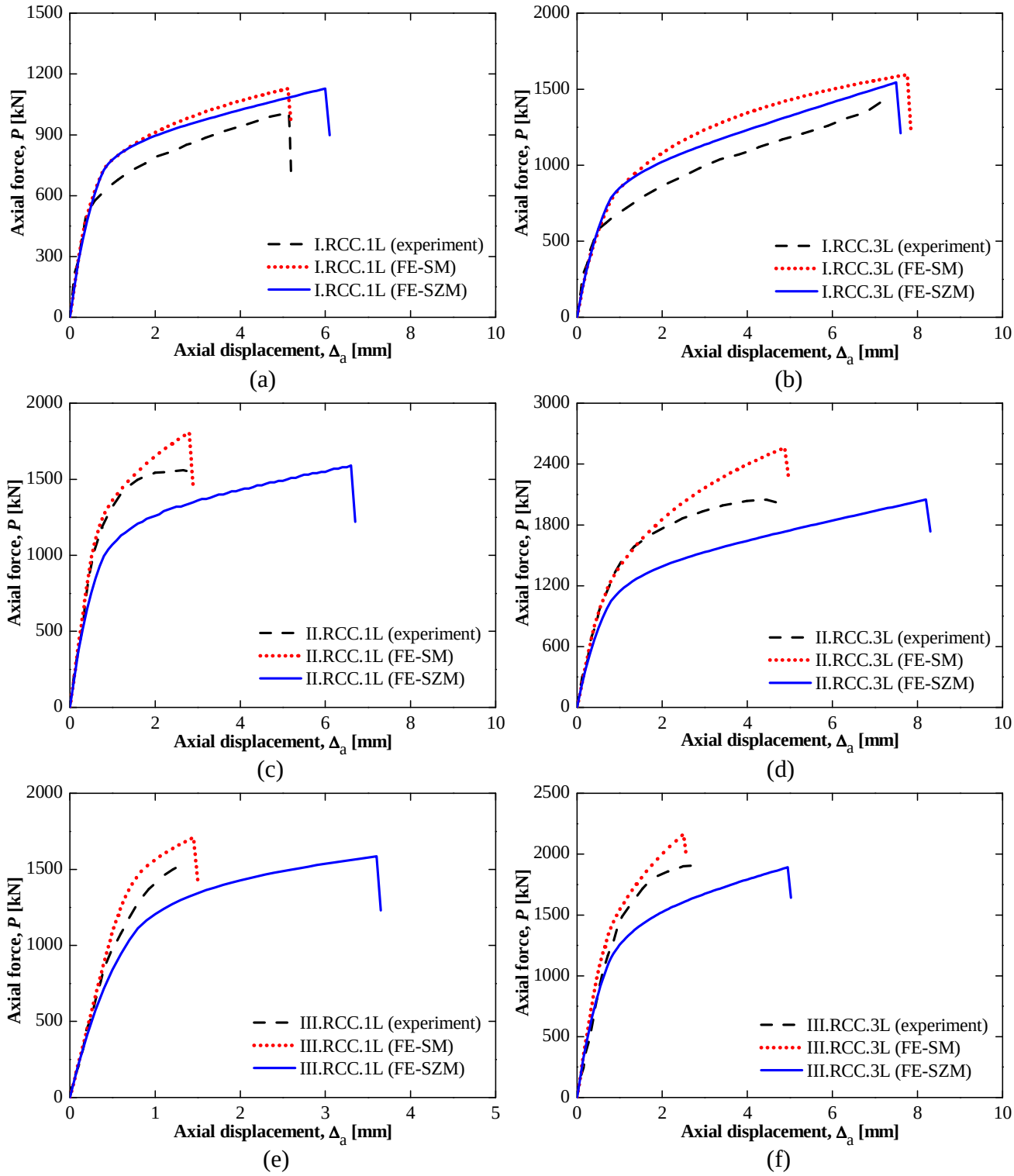

Figure A.14 - Comparison between experimental and numerical results for FRP-confined RC columns subjected to concentric axial loading in [68]: force-displacement response (a) I.RCC.1L specimen, (b) I.RCC.3L specimen, (c) II.RCC.1L specimen, (d) II.RCC.3L specimen, (e) III.RCC.1L specimen, (f) III.RCC.3L specimen

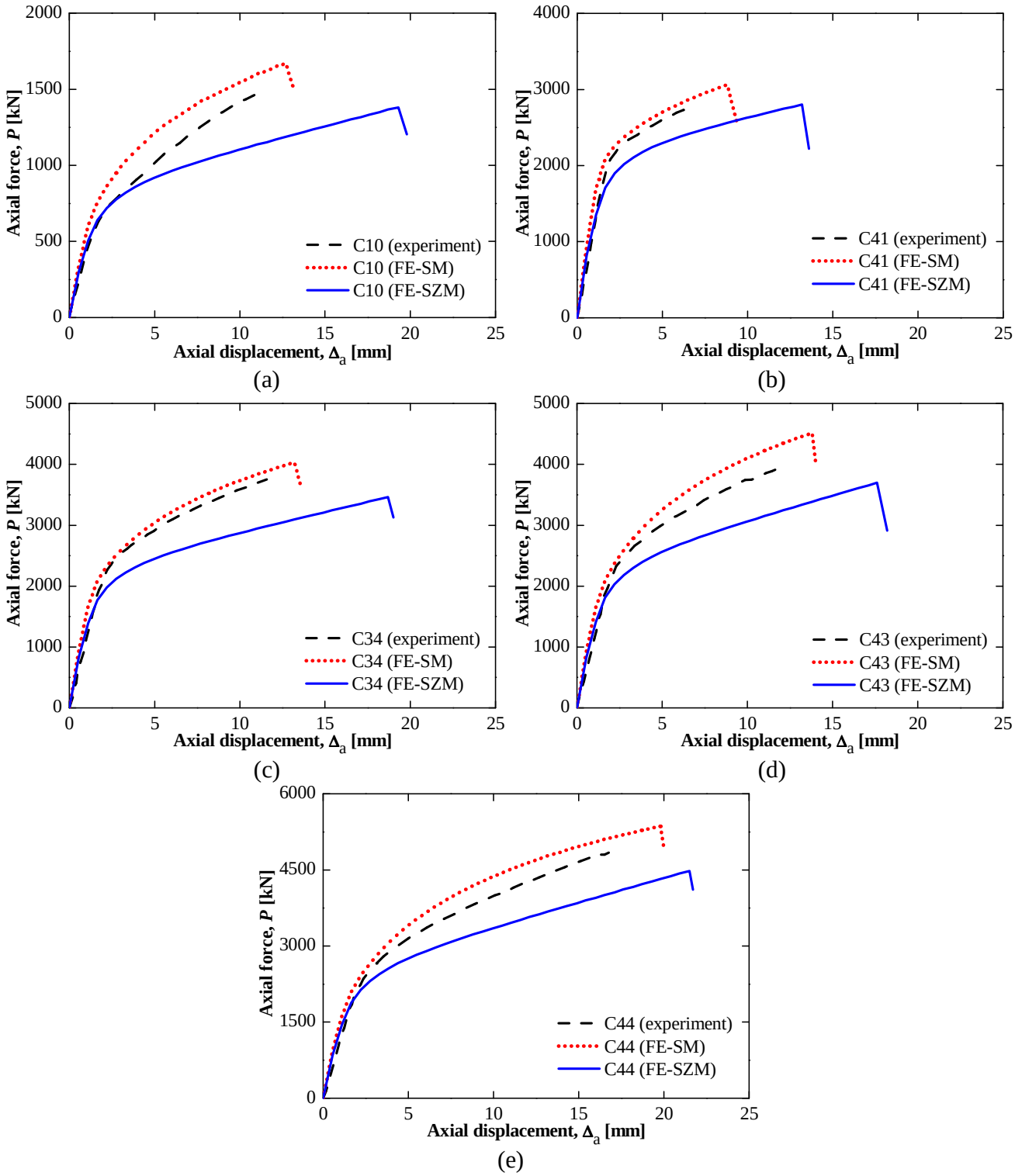

Figure A.15 - Comparison between experimental and numerical results for FRP-confined RC columns subjected to concentric axial loading in [69]: force-displacement response (a) C10 specimen, (b) C41 specimen, (c) C34 specimen, (d) C43 specimen, (e) C44 specimen

Figure A.16 to A.23 show the comparisons of the experimental and FE simulated force-displacement responses of the RC columns subjected to eccentric axial loading.

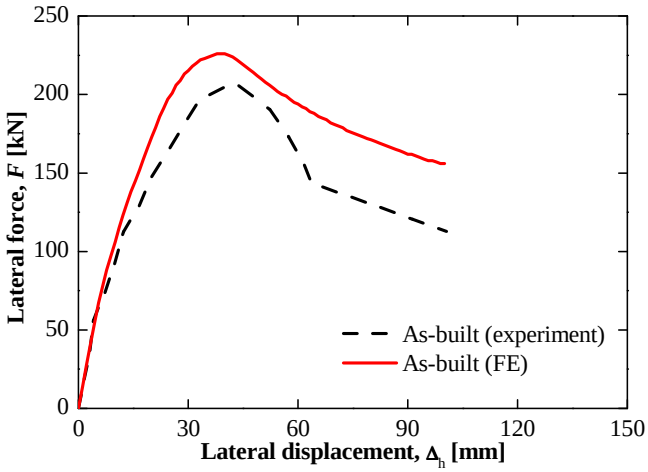

Figure A.16 - Comparison between experimental and numerical result for RC column subjected to eccentric axial loading in [3]: lateral force-displacement response

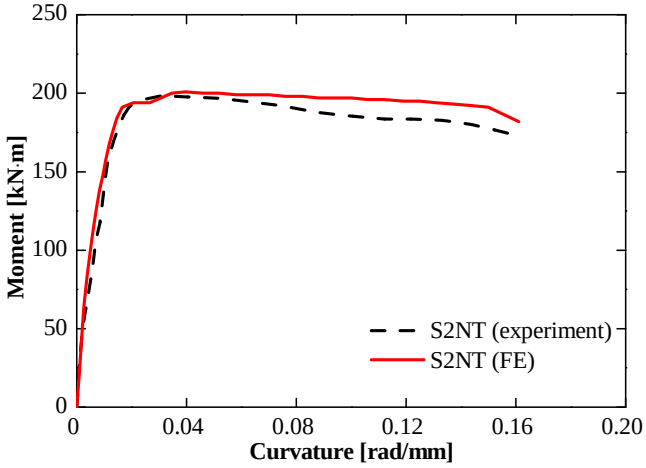

(a)

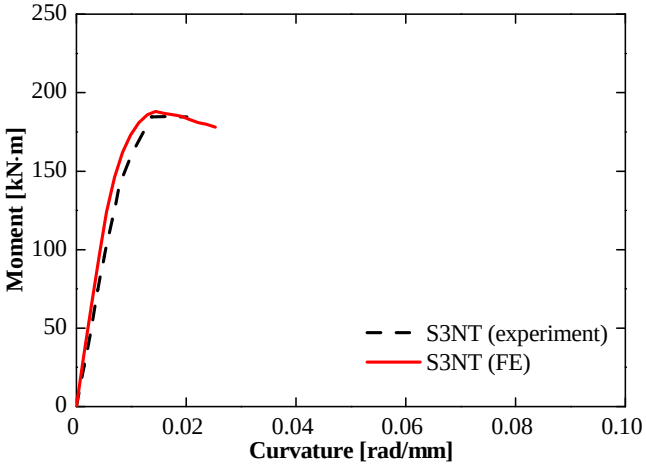

(b)

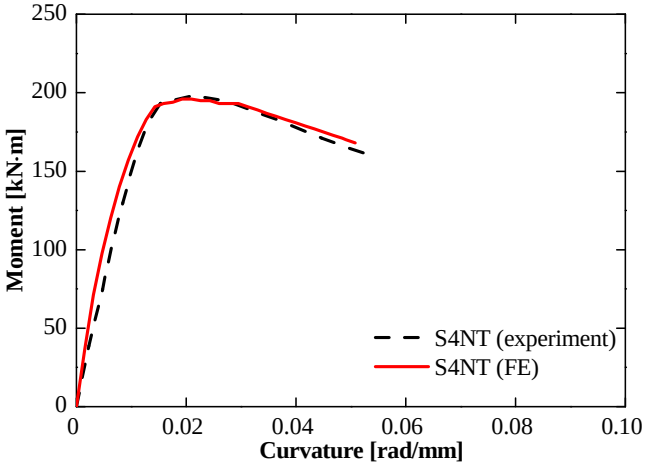

(c)

Figure A.17 - Comparison between experimental and numerical results for RC columns subjected to eccentric axial loading in [60]: moment-curvature response (a) S2NT specimen, (b) S3NT specimen, (c) S4NT specimen

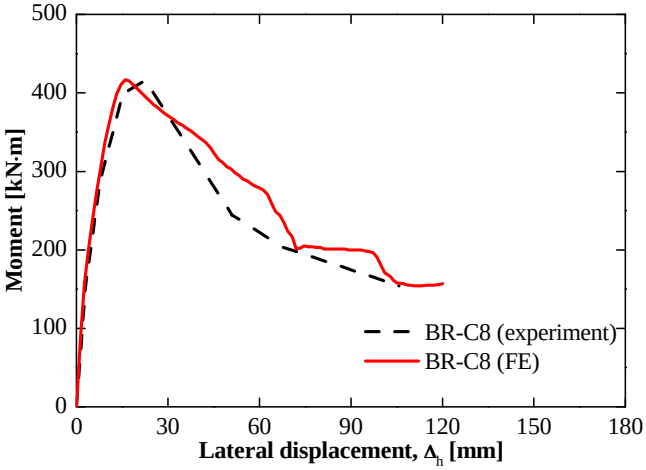

Figure A.18 - Comparison between experimental and numerical result for RC column subjected to eccentric axial loading in [65]: moment-displacement response

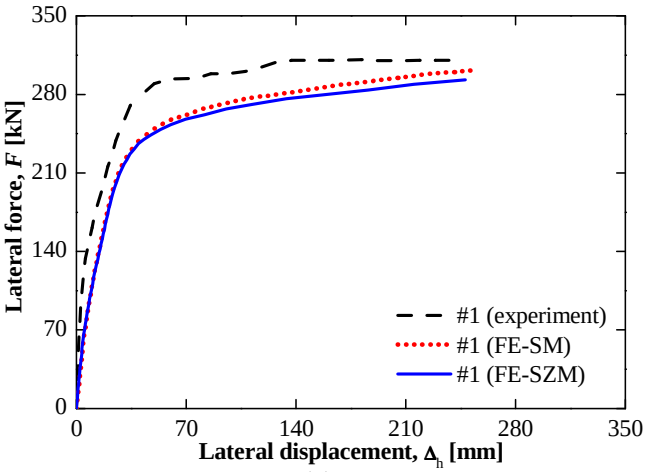

(a)

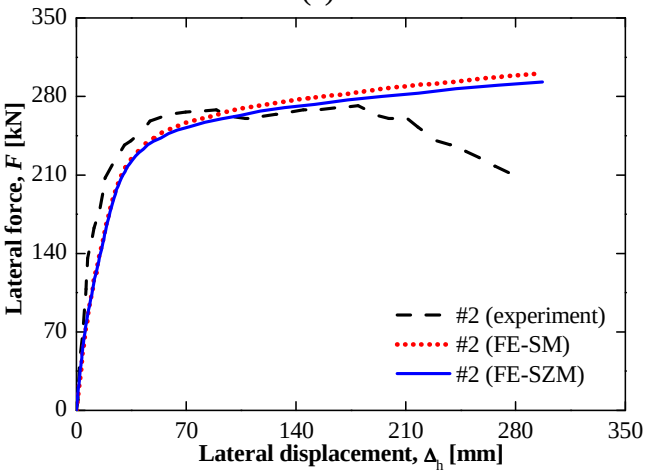

(b)

Figure A.19 - Comparison between experimental and numerical results for FRP-confined RC columns subjected to eccentric axial loading in [3]: lateral force-displacement response (a) #1 specimen，(b) #2 specimen

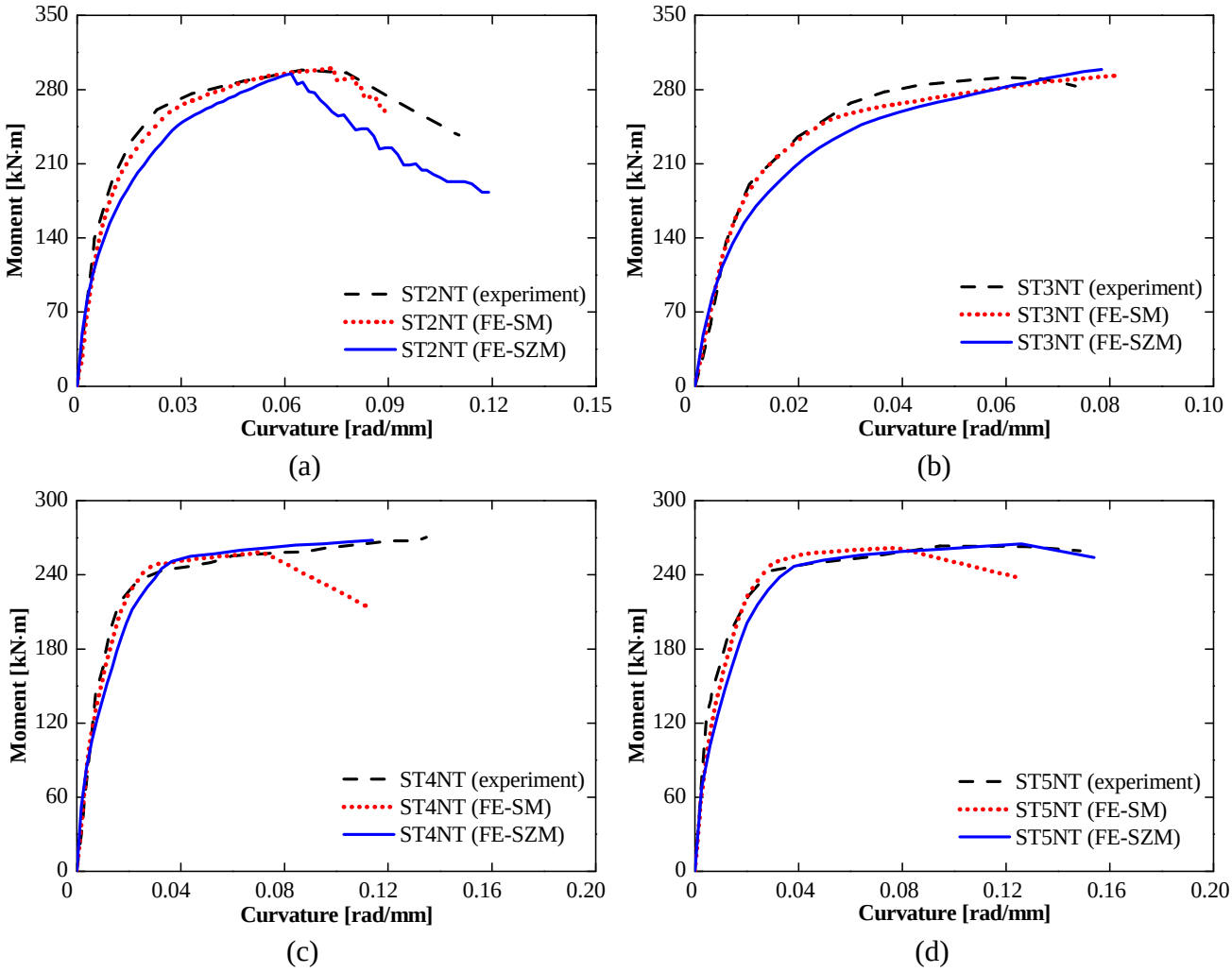

Figure A.20 - Comparison between experimental and numerical results for FRP-confined RC columns subjected to eccentric axial loading in [60]: moment-curvature response (a) ST2NT specimen, (b) ST3NT specimen, (c) ST4NT specimen, (d) ST5NT specimen

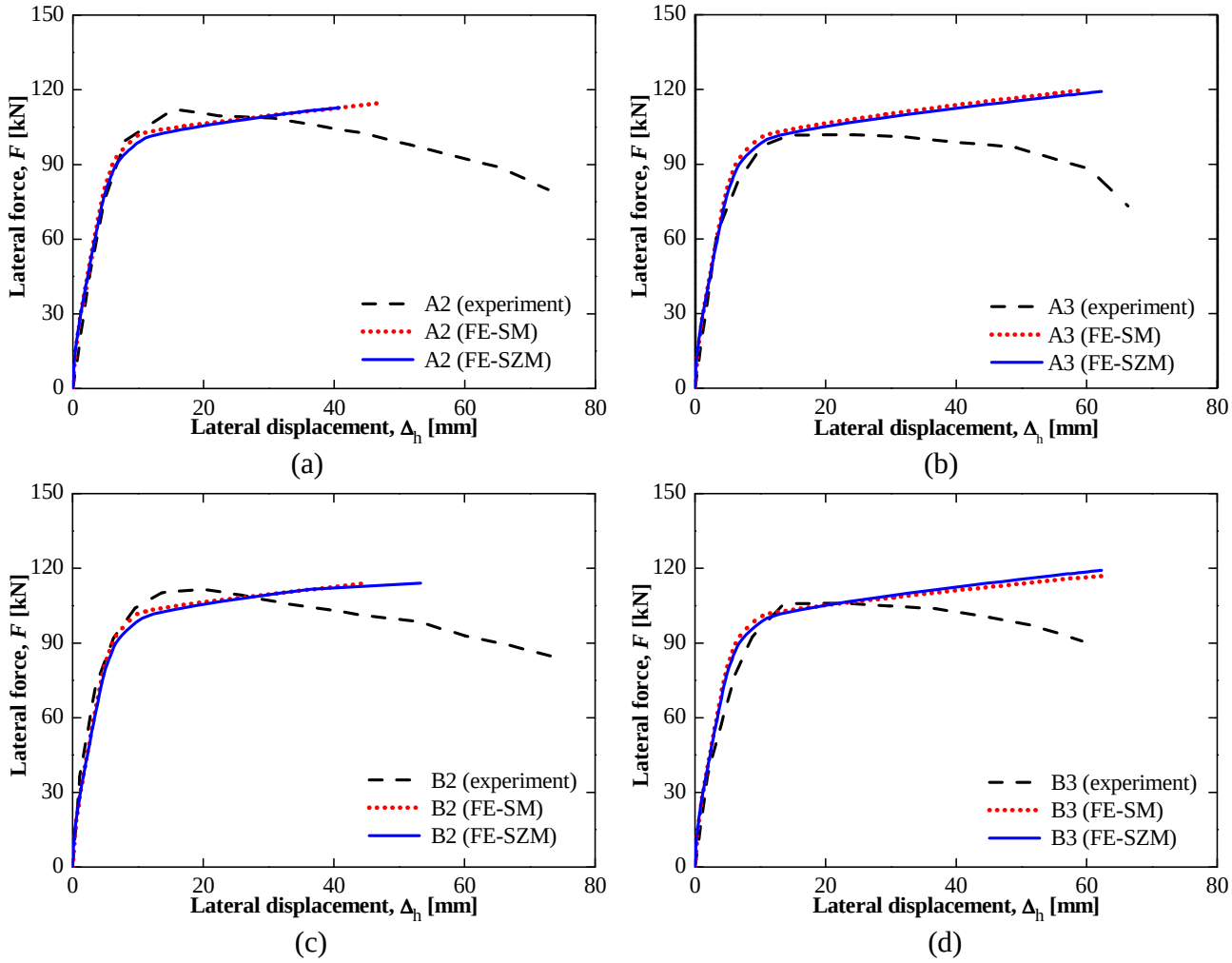

Figure A.21 - Comparison between experimental and numerical results for FRP-confined RC columns subjected to eccentric axial loading in [74]: lateral force-displacement response (a) A2 specimen, (b) A3 specimen, (c) B2 specimen, (d) B3 specimen

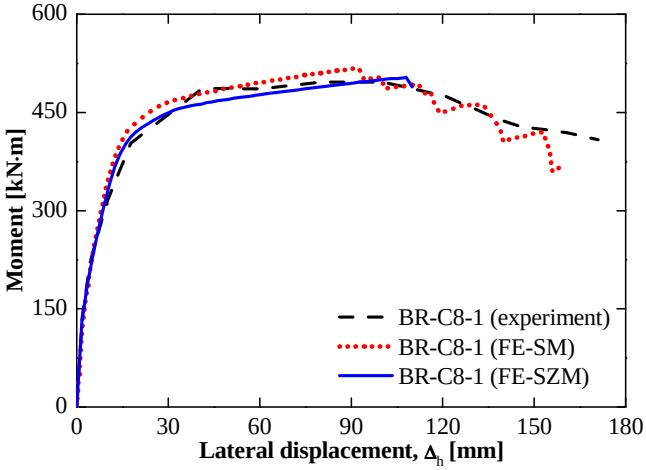

(a)

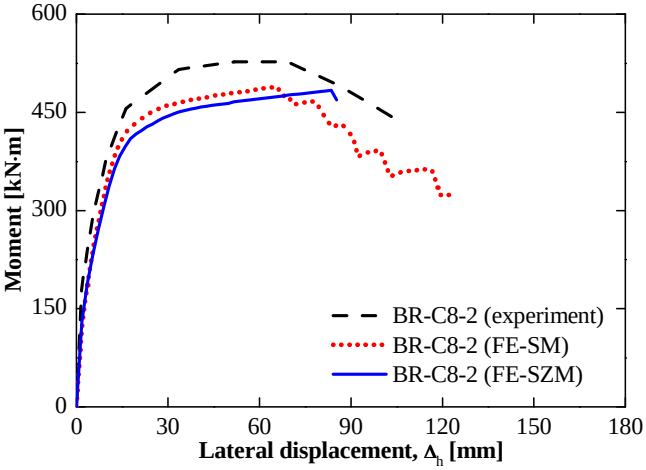

(b)

Figure A.22 - Comparison between experimental and numerical results for FRP-confined RC columns subjected to eccentric axial loading in [75]: moment-displacement response (a) BR-C8-1 specimen, (b) BR-C8-2 specimen

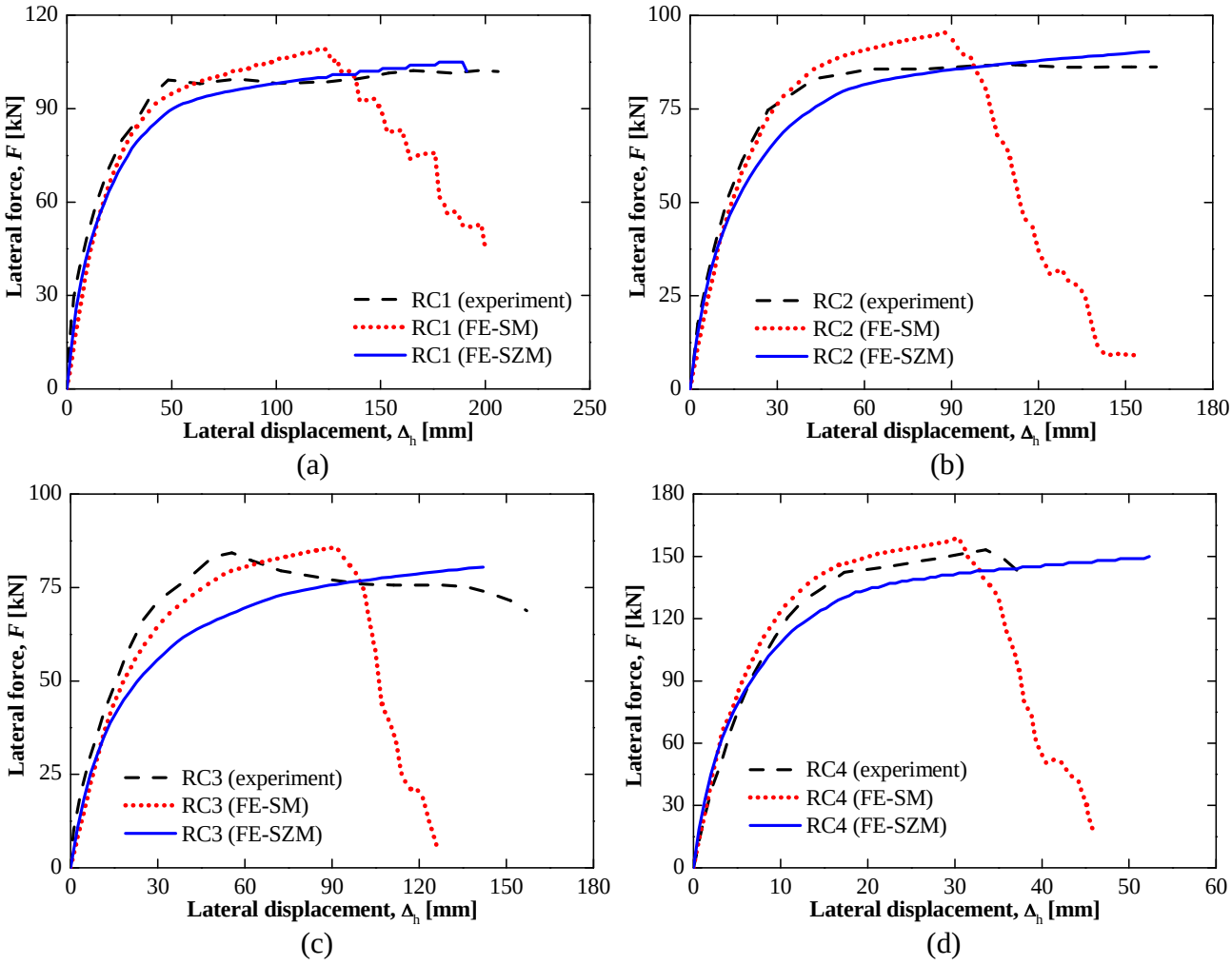

Figure A.23 - Comparison between experimental and numerical results for FRP-confined RC columns subjected to eccentric axial loading in [76]: lateral force-displacement response (a) RC1 specimen, (b) RC2 specimen, (c) RC3 specimen, (d) RC4 specimen

APPENDIX B : EXTENSION OF THE FRAME FE TO FRP-CONFINED RC COLUMNS WITH RECTANGULAR SECTION

This appendix provides the comparison between experimentally recorded and numerically simulated force-displacement responses of several FRP-confined RC columns with square/rectangular cross-sections by using the material constitutive models discussed in the previous chapters of this thesis.

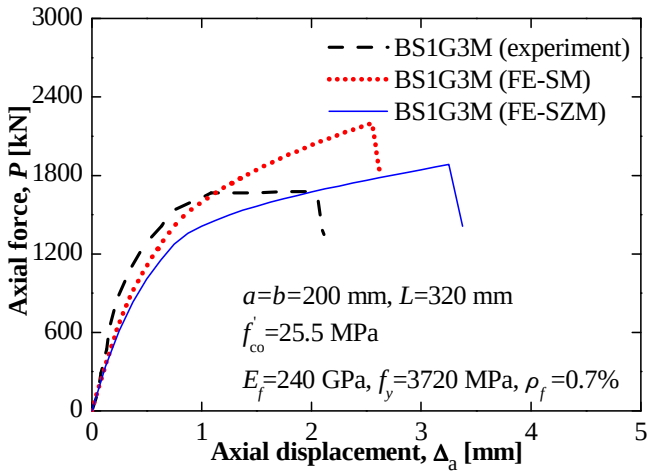

Figure B.1 - Comparison between experimental and numerical result for FRP-confined RC square column subjected to concentric axial loading in [84]: force-displacement response

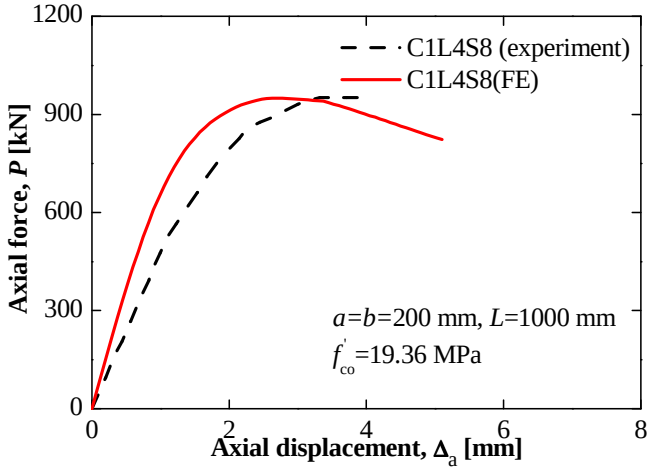

Figure B.2 - Comparison between experimental and numerical result for reference RC square column subjected to concentric axial loading in [85]: force-displacement response

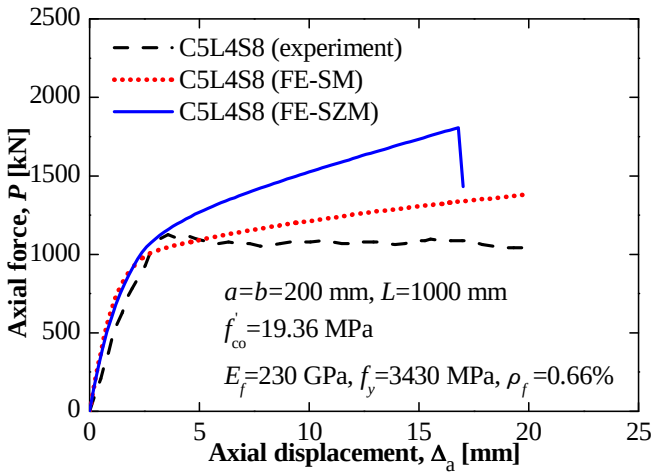

Figure B.3 - Comparison between experimental and numerical result for FRP-confined RC square column subjected to concentric axial loading in [85]: force-displacement response

APPENDIX C : FEDEASLAB CODE FOR CIRCULAR SECTIONAL ANALYSIS

```
function varargout = Sect19 (action,Sec_no,ndm,SecData,State)
% SECT19 2D response of RC circular section with integration over area
% varargout = Sect19 (action,Sec_no,ndm,SecData,State)
%
% varargout : variable return argument list
% varargout = SecData   for action 'chec'
% varargout = State for action 'init' with fields s, ks and Pres
% varargout = State for action 'stif' with updated fields s, ks and Pres
% varargout = State for action 'forc' with updated field  s     and Pres
% varargout = [s Post]  for action 'post'
%          where ks   = current section stiffness
%                  s    = current section force
%                Pres = data structure with current values of section history variables
%                Post = data structure with section post-processing information
% action    : switch with following possible values
%              'chec' section checks data for omissions
%              'data' section prints properties
%              'init' section initializes and reports history variables
%              'stif' section returns current stiffness and force
%              'forc' section returns current force only
%              'post' section stores information for post-processing
% Sec_no    : section number
% SecData   : data structure of section properties
% State     : current section state; data structure with updated fields e, Past and Pres
%     .e(:,1) : total section deformations
%     .e(:,2) : section deformation increments from last convergence
%     .e(:,3) : section deformation increments from last iteration
%     .e(:,4) : section deformation rates
%     .Past   : history variables at last convergence
%     .Pres   : history variables at last iteration

% ==========================================================================
% FEDEAS Lab - Release 2.3, March 2001
% Matlab Finite Elements for Design, Evaluation and Analysis of Structures
%
% Copyright (c) 1998, Professor Filip C. Filippou, filippou@ce.berkeley.edu
% Department of Civil and Environmental Engineering, UC Berkeley
% ==========================================================================
% Created by Dan Hu,2011

% Section Properties
% SecData.Re     : external radius
%       .Rc     : steel confined radius (Rc=Re-cov)
%       .Ri     : internal radius
%       .Ang  : angle
%       .nl1    : no of layers from internal radius to stirrups
%       .nl2    : no of layers from stirrups to external radius
```

```
%       .m      : no of subdivisions
%       .n      : no of steel bars
%       .IntTyp : integration type of section response
%       .As     : area of reinforcing steel
%       .cov    : cover of outside reinforcing steel
%       .MatName: array with material names
%       .MatData: data structure of material properties

% GLOBAL VARIABLES
global IOW;         % output file number
global HEAD_PR;     % header print indicator

% check section data, set default values, if any, and retrieve data
% ====================================================================
switch action
case 'chec'
   if (~isfield(SecData,'Ri'))       disp('Section');disp(Sec_no); error('internal radius missing');end
   if (~isfield(SecData,'Rc'))       disp('Section');disp(Sec_no); error('steel confined radius missing');end
   if (~isfield(SecData,'Re'))       disp('Section');disp(Sec_no); error('external radius missing');end
   if (~isfield(SecData,'MatName'))  disp('Section');disp(Sec_no); error('material name missing');end
   if (~isfield(SecData,'As'))       disp('Section');disp(Sec_no); error('area of reinforcing steel missing');end
   if (~isfield(SecData,'Ang'))      disp('Section');disp(Sec_no);
      warning('value of angle missing, 2*pi assumed');
      SecData.Ang = 2*pi;end
   if (~isfield(SecData,'nl1')) disp('Section');disp(Sec_no);
      warning('no of layers missing, 10 layers assumed');
      SecData.nl1 = 10;end
   if (~isfield(SecData,'nl2')) disp('Section');disp(Sec_no);
      warning('no of layers missing, 10 layers assumed');
      SecData.nl2 = 2;end
   if (~isfield(SecData,'m')) disp('Section');disp(Sec_no);
      warning('no of subdivisions missing, 12 subdivision assumed');
      SecData.m  = 12;end
   if (~isfield(SecData,'n')) disp('Section');disp(Sec_no);
      warning('no of steel bars missing, 12 subdivision assumed');
      SecData.n  = 12;end
   if (~isfield(SecData,'IntTyp')) disp('Section');disp(Sec_no);
      warning('integration type missing, midpoint assumed');
      SecData.IntTyp = 'Midpoint';end
   SecData.MatData{1} = feval (SecData.MatName(1,:),'chec',1,SecData.MatData{1});
   SecData.MatData{2} = feval (SecData.MatName(2,:),'chec',2,SecData.MatData{2});
   SecData.MatData{3} = feval (SecData.MatName(3,:),'chec',3,SecData.MatData{3});
   varargout = {SecData};
otherwise
   % extract section properties
   Ri     = SecData.Ri;     % internal radius
   Rc     = SecData.Rc;     % steel confined radius
   Re     = SecData.Re;     % external radius
   Ang    = SecData.Ang;    % Angle
   nl1    = SecData.nl1;    % no of layers from internal radius to stirrups
   nl2    = SecData.nl2;    % no of layers from stirrups to external radius
```

```
    m      = SecData.m;       % no of subdivisions
    n      = SecData.n;       % no of steel bars
    IntTyp  = SecData.IntTyp;  % integration type
    As     = SecData.As;          % area of reinforcing steel
    cov    = SecData.cov;         % cover of reinforcing steel
    MatName = SecData.MatName;  % array of material names
    MatData = SecData.MatData;      % material data
end
% section actions
% ========================================================================
switch action
case 'data'
    fprintf (IOW,'\n      Circular RC Layer Section');
    fprintf (IOW,'\n      Sec no     intRad      extRad      No_Layers');
    fprintf (IOW,'\n     %4d  %11.3e %11.3e    %4d', Sec_no,ri,re,nl);
    HEAD_PR = 1;
    feval (MatName(1,:),'data',1,   SecData.MatData{1});   % first m layers are the same, print only 1
    feval (MatName(2,:),'data',nl*m+1,SecData.MatData{2});
% ========================================================================
case 'init'
    % discretization of section
    patcoor1    = [0 Ri;0 Rc];
    patcoor2    = [0 Rc;0 Re];
    [yfib(1:nl1*m) Afib(1:nl1*m)] = CircularPatch_Layer (patcoor1,IntTyp,nl1,m);
    [yfib((nl1)*m+1:(nl1+nl2)*m) Afib((nl1)*m+1:(nl1+nl2)*m)] = CircularPatch_Layer
    (patcoor2,IntTyp,nl2,m);
    % initialize before assembly
    s  = zeros(ndm,1);         % current section force
    ks = zeros(ndm,ndm);    % current section stiffness

    % concrete layers
    for i=1:nl1*m
       as  = [1 -yfib(i)];
       MatState = feval (MatName(1,:),'init',i,MatData{1});
       s   = s  + Afib(i).*(as'*MatState.sig);
       ks  = ks + Afib(i).*(as'*MatState.Et*as);
       State.Pres.Mat{i} = MatState.Pres;
    end

    for i=(nl1)*m+1:(nl1+nl2)*m
       as  = [1 -yfib(i)];
       MatState = feval (MatName(2,:),'init',i,MatData{2});
       s   = s  + Afib(i).*(as'*MatState.sig);
       ks  = ks + Afib(i).*(as'*MatState.Et*as);
       State.Pres.Mat{i} = MatState.Pres;
    end

    % steel reinforcing layers
    betastr = pi/n;
    betaend = pi*(2*n-1)/n;
    beta    = linspace(betastr,betaend,n);
```

```
    sfib    = zeros(n,1);
    for j=1:n
       sfib(j) = (Re-cov-(As/pi)^0.5)*sin(beta(1,j));
       as  = [1 -sfib(j)];
       MatState = feval (MatName(3,:),'init',i+j,MatData{3});
       s   = s  + As.*(as'*MatState.sig);
       ks  = ks + As.*(as'*MatState.Et*as);
       State.Pres.Mat{i+j} = MatState.Pres;
    end

    State.s   = s;
    State.ks  = ks;
    varargout = {State};
% ========================================================================
case {'stif','forc'}
    % discretization of section
    patcoor1     = [0 Ri;0 Rc];
    patcoor2     = [0 Rc;0 Re];
    [yfib(1:nl1*m) Afib(1:nl1*m)] = CircularPatch_Layer (patcoor1,IntTyp,nl1,m);
    [yfib((nl1)*m+1:(nl1+nl2)*m) Afib((nl1)*m+1:(nl1+nl2)*m)] = CircularPatch_Layer
    (patcoor2,IntTyp,nl2,m);

    % initialize before assembly
    s  = zeros(ndm,1);
    ks = zeros(ndm,ndm);

    % concrete layers
    for i=1:nl1*m
       as  = [1 -yfib(i)];
       MatState.eps  = as*State.e;
       MatState.Pres = State.Pres.Mat{i};
       MatState.Past = State.Past.Mat{i};
       MatState = feval (MatName(1,:),'stif',i,MatData{1},MatState);
       s   = s  + Afib(i).*(as'*MatState.sig);
       ks  = ks + Afib(i).*(as'*MatState.Et*as);
       State.Pres.Mat{i} = MatState.Pres;
    end

    for i=(nl1)*m+1:(nl1+nl2)*m
       as  = [1 -yfib(i)];
       MatState.eps  = as*State.e;
       MatState.Pres = State.Pres.Mat{i};
       MatState.Past = State.Past.Mat{i};
       MatState = feval (MatName(2,:),'stif',i,MatData{2},MatState);
       s   = s  + Afib(i).*(as'*MatState.sig);
       ks  = ks + Afib(i).*(as'*MatState.Et*as);
       State.Pres.Mat{i} = MatState.Pres;
    end

    % steel reinforcing layer
    betastr = pi/n;
```

```
    betaend = pi*(2*n-1)/n;
    beta    = linspace(betastr,betaend,n);
    sfib    = zeros(n,1);
    for j=1:n
       sfib(j) = (Re-cov-(As/pi)^0.5)*sin(beta(1,j));
       as  = [1 -sfib(j)];
       MatState.eps  = as*State.e;
       MatState.Pres = State.Pres.Mat{i+j};
       MatState.Past = State.Past.Mat{i+j};
       MatState = feval (MatName(3,:),'stif',i+j,MatData{3},MatState);
       s   = s  + As.*(as'*MatState.sig);
       ks  = ks + As.*(as'*MatState.Et*as);
       State.Pres.Mat{i+j} = MatState.Pres;
    end

    State.s   = s;
    if (action=='stif') State.ks  = ks; end
    varargout = {State};
% ========================================================================
case 'post'
    % discretization of section
    patcoor1     = [0 Ri;0 Rc];
    patcoor2     = [0 Rc;0 Re];
    [yfib(1:nl1*m) Afib(1:nl1*m)] = CircularPatch_Layer (patcoor1,IntTyp,nl1,m);
    [yfib((nl1)*m+1:(nl1+nl2)*m) Afib((nl1)*m+1:(nl1+nl2)*m)] = CircularPatch_Layer
    (patcoor2,IntTyp,nl2,m);

    s  = zeros(ndm,1);      % initialize before assembly

    % concrete core
    for i=1:nl1*m
       as = [1 -yfib(i)];
       MatState.eps  = as*State.e;
       MatState.Pres = State.Pres.Mat{i};
       MatState.Past = State.Past.Mat{i};
       [sig Post.Mat{i}] = feval (MatName(1,:),'post',i,MatData{1},MatState);
       s = s  + Afib(i).*(as'*sig);
    end

    for i=(nl1)*m+1:(nl1+nl2)*m
       as = [1 -yfib(i)];
       MatState.eps  = as*State.e;
       MatState.Pres = State.Pres.Mat{i};
       MatState.Past = State.Past.Mat{i};
       [sig Post.Mat{i}] = feval (MatName(2,:),'post',i,MatData{2},MatState);
       s = s  + Afib(i).*(as'*sig);
    end

    % steel reinforcing layer
    betastr = pi/n;
    betaend = pi*(2*n-1)/n;
```

```
    beta    = linspace(betastr,betaend,n);
    sfib    = zeros(n,1);
    for j=1:n
       sfib(j) = (Re-cov-(As/pi)^0.5)*sin(beta(1,j));
       as  = [1 -sfib(j)];
       MatState.eps  = as*State.e;
       MatState.Pres = State.Pres.Mat{i+j};
       MatState.Past = State.Past.Mat{i+j};
       [sig Post.Mat{i+j}] = feval (MatName(3,:),'post',i+j,MatData{3},MatState);
       s   = s  + As.*(as'*sig);
    end

    % add section post-processing information
    Post.e = State.e(:,1);
    Post.s = s;
    varargout = {s Post};
otherwise
    % add further actions
end
```

APPENDIX D : FEDEASLAB CODE FOR RESPONSE COMPUTATION FOR MANDER MODEL AND THE SM MODEL

```
function varargout = Mate12 (action,Mat_no,MatData,State)
% MATE12 cyclic stress-strain relation for confined concrete
% ========================================================================
% FEDEAS Lab - Release 2.3, March 2001
% Matlab Finite Elements for Design, Evaluation and Analysis of Structures
%
% Copyright (c) 1998, Professor Filip C. Filippou, filippou@ce.berkeley.edu
% Department of Civil and Environmental Engineering, UC Berkeley
% ========================================================================

% Material Properties of unconfined concrete
% MatData.fc0  : concrete compressive strength
%       .ec0  : strain at compressive strength
%       .Ec   : initial tangent modulus
%       .beta : constant relating Ec with Esec
%       .nu   : Poisson's ratio
%       .elim : limit axial strain beyond which microcracking starts to occur
%       .alpha: constant relating ec0 with the axial at volume strain equal zero
%       .eult : ultimate strain
%
% Confining Properties
% MatData.type_conf  : type of confinement ('unconf','steel','FRP')
%       .sect_shape : section shape ('oval','rect')
%       .reinf_disp : reinforcement disposition ('cont', 'discont')
%
% Material Properties of confined concrete
% MatData.kg   : arching-effect coeff.
%       .roj  : transverse FRP or steel volumetric ratio
%       .Ej   : FRP or steel Young modulus
%       .fy   : steel yield strength
%       .fjult: ultimate FRP strength
%       .ejult: ultimate FRP or steel strain
%       .ks   : corner curvature coeff.

% Material History Variables
% State._.sig  : stress
%       .Et   : tangent modulus
%       .eps  : strain
%       .emin : minimum strain (compression)
%       .eunl : strain at stress equal zero
%       .Eunl : unloading-reloading modulus
%       .sunl : unloading stress
%       .ecc  : strain at peach strength
%       .fcc  : peak strength
%       .fl   : confinement pressure
%       .elunl: unloading lateral strain
%       .flunl: unloading lateral stress
```

```
%       .muunl: unloading Del to De ratio

global IOW;       % output file number
global HEAD_PR;   % header print indicator

% check material data, set default values, if any, and retrieve data
% ========================================================================
switch action
case 'chec'
  if (~isfield(MatData,'ec0')) MatData.ec0 = -0.002; end
  if (~isfield(MatData,'Ec'))  disp('Material');disp(Mat_no); error('tangent modulus missing'); end
  if (~isfield(MatData,'fc0')) disp('Material');disp(Mat_no); error('compressive strength missing'); end
  if (~isfield(MatData,'beta')) MatData.beta = (MatData.Ec/abs(MatData.fc0)-1/abs(MatData.ec0)); end
  if (~isfield(MatData,'type_conf')) disp('Material');disp(Mat_no); error('confinement type missing'); end
  switch MatData.type_conf
  case 'unconf'
    if (~isfield(MatData,'nu'))    MatData.nu = 0.2; end
    if (~isfield(MatData,'alpha')) MatData.alpha = 0.9; end
    if (~isfield(MatData,'elim')) MatData.elim = -0.001; end
    if (~isfield(MatData,'eult')) MatData.eult = -0.005; end
  case 'steel'
    if (~isfield(MatData,'Ej')) disp('Material');disp(Mat_no); error('steel Young''s modulus missing'); end
    if (~isfield(MatData,'fy')) disp('Material');disp(Mat_no); error('steel yield strength missing'); end
    if (~isfield(MatData,'roj')) disp('Material');disp(Mat_no); error('transverse steel volumetric ratio
missing'); end
    if (~isfield(MatData,'kg')) MatData.kg = 0.8; end
    if (~isfield(MatData,'ks')) MatData.ks = 1; end
    if (~isfield(MatData,'ejult')) MatData.ejult = 0.1; end
    flmax    = 0.5*MatData.kg*MatData.ks*MatData.roj*MatData.fy;
    fccmax = (2.254*(1+7.94*flmax/abs(MatData.fc0))^0.5-2*flmax/abs(MatData.fc0)-1.254)*
              abs(MatData.fc0);
    MatData.eult = -0.004 - 1.4*MatData.roj*MatData.fy*MatData.ejult/fccmax;
    % Priestley equation (based on energy-balance method)
  case 'FRP'
    if (~isfield(MatData,'Ej')) disp('Material');disp(Mat_no); error('FRP Young''s modulus missing'); end
    if (~isfield(MatData,'fjult')) disp('Material');disp(Mat_no); error('FRP ultimate strenght missing'); end
    if (~isfield(MatData,'ejult')) disp('Material');disp(Mat_no); error('FRP ultimate strain missing'); end
    if (~isfield(MatData,'tj')) disp('Material');disp(Mat_no); error('FRP thickness missing'); end
    if (~isfield(MatData,'sect_shape')) disp('Material');disp(Mat_no); error('section shape missing'); end
    switch MatData.sect_shape
    case 'oval'
      if (~isfield(MatData,'a')) disp('Material');disp(Mat_no); error('a semi-axis missing'); end
      if (~isfield(MatData,'b')) disp('Material');disp(Mat_no); error('b semi-axis missing'); end
      MatData.Dj = 4*MatData.a*MatData.b/(1.5*(MatData.a+MatData.b)-(MatData.a*MatData.b)^0.5);
      MatData.ks = 1;
    case 'rect'
      if (~isfield(MatData,'a')) disp('Material');disp(Mat_no); error('a dimension missing'); end
      if (~isfield(MatData,'b')) disp('Material');disp(Mat_no); error('b dimension missing'); end
      MatData.Dj = max(MatData.a,MatData.b);
      if (~isfield(MatData,'Rc')) disp('Material');disp(Mat_no); error('Rc curvature missing'); end
      MatData.ks = 2*MatData.Rc/MatData.Dj;
```

```
    end
    MatData.roj = 4*MatData.tj/MatData.Dj;
    if (~isfield(MatData,'reinf_disp')) disp('Material');disp(Mat_no); error('reinforcement disposition
missing'); end
    switch MatData.reinf_disp
    case 'cont'
      MatData.kg = 1;
    case 'discont'
      if (~isfield(MatData,'s')) disp('Material');disp(Mat_no); error('reinforcement spacing missing'); end
      MatData.kg = (1-0.5*MatData.s/MatData.Dj)^2/(1-MatData.roj);
    end
  otherwise
    % no further options are currently supported
  end
  varargout = {MatData};

otherwise
  % extract material properties
  fc0   = MatData.fc0;
  Ec    = MatData.Ec;
  ec0   = MatData.ec0;
  beta  = MatData.beta;
  type_conf = MatData.type_conf;
  switch type_conf
  case 'unconf'
    nu    = MatData.nu;
    alpha = MatData.alpha;
    elim  = MatData.elim;
    eult  = MatData.eult;
  case 'steel'
    Ej    = MatData.Ej;
    fy    = MatData.fy;
    roj   = MatData.roj;
    ks    = MatData.ks;
    kg    = MatData.kg;
    eult  = MatData.eult;
  case 'FRP'
    Ej    = MatData.Ej;
    fjult = MatData.fjult;
    ejult = MatData.ejult;
    Dj    = MatData.Dj;
    ks    = MatData.ks;
    roj   = MatData.roj;
    kg    = MatData.kg;
  otherwise
  end
end


% material actions
% ========================================================================
```

```
switch action
case 'data'
  if (HEAD_PR)
    fprintf (IOW,'\n              Confined Concrete Material Model');
    fprintf (IOW,'\n              Mat no       fc0          ec0          Ec');
  end
  fprintf (IOW,'\n              %4d   %11.3e  %11.3e  %11.3e', Mat_no,fc0,ec0,Ec);
% ======================================================================
case 'init'
  sig  = 0;
  Et   = Ec;
  State.sig  = sig;
  State.Et   = Et;
  State.Pres.sig  = sig;
  State.Pres.Et   = Et;
  switch type_conf
  case 'unconf'
    State.Pres.emin = 0;
    State.Pres.eunl = 0;
    State.Pres.Eunl = fc0/ec0;
    State.Pres.sunl = 0;
  case 'steel'
    State.Pres.emin  = 0;
    State.Pres.eunl  = 0;
    State.Pres.Eunl  = fc0/ec0;
    State.Pres.sunl  = 0;
    State.Pres.el    = 0;
    State.Pres.ecc   = ec0;
    State.Pres.fl    = 0;
    State.Pres.flunl = 0;
  case 'FRP'
    State.Pres.emin  = 0;
    State.Pres.eunl  = 0;
    State.Pres.Eunl  = fc0/ec0;
    State.Pres.sunl  = 0;
    State.Pres.el    = 0;
    State.Pres.ecc   = ec0;
    State.Pres.fcc   = fc0;
    State.Pres.fl    = 0;
    State.Pres.flunl = 0;
    State.Pres.elunl = 0;
    State.Pres.muunl = 0;
  otherwise
  end
  varargout = {State};
% ======================================================================
case {'stif','forc'}
  % extract material properties
  fc0   = MatData.fc0;
  Ec    = MatData.Ec;
  ec0   = MatData.ec0;
```

```
beta  = MatData.beta;
type_conf = MatData.type_conf;
switch type_conf
case 'unconf'
  nu    = MatData.nu;
  alpha  = MatData.alpha;
  elim   = MatData.elim;
  eult   = MatData.eult;
case 'steel'
  Ej    = MatData.Ej;
  fy    = MatData.fy;
  roj   = MatData.roj;
  ks    = MatData.ks;
  kg    = MatData.kg;
  eult   = MatData.eult;
case 'FRP'
  Ej    = MatData.Ej;
  fjult  = MatData.fjult;
  ejult  = MatData.ejult;
  Dj    = MatData.Dj;
  ks    = MatData.ks;
  roj   = MatData.roj;
  kg    = MatData.kg;

otherwise
end
% Retrieve history variables from Past
sigp = State.Past.sig;
Ep   = State.Past.Et;
eps  = State.eps(1,1); % total strain
De   = State.eps(1,2); % total strain increment

switch type_conf
case 'unconf'
  % Retrieve history variables from Past
  emin = State.Past.emin;
  eunl = State.Past.eunl;
  Eunl = State.Past.Eunl;
  sunl = State.Past.sunl;
  % State determination
  if (De == 0)    % total strain is not changing
    sig = sigp;
    Et  = Ep;
  else
    if (eps <= eult) | (emin <= eult)  % material strength is failed
      sig = 0;
      Et  = 0;
      emin = min(eps,emin);
    else                          % material streng is not failed
      if (De < 0) % negative strain increment: loading
        if ((emin == 0)& eps < 0) % virgin material
```

```
            [sig,Et] = Unconfined_Envelope (MatData,eps,sigp,De);
          else % non-virgin material
            if (eps > eunl) % closure of a previously open crack
              sig = 0;
              Et  = 0;
            elseif (eps < emin) % the strain increment brings back on the envelope
              if eps-De > emin
                sigp = sunl;
                De   = eps-emin;
              end
              [sig,Et] = Unconfined_Envelope (MatData,eps,sigp,De);
            else % loading inside the envelope
              sig = Eunl*(eps-eunl);
              Et  = Eunl;
            end
          end
        else % positive strain increment: unloading (De > 0)
          if ((eps-De) < emin)    % unloading from the envelope
            emin = eps-De;
            Eunl = Ec*(abs(sigp/(Ec*ec0))+0.57)/(abs(emin/ec0)+0.57);
            sunl = sigp;
            eunl = emin-sunl/Eunl;
            sig  = Eunl*(eps-eunl);
            Et   = Eunl;
          elseif (eps > eunl)     % crack has opened
            sig = 0;
            Et  = 0;
          else                    % unloading inside the envelope
            sig  = Eunl*(eps-eunl);
            Et   = Eunl;
          end
        end
      end
    end
    % save history variables
    State.Pres.sig  = sig;
    State.Pres.Et   = Et;
    State.Pres.emin = emin;
    State.Pres.eunl = eunl;
    State.Pres.Eunl = Eunl;
    State.Pres.sunl = sunl;

  case 'steel'
    % Retrieve history variables from Past
    emin  = State.Past.emin;
    eunl  = State.Past.eunl;
    Eunl  = State.Past.Eunl;
    sunl  = State.Past.sunl;
    el    = State.Past.el;
    ecc   = State.Past.ecc;
    flp   = State.Past.fl;
```

```
flunl = State.Past.flunl;
% State determination
if (De == 0)    % total strain is not changing
  sig = sigp;
  Et  = Ep;
  fl  = flp;
else          % total strain is changing
  if (eps <= eult) | (emin <= eult)  % material strength is failed
    sig  = 0;
    Et   = 0;
    emin = min(eps,emin);
    fl   = 0;
  else                        % material strength is not failed
    if (De < 0) % negative strain increment: loading
      if ((emin == 0)& eps <= 0) % virgin material
        [fc,el,fl,ecc]= Conf_Pressure(fc0,flp,ec0,Ec,eps,beta,roj,Ej,ks,kg);
        fs=Ej*el;
        if fs <= fy
          cont=0;
          while abs(fl-flp) > max(fl/10000,0.0000001)
            cont = cont+1;
            flp  = fl;
            [fc,el,fl,ecc]= Conf_Pressure(fc0,flp,ec0,Ec,eps,beta,roj,Ej,ks,kg);
            if cont>10, break, end
          end
        else
          flp   = 0.5*ks*kg*roj*fy;
          fcc   = (2.254*(1+7.94*flp/abs(fc0))^0.5-2*flp/abs(fc0)-1.254)*fc0;
          ecc   = ec0*(1+5*(fcc/fc0-1));
          x     = eps/ecc;
          Esecc = fcc/ecc;
          r     = Ec/(Ec-Esecc);
          fc    = fcc*x*r/(r-1+x^r);
          el    = (Ec*eps-fc)/(2*beta*fc);
          fl    = flp;
        end
        sig = fc;
        Et  = (sig-sigp)/De;
      else % non-virgin material
        if (eps > eunl) % closure of a previously open crack
          sig = 0;
          Et  = 0;
          fl  = flp;
        elseif (eps < emin) % the strain increment brings back on the envelope
          [fc,el,fl,ecc]= Conf_Pressure(fc0,flp,ec0,Ec,eps,beta,roj,Ej,ks,kg);
          fs=Ej*el;
          if fs <= fy
            cont=0;
            while abs(fl-flp) >  max(fl/10000,0.0000001)
              cont = cont+1;
              flp  = fl;
```

```
            [fc,el,fl,ecc]= Conf_Pressure(fc0,flp,ec0,Ec,eps,beta,roj,Ej,ks,kg);
            if cont>10, break, end
          end
        else
          flp=0.5*ks*kg*roj*fy;
          [fc,el,fl,ecc]= Conf_Pressure(fc0,flp,ec0,Ec,eps,beta,roj,Ej,ks,kg);
        end
        if eps-De > emin
          sigp = sunl;
          De   = eps-emin;
        end
        sig = fc;
        Et  = (sig-sigp)/De;
      else % loading inside the envelope
        sig = Eunl*(eps-eunl);
        Et  = Eunl;
        fl  = flunl;
      end
    end
  else % positive strain increment: unloading (De > 0)
    if ((eps-De) < emin)    % unloading from the envelope
      emin  = eps-De;
      Eunl  = Ec*(abs(sigp/(Ec*ecc))+0.57)/(abs(emin/ecc)+0.57);
      sunl  = sigp;
      eunl  = emin-sigp/Eunl;
      flunl = flp;
      sig   = Eunl*(eps-eunl);
      Et    = Eunl;
      fl    = flunl;
    elseif (eps > eunl)     % crack has opened
      sig = 0;
      Et  = 0;
      fl  = flp;
    else                    % unloading inside the envelope
      sig  = Eunl*(eps-eunl);
      Et   = Eunl;
      fl   = flunl;
    end
  end
 end
end
% save history variables
State.Pres.sig   = sig;
State.Pres.Et    = Et;
State.Pres.emin  = emin;
State.Pres.eunl  = eunl;
State.Pres.Eunl  = Eunl;
State.Pres.sunl  = sunl;
State.Pres.el    = el;
State.Pres.ecc   = ecc;
State.Pres.fl    = fl;
```

```
  State.Pres.flunl  = flunl;

case 'FRP'
  % Retrieve history variables from Past
  emin  = State.Past.emin;
  eunl  = State.Past.eunl;
  Eunl  = State.Past.Eunl;
  sunl  = State.Past.sunl;
  el    = State.Past.el;
  ecc   = State.Past.ecc;
  fcc   = State.Past.fcc;
  flp   = State.Past.fl;
  flunl = State.Past.flunl;
  elunl = State.Past.elunl;
  muunl  = State.Past.muunl;
  % State determination
  if (De == 0)    % total strain is not changing
    sig = sigp;
    Et  = Ep;
    fl   = flp;
  else           % total strain is changing
    if el >= ejult    % confining FRP is failed
      sig = 0;
      Et  = 0;
      fl  = 0;
      el  = ejult;
    else            % confining FRP is not failed
      if (De < 0) % negative strain increment: loading
        if ((emin == 0)& eps < 0) % virgin material
          [fc,el,fl,ecc]= Conf_Pressure(fc0,flp,ec0,Ec,eps,beta,roj,Ej,ks,kg);
          cont=0;
          while abs(fl-flp) > max(fl/10000,0.0000001)
            cont = cont+1;
            flp  = fl;
            [fc,el,fl,ecc]= Conf_Pressure(fc0,flp,ec0,Ec,eps,beta,roj,Ej,ks,kg);
           if cont>10, break, end
          end
          if el >= ejult    % confining FRP is failing
            sig = 0;
            Et  = 0;
            fl  = 0;
            el  = ejult;
          else
            sig = fc;
            Et  = (sig-sigp)/De;
          end
        else % non-virgin material
          if (eps >= eunl) % closure of a previously open crack
            sig = 0;
            Et  = 0;
            fl  = flp;
```

```
    elseif (eps <= emin) % the strain increment brings back on the envelope
      if eps-De > emin      % loading from reloading to envelope
        sigp = sunl;
        De   = eps-emin;
        flp   = flunl;
      end
      [fc,el,fl,ecc]= Conf_Pressure(fc0,flp,ec0,Ec,eps,beta,roj,Ej,ks,kg);
      cont=0;
      while abs(fl-flp) >  max(fl/10000,0.0000001)
        cont = cont+1;
        flp  = fl;
        [fc,el,fl,ecc]= Conf_Pressure(fc0,flp,ec0,Ec,eps,beta,roj,Ej,ks,kg);
        if cont>10, break, end
      end
      if el >= ejult % confining FRP is failing
        sig = 0;
        Et  = 0;
        fl  = 0;
        el  = ejult;
      else
        sig = fc;
        Et  = (sig-sigp)/De;
      end
    else % loading inside the envelope
      sig = Eunl*(eps-eunl);
      Et  = Eunl;
      el  = elunl-muunl*(eps-emin);
      fl  = 0.5*ks*kg*roj*Ej*el;
    end
  end
else % positive strain increment: unloading (De > 0)
  if ((eps-De) <= emin)    % unloading from the envelope
    emin  = eps-De;
    elunl = el;
    Eunl  = Ec/(1+2*20*elunl);
    sunl  = sigp;
    eunl  = emin-sigp/Eunl;
    flunl = flp;
    muunl = -20*elunl*Eunl/(beta*sunl);
    el    = elunl-muunl*(eps-emin);
    sig   = Eunl*(eps-eunl);
    Et    = Eunl;
    fl    = 0.5*ks*kg*roj*Ej*el;
  elseif (eps >= eunl)     % crack has opened
    sig = 0;
    Et  = 0;
    fl   = flp;
  else                  % unloading inside the envelope
    sig  = Eunl*(eps-eunl);
    Et   = Eunl;
    el   = elunl-muunl*(eps-emin);
```

```
            fl   = 0.5*ks*kg*roj*Ej*el;
          end
        end
      end
    end
    % save history variables
    State.Pres.sig   = sig;
    State.Pres.Et    = Et;
    State.Pres.emin  = emin;
    State.Pres.eunl  = eunl;
    State.Pres.Eunl  = Eunl;
    State.Pres.sunl  = sunl;
    State.Pres.el    = el;
    State.Pres.ecc   = ecc;
    State.Pres.fcc   = fcc;
    State.Pres.fl    = fl;
    State.Pres.flunl = flunl;
    State.Pres.elunl = elunl;
    State.Pres.muunl = muunl;
  otherwise
  end

  if action == 'stif'
    State.sig = sig;
    State.Et  = Et;
  else
    State.sig = sig;
  end
  varargout = {State};
% ========================================================================
case 'post'
  sig      = State.Past.sig;
  Post.eps  = State.eps(1,1);
  Post.sig  = sig;
  switch type_conf
  case {'steel','FRP'}
    Post.el   = State.Past.el;
  otherwise
  end
  varargout = {sig Post};
% ========================================================================
otherwise
  % no further actions are currently supported
end

% ++++++++++++++++++++++++++++++++++++++++++++++++++++++++++++++++++++++++
function [sig,Et] = Unconfined_Envelope(MatData,eps,sigp,De)
% Pantazopoulou-Mills concrete stress-strain relationship
nu      = MatData.nu;
alpha = MatData.alpha;
ec0    = MatData.ec0;
```

```
elim  = MatData.elim;
beta  = MatData.beta;
Ec    = MatData.Ec;
el    = -nu*eps-0.5*(1-2*nu)*alpha*ec0*(0.5*((elim-eps)+abs(elim-eps))/(elim-alpha*ec0))^2;
Esec  = Ec/(1+2*beta*el);
sig   = Esec*eps;
if eps >= elim
   Et = Ec/(1+2*beta*el)^2;
else
   Et = (sig-sigp)/De;
End

% ++++++++++++++++++++++++++++++++++++++++++++++++++++++++++++++++++++++++++++++
function [fc,el,fl,ecc]= Conf_Pressure(fc0,flp,ec0,Ec,eps,beta,roj,Ej,ks,kg)
% Confinement pressure on Mander-Popovics curve
fcc   = (2.254*(1+7.94*flp/abs(fc0))^0.5-2*flp/abs(fc0)-1.254)*fc0;
ecc   = ec0*(1+5*(fcc/fc0-1));
x     = eps/ecc;
Esecc = fcc/ecc;
r     = Ec/(Ec-Esecc);
fc    = fcc*x*r/(r-1+x^r);
el    = (Ec*eps-fc)/(2*beta*fc);
fl    = 0.5*ks*kg*roj*Ej*el;
```

APPENDIX E : FEDEASLAB CODE FOR RESPONSE COMPUTATION FOR THE SZM MODEL

```
function varargout = Mate17 (action,Mat_no,MatData,State,varargin)
% MATE17 cyclic stress-strain relation for SZM confined concrete 2006
% With Sensitivity Analysis
% ========================================================================
% FEDEAS Lab - Release 2.3, March 2001
% Matlab Finite Elements for Design, Evaluation and Analysis of Structures
%
% Copyright (c) 1998, Professor Filip C. Filippou, filippou@ce.berkeley.edu
% Department of Civil and Environmental Engineering, UC Berkeley
% ========================================================================
% Material Properties of unconfined concrete
% MatData.fcc  : peak strength of unconfined concrete

% Confining Properties
% MatData.type_conf  : type of confinement ('FRP')
%              .reinf_disp : reinforcement disposition ('cont', 'discont')
%
% Material Properties of confined concrete
% MatData.Ej  : FRP Young modulus
%              .tj   : FRP thickness
%              .fj   : hoop strength of FRP
%              .D   : diameter of concrete core

% Material History Variables
% State._.sig  : stress
%          .eps  : strain
%          .Et   : tangent modulus
%         .emax : maximum strain (compression)
%          .epl  : strain at stress equal zero
%         .Eunl : unloading-reloading modulus
%          .sunl : unloading stress
%          .eunl : unloading strain
%          .ero  : reloading strain
%          .fro  : reloading stress
%          .ere  : return strain
%          .fre  : return stress

global IOW;      % output file number
global HEAD_PR;   % header print indicator

% check material data, set default values, if any, and retrieve data
% ========================================================================
switch action
   case 'chec'
      if (~isfield(MatData,'fcc'))disp('Material');disp(Mat_no);error('peak compressive strength missing');
         end
```

```
      if (~isfield(MatData,'Ej')) disp('Material');disp(Mat_no); error('FRP Young"s modulus missing'); end
      if (~isfield(MatData,'tj')) disp('Material');disp(Mat_no); error('FRP thickness missing'); end
      if (~isfield(MatData,'fj')) disp('Material');disp(Mat_no); error('FRP hoop strength missing'); end
      if (~isfield(MatData,'D'))  disp('Material');disp(Mat_no); error('diameter of concrete core missing');
         end
      MatData.fcc = abs(MatData.fcc);
      MatData.E1  = 3950*(MatData.fcc)^0.5;
      MatData.E2  = 245.61*(MatData.fcc)^0.2+1.3456*MatData.Ej*MatData.tj/MatData.D;
      MatData.fl    = 2*MatData.fj*MatData.tj/MatData.D;
      MatData.f0   = 0.872*(MatData.fcc)+0.371*MatData.fl+6.258;
      MatData.fcu = MatData.fcc+6.0*MatData.fl^0.7;
      MatData.ecu = (MatData.fcu-MatData.f0)/MatData.E2;
      MatData.a   = (MatData.E1-MatData.E2)*MatData.ecu/(1+((MatData.E1-MatData.E2)*MatData.cu/
                    MatData.f0)^1.5)^(1/1.5)+MatData.E2*MatData.ecu;
      MatData.b   = MatData.E2+(MatData.E1-MatData.E2)/((MatData.ecu*(MatData.E1-MatData.E2)/
                    MatData.f0)^1.5+1)^(2/3)-MatData.ecu*(MatData.E1-MatData.E2)^2*
                    (MatData.ecu*(MatData.E1-MatData.E2)/MatData.f0)^0.5/(MatData.f0*
                    ((MatData.ecu*(MatData.E1- MatData.E2)/MatData.f0)^1.5+1)^(5/3));
      MatData.c   = (-200*MatData.b*MatData.ecu-3e4*MatData.a)/(MatData.ecu)^2;
      MatData.d   = (MatData.b*MatData.ecu+200*MatData.a)*10^4/(MatData.ecu)^3;
      varargout = {MatData};
   otherwise
      %  extract material properties
      fcc   = MatData.fcc;
      Ej    = MatData.Ej;
      tj    = MatData.tj;
      fj    = MatData.fj;
      E1    = MatData.E1;
      E2    = MatData.E2;
      D     = MatData.D;
      fl    = MatData.fl;
      f0    = MatData.f0;
      fcu   = MatData.fcu;
      ecu   = MatData.ecu;
      a     = MatData.a;
      b     = MatData.b;
      c     = MatData.c;
      d     = MatData.d;
end

% material actions
% =====================================================================
switch action
   case 'data'
      if (HEAD_PR)
         fprintf (IOW,'\n       Confined Concrete Material Model');
         fprintf (IOW,'\n       Mat no       fcc              ');
      end
      fprintf (IOW,'\n          %4d   %11.3e  %11.3e  %11.3e', Mat_no,fcc);
% =====================================================================
   case 'init'
```

```
        sig  = 0;
        Et   = E1;
        State.sig  = sig;
        State.eps  = 0;
        State.Et   = Et;
        State.Pres.sig  = sig;
        State.Pres.Et   = Et;
        State.Pres.emax = 0;
        State.Pres.epl  = 0;
        State.Pres.Eunl = E1;
        State.Pres.sunl  = 0;
        State.Pres.eunl  = 0;
        State.Pres.sun   = 0;
        State.Pres.eun   = 0;
        State.Pres.ero    = 0;
        State.Pres.fro    = 0;
        State.Pres.ere    = 0;
        State.Pres.fre    = 0;
        State.Pres.flag  = 0; % 0 = virgin material;1 = loading;2 = unloading
        varargout = {State};
% ======================================================================
    case {'stif','forc'}
        % extract material properties
        fcc   = MatData.fcc;
        Ej    = MatData.Ej;
        D     = MatData.D;
        fcu   = MatData.fcu;
        ecu   = MatData.ecu;
        % Retrieve history variables from Past
        sigp  = -State.Past.sig;
        Ep    = State.Past.Et;
        eps   = -State.eps(1,1); % total strain
        De    = -State.eps(1,2); % total strain increment
        epl    = State.Past.epl;
        emax  = State.Past.emax;
        Eunl   = State.Past.Eunl;
        sunl    = State.Past.sunl;
        eunl   = State.Past.eunl;
        sun    = State.Past.sun;
        eun    = State.Past.eun;
        ero     = State.Past.ero;
        fro     = State.Past.fro;
        ere     = State.Past.ere;
        fre      = State.Past.fre;
        flag     = State.Past.flag;
        emax  = max(emax,eps);

 % State determination
        if (De == 0)        % total strain is not changing
            sig = sigp;
            Et  = Ep;
```

```
else              % total strain is changing
  if (emax >= 1.01*ecu) || (eps <= 0)    % confining FRP is failed
    sig = 0;
    Et  = 0;
  else            % confining FRP is not failed
    if (De > 0)  % loading
      if (flag==0)    % material on the envelope
        if eps<ecu
          sig = (E1-E2)*eps/(1+((E1-E2)*eps/f0)^1.5)^(1/1.5)+E2*eps;
          Et  = E2+(E1-E2)/((eps*(E1-E2)/f0)^1.5+1)^(2/3)-eps*(E1-E2)^2*(eps*(E1-E2)/
                f0)^0.5/(f0* ((eps*(E1-E2)/f0)^1.5+1)^(5/3));
        else
          sig= a+b*(eps-ecu)+c*(eps-ecu)^2+d*(eps-ecu)^3;
          Et = b+2*c*(eps-ecu)+3*d*(eps-ecu)^2;
        end
      else
        if eps<=epl % closure of a previously open crack
          sig = 0;
          Et  = 0;
          flag= 1;
        else
          if (flag==1)
            if eun<=eunl
              if fro>=0.9*sunl % return to the unloading point
                if eps<=eunl
                  Et  = (sunl-fro)/(eunl-ero);
                  sig = fro+Et*(eps-ero);
                elseif eps>eunl && eps<=ecu
                   sig = (E1-E2)*eps/(1+((E1-E2)*eps/f0)^1.5)^(1/1.5)+E2*eps;
                   Et  = E2+(E1-E2)/((eps*(E1-E2)/f0)^1.5+1)^(2/3)-eps*(E1-E2)^2*(eps*(E1-
                         E2)/f0)^0.5/(f0*((eps*(E1-E2)/f0)^1.5+1)^(5/3));
                   flag= 0;
                elseif eps>ecu
                   sig = a+b*(eps-ecu)+c*(eps-ecu)^2+d*(eps-ecu)^3;
                   Et  = b+2*c*(eps-ecu)+3*d*(eps-ecu)^2;
                end
              else
                if eps<=eunl
                  Et  = (0.9*sunl-fro)/(eunl-ero);
                  sig = fro+Et*(eps-ero);
                elseif eps>eunl && eps<=ere
                  Et  = 0.9*sunl/(eunl-epl);
                  sig = 0.9*sunl+Et*(eps-eunl);
                elseif eps>ere
                  if eps<=ecu
                    sig = (E1-E2)*eps/(1+((E1-E2)*eps/f0)^1.5)^(1/1.5)+E2*eps;
                    Et  = E2+(E1-E2)/((eps*(E1-E2)/f0)^1.5+1)^(2/3)-eps*(E1-E2)^2*
                          (eps*(E1-E2)/f0)^0.5/(f0*((eps*(E1-E2)/f0)^1.5+1)^(5/3));
                    flag= 0;
                  else % eps>ecu
                     sig = a+b*(eps-ecu)+c*(eps-ecu)^2+d*(eps-ecu)^3;
```

```
                Et  = b+2*c*(eps-ecu)+3*d*(eps-ecu)^2;
            end
        end
    end

  else %eun>eunl
    if eps<=eun
        Et  = (sun-fro)/(eun-ero);
        sig = fro+Et*(eps-ero);
    elseif  eps>eun && eps<=ere
        Et  = 0.9*sunl/(eunl-epl);
        sig = sun+Et*(eps-eun);
    elseif eps>ere
        if eps<=ecu
            sig = (E1-E2)*eps/(1+((E1-E2)*eps/f0)^1.5)^(1/1.5)+E2*eps;
            Et  = E2+(E1-E2)/((eps*(E1-E2)/f0)^1.5+1)^(2/3)-eps*(E1-E2)^2*(eps*(E1-
                  E2)/f0)^0.5/ (f0*((eps*(E1-E2)/f0)^1.5+1)^(5/3));
            flag= 0;
        else % eps>ecu
            sig = a+b*(eps-ecu)+c*(eps-ecu)^2+d*(eps-ecu)^3;
            Et  = b+2*c*(eps-ecu)+3*d*(eps-ecu)^2;
        end
    end
  end

else %flag==2
  ero = eps-De;
  if ero<epl
    ero = epl;
  end
  fro = sigp;
  flag=1;
  if eun<=eunl
    if fro>=0.9*sunl
        if eps<=eunl
            Et  = (sunl-fro)/(eunl-ero);
            sig = fro+Et*(eps-ero);
        else %eps>eunl
            sig = (E1-E2)*eps/(1+((E1-E2)*eps/f0)^1.5)^(1/1.5)+E2*eps;
            Et  = E2+(E1-E2)/((eps*(E1-E2)/f0)^1.5+1)^(2/3)-eps*(E1-E2)^2*(eps*(E1-
                  E2)/f0)^0.5/ (f0*((eps*(E1-E2)/f0)^1.5+1)^(5/3));
            flag= 0;
        end
    else
        if eps<=eunl
            Et  = (0.9*sunl-fro)/(eunl-ero);
            sig = fro+Et*(eps-ero);
        elseif eps>eunl && eps<=ere
            Et  = 0.9*sunl/(eunl-epl);
            sig = 0.9*sunl+Et*(eps-eunl);
        elseif eps>ere
```

```
                    if eps<=ecu
                      sig = (E1-E2)*eps/(1+((E1-E2)*eps/f0)^1.5)^(1/1.5)+E2*eps;
                      Et  = E2+(E1-E2)/((eps*(E1-E2)/f0)^1.5+1)^(2/3)-eps*(E1-E2)^2*(eps*
                            (E1-E2)/f0)^0.5/(f0*((eps*(E1-E2)/f0)^1.5+1)^(5/3));
                      flag= 0;
                    else % eps>ecu
                       sig = a+b*(eps-ecu)+c*(eps-ecu)^2+d*(eps-ecu)^3;
                       Et  = b+2*c*(eps-ecu)+3*d*(eps-ecu)^2;
                    end
                 end
              end

           else %eun>eunl
              if eps<=eun
                 Et  = (sun-fro)/(eun-ero);
                 sig = fro+Et*(eps-ero);
              elseif  eps>eun && eps<=ere
                 Et  = 0.9*sunl/(eunl-epl);
                 sig = sun+Et*(eps-eun);
              elseif eps>ere
                 if eps<=ecu
                    sig = (E1-E2)*eps/(1+((E1-E2)*eps/f0)^1.5)^(1/1.5)+E2*eps;
                    Et  = E2+(E1-E2)/((eps*(E1-E2)/f0)^1.5+1)^(2/3)-eps*(E1-E2)^2*(eps*(E1-
                          E2)/f0)^0.5/ (f0*((eps*(E1-E2)/f0)^1.5+1)^(5/3));
                    flag= 0;
                 else % eps>ecu
                    sig = a+b*(eps-ecu)+c*(eps-ecu)^2+d*(eps-ecu)^3;
                    Et  = b+2*c*(eps-ecu)+3*d*(eps-ecu)^2;
                 end
              end
           end
        end
     end

else %(De < 0)    unloading
   if (flag == 0) %from loading
      eunl = eps-De;
      if eunl<=ecu
         sunl = (E1-E2)*eunl/(1+((E1-E2)*eunl/f0)^1.5)^(1/1.5)+E2*eunl;
      elseif eunl>ecu && eunl<=1.01*ecu
         sunl=a+b*(eunl-ecu)+c*(eunl-ecu)^2+d*(eunl-ecu)^3;
      else
         disp('error1');
      end
      eun=eunl;
      sun=sunl;
      if (sunl/fcc) >= 0 && (sunl/fcc) <1
         Eunl = E1;
      elseif sunl/fcc>=1 && sunl/fcc <2.5
         Eunl = (-0.44*sunl/fcc+1.44)*E1;
```

```
    elseif sunl/fcc >= 2.5
       Eunl =0.34*E1;
    else
       disp('error2');
    end
    epl = eunl-sunl/Eunl;
    ff = 0.9*sunl/(eunl-epl);
    ere = fzero(@(x)myfun_ere(x,ff,E1,E2,f0,epl,ecu,a,b,c,d),[eunl,1.01*ecu]);
    fre = (E1-E2)*ere/(1+((E1-E2)*ere/f0)^1.5)^(1/1.5)+E2*ere;
    flag = 2; %unloading already started
    x = (eps-eunl)/(epl-eunl);
    if x>=0 && x<=1
       sig = ((1-x)^2/(1+2*x)^2)*sun;
       Et = (2*(1-x)*(1+2*x)+4*(1-x)^2)*Eunl/(1+2*x)^3;
    elseif x>1
       sig = 0;
       Et  = 0;
    else
       disp('error3');
    end

elseif (flag == 1)
    if eps>epl
       eun = eps-De;
       sun = sigp;
    end
    flag = 2; %unloading already started
    x = (eps-eun)/(epl-eun);
    if x>=0 && x<=1
       sig = ((1-x)^2/(1+2*x)^2)*sun;
       Et  = (2*(1-x)*(1+2*x)+4*(1-x)^2)*Eunl/(1+2*x)^3;
    elseif x>1
       sig = 0;
       Et  = 0;
    else
       disp('error4');
    end

elseif (flag == 2)
    x = (eps-eun)/(epl-eun);
    if x>=0 && x<=1
       sig = ((1-x)^2/(1+2*x)^2)*sun;
       Et = (2*(1-x)*(1+2*x)+4*(1-x)^2)*Eunl/(1+2*x)^3;
       fro = sig;
       ero = eps;
    elseif x>1
       sig = 0;
       Et  = 0;
       fro = 0;
       ero = epl;
    else
```

```
                    disp('error5');
                end
            end
        end
    end
    % save history variables
    State.Pres.sig    = -sig;
    State.Pres.Et     = Et;
    State.Pres.epl    = epl;
    State.Pres.Eunl   = Eunl;
    State.Pres.eunl   = eunl;
    State.Pres.sunl   = sunl;
    State.Pres.eun    = eun;
    State.Pres.sun    = sun;
    State.Pres.emax   = emax;
    State.Pres.ero    = ero;
    State.Pres.fro    = fro;
    State.Pres.ere    = ere;
    State.Pres.fre    = fre;
    State.Pres.flag   = flag;

    if action == 'stif'
       State.sig = -sig;
       State.Et  = Et;
    else
       State.sig = -sig;
    end
    varargout = {State};
% ========================================================================
  case 'post'
    sig          = State.Past.sig;
    Post.eps  = State.eps(1,1);
    Post.sig   = sig;
    Post.flag = State.Past.flag;
    Post.ero  = State.Past.ero;
    Post.fro  = State.Past.fro;
    Post.ere   = State.Past.ere;
    varargout = {sig Post};
   otherwise
end

% ========================================================================
function f=myfun_ere(x,ff,E1,E2,f0,epl,ecu,a,b,c,d)
if x<=ecu
   f=ff*(x-epl)-(E1-E2)*x/(1+((E1-E2)*x/f0)^1.5)^(1/1.5)-E2*x;
elseif x>ecu && x<=1.01*ecu
   f=ff*(x-epl)- (a+b*(x-ecu)+c*(x-ecu)^2+d*(x-ecu)^3);
else % ere>1.01*ecu
   f=ff*(x-epl);
end
```

VITA

Dan Hu was born in 1988 in Jiangxi, China. She graduated with her bachelor's degree from Southwest Jiaotong University, China, in civil engineering in June 2009. After her graduation, she moved to the United States to continue her education. She got admitted in structural engineering program in the Department of Civil and Environmental Engineering at Louisiana State University in spring 2010. She has been working as a graduate research assistant under the supervision of Dr. Barbato and is a candidate for degree of Master of Science in Civil Engineering to be awarded in December 2012. Her main area of interests is modeling and analysis of reinforced concrete structures retrofitted with fiber reinforced polymers.